VOLUME CHANGE AND RESIDUAL PORE WATER PRESSURE OF SATURATED GRANULAR SOILS TO BLAST LOADS

A Research Report Submitted to NSERC

by

Guoxi Wu, Ph.D.

NSERC Industrial Research Fellow

Reviewed by:

W. Blair Gohl, Ph.D., P.Eng.

AGRA Earth & Environmental Limited
2227 Douglas Road, Burnaby, BC, V5C 5A9
(604) 294-3811

December 3, 1996

Volume Change and Residual Pore Water Pressure
of Saturated Granular Soils to Blast Loads
A Research Report Submitted to NSERC

ABSTRACT:

This report presents the results of the continued research on soil response to blast loads. The research program is financially supported by the Natural Sciences and Engineering Research Council of Canada (NSERC) by means of an Industrial Research Fellowship.

The numerical model (Wu, 1995) for the analysis of dynamic response of granular soil to blast loads has been used for computing peak dynamic water pressures, peak dynamic volumetric strains and peak dynamic shear strains. Vibrations of soil induced by blast loads result in increasing hydrostatic pore water pressures and residual pore water pressures. Subsequent settlements or plastic non-recoverable volumetric strains occur as the residual pore water pressures dissipate with time. Full dissipation of residual pore water pressures for granular soils usually occurs within hours after blasting.

An empirical formulation has been proposed for analysis of plastic volumetric strain using peak dynamic volumetric strain computed from the dynamic response analysis. The plastic volumetric strains caused by multiple charges are accumulated from each individual charge. This formulation has been extensively verified using settlement data from field blasting trials with single charges and multiple charges.

A methodology is presented in this report for computing residual pore water pressures according to the amount of plastic volumetric strain. The method uses a concept that the potential volumetric strain required to trigger initial liquefaction only depends on the relative density of the sample, but does not depend on other factors such as loading path, initial soil stiffness and the effective vertical stress. The residual pore water pressure ratios predicted by the proposed model have been compared to available measured data.

The analysis of dynamic transient response and the residual response of saturated granular soils to blast loads has been implemented in the computer program BLAST. The program BLAST is then used for generating curves describing the relationships between the plastic volumetric strain, residual pore water pressures and the scaled distance $R/W^{0.333}$ for sands of different $(N_1)_{60}$ values. These curves are expected to be used in the design of controlled blasting for soil densification.

Volume Change and Residual Pore Water Pressure
of Saturated Granular Soils to Blast Loads
A Research Report Submitted to NSERC

TABLE OF CONTENTS

List of Figures

1.0 INTRODUCTION

Prediction of plastic (or permanent) volumetric strain in saturated sands subjected to blast loads is of great importance in the design of controlled blasting for densification of granular soils. Densification of sand is considered herein although the numerical model developed is considered equally applicable to a wide range of granular soil types using appropriate calibration of model parameters. In this report, an empirical relationship is presented for computing the plastic volumetric strain using the level of dynamic strain developed in the sand and the rebound deformation characteristics of the sand. The method for computing dynamic transient response of sand subjected to blast loads has been described in the first report to NSERC (Wu, 1995).

It has been well recognized that the plastic volumetric strain (or potential volumetric strain under undrained conditions) developed under cyclic loading depends mainly on the dynamic shear strain history. Under cyclic loading, sand tends to vibrate into a more compact state. Drained volume change occurs simultaneously with vibration for dry sand or saturated sand in drained conditions. However, pore water pressure arises for saturated sand in undrained conditions. Reconsolidation volume change will occur when the pore water pressures are allowed to dissipate with time.

Martin - Finn - Seed (1975) developed a procedure for computing the potential volumetric strain in undrained conditions. The potential volumetric strain can be obtained in an experimental test by changing the drainage condition from undrained to drained and measuring the volume change following the dissipation of pore water pressure. The work of Bhatia (1980) and Byrne (1991) showed that the potential volumetric strain can also be determined quite accurately using an analytical tool when the shear strain history is known.

In this report, a formulation similar to the Martin - Finn - Seed (1975) model has been proposed for computing the plastic volumetric strain of sands subjected to blast loads. The plastic volumetric strain is computed from the level of dynamic volumetric strain rather than the shear strain as used in the Martin -- Finn - Seed (1975) model. The volumetric strain constants are presented as a function of the normalized SPT $(N_1)_{60}$ in clean sand, i.e., fines content (grain size $<$ 0.075 mm) less than 5%. The proposed relationship has been extensively examined using settlement data from field blasting trials.

In the field blasting trials residual pore water pressures will develop prior to the development of plastic

volumetric strain. The amount of residual pore water pressures is determined from the potential volumetric strain and the rebound characteristics of the sand. Martin et al. (1975) proposed that within a segment of strain increment, the pore water pressure increment can be computed by the product of the potential volumetric strain increment and a stress - level - dependent rebound modulus E_r. They further suggested that the rebound modulus be determined by static unloading tests. Bhatia (1980) showed that the rebound modulus E_r measured from static unloading conditions is too high and leads to overestimation of pore water pressure in stress controlled undrained conditions. She also showed that the rise of pore water pressures can be predicted if the rebound modulus measured under cyclic loading conditions was used. However, this method remains experimental and can not immediately be applied to analysis.

A methodology is presented in this report for computing the rise of residual pore water pressure according to the accumulated potential volumetric strain. The method uses a concept that the potential volumetric strain required to trigger initial liquefaction only depends on the relative density of the sample, but does not depend on other factors such as loading path, initial soil stiffness and the effective vertical stress. The method basically involves a modification of the expression of the rebound modulus E_r which was originally proposed by Martin et al. (1975). The proposed expression for E_r only contains one single parameter, the rebound modulus constant M. The values of M are explicitly given corresponding to relative density D_r or the $(N_1)_{60}$. The performance of the proposed model for prediction of residual pore water pressure in strain controlled tests has been evaluated.

Finally the theory is applied for generating curves describing the relationship between the plastic volumetric strain, residual pore water pressures and the scaled distance $R/W^{0.333}$ for sands having different $(N_1)_{60}$ values. These curves are expected to be useful in the design of controlled blasting for granular soil densification.

2.0 THEORY FOR DETERMINATION OF VOLUME CHANGES AND PORE WATER PRESSURES

2.1 A Formulation for Computing Plastic Volumetric Strains

It has been reported from strain controlled tests that under simple shear conditions the drained volume change or the reconsolidation volume change depends mainly on the shear strain history (Martin et al., 1975; Bhatia, 1980; Byrne, 1991; Ishihara and Yoshimine, 1992). However, under blast loads, large radial and tangential normal strains occur which generate a significant amount of dynamic volumetric strain. Therefore an empirical formulation is proposed to correlate the plastic volumetric strain increment to the level of dynamic volumetric strain ε_v as

[1] $$\Delta\varepsilon_v^p = B_1 \cdot \varepsilon_v \cdot EXP(-B_2 \varepsilon_v^p / \varepsilon_v)$$

where

$\Delta\varepsilon_v^p$ = the plastic volumetric strain increment (%) caused by dynamic current strain

ε_v^p = the total plastic volumetric strain (%) accumulated from previous strain history

ε_v = the amplitude of dynamic volumetric strain (%)

B_1, B_2 = volumetric strain constants of the sand

The relationship between the volumetric strain constants B_1 and the $(N_1)_{60}$ as shown in Fig. 2-1(a) has been established using the technique of back-analysis. Ground surface settlement data obtained from field blast trials have been used in these analyses which are detailed in the following section. The volumetric strain constant B_2 is given by

[2] $$B_2 = \frac{0.2}{B_1}$$

The compressive shear wave velocity V_P for saturated sand and the viscosity number K_η (Wu, 1995) are also presented in Fig. 2-1(b) and Fig. 2-1(c), respectively, as a function of $(N_1)_{60}$. A correlation between $(N_1)_{60}$ and the relative density D_r of the sand is given in Fig. 2-2 (after Tokimatsu and Seed, 1987). A loose sand may be represented by $(N_1)_{60}$ = 8 or D_r = 45 %, a medium dense sand by $(N_1)_{60}$ = 16 or D_r = 60 %, and a dense sand by $(N_1)_{60}$ = 25 or D_r = 75 %.

The plastic volumetric strain in a soil element caused by multiple charges are accumulated using eq. [1] by treating these charges as subsequent single charges. Because plastic volumetric strain increment is not a linear function of dynamic volumetric strain, the plastic volumetric strain increment per single charge decreases as total plastic volumetric strain accumulates as shown in Fig. 2-3.

2.2 A Volume-Constant Pore Water Pressure Model for Saturated Granular Soils in Undrained Conditions

For saturated sand in undrained conditions, water may be assumed to be effectively incompressible compared to the sand skeleton. Thus under conditions of zero volume change Martin et al. (1975) proposed the following relationship for computing the pore water pressure increment Δu

[3] $$\Delta u = E_r \cdot \Delta \varepsilon_v^p$$

where

$\Delta \varepsilon_v^p$ = plastic volumetric strain increment accumulated during a period of strain history

Δu = residual pore water pressure increment corresponding to the plastic volumetric strain increment ε_v^p

E_r = rebound modulus of the sand skeleton corresponding to the current effective vertical stress σ_v'

Under harmonic loads, $\Delta \varepsilon_v^p$ is usually accumulated at each cycle or at each half cycle of strain. Under irregular earthquake loads, $\Delta \varepsilon_v^p$ may be accumulated at points of strain reversal. As the potential volumetric strain is known, the increment in pore water pressure Δu can be determined from the rebound modulus of the sand skeleton E_r. Martin et al. (1975) suggested that the rebound modulus of sand under one dimensional conditions should be determined from static unloading tests. However Bhatia (1980) showed that " the rebound modulus must be measured under cyclic loading conditions. The static rebound modulus used in conjunction with volumetric strain data overestimates pore water pressures in stress controlled undrained conditions."

A simple one-parameter equation is proposed herein to determine the rebound modulus E_r according to the current effective vertical stress σ_v' as

[4] $$E_r = M \cdot \sigma_v'$$

or

[5] $$E_r = M \cdot (\sigma_{v0}' - u)$$

where

M = rebound modulus constant, M = f(D_r or $(N_1)_{60}$)

σ_{v0}' = initial effective vertical stress

The determination of the rebound modulus constant M is based on the volume-constant concept that there is a unique relationship between the relative density of sand and the amount of potential volumetric strain required to trigger initial liquefaction. Ishihara and Yoshimine (1992) stated that " the volume change characteristics of sand during reconsolidation following the cyclic loading is uniquely correlated with the amount of developed pore water pressure, no matter what types of irregular loads are used, and irrespective of whether the irregular load is applied in one-direction or in a multi-directional manner." Their work strongly supports that at a specific relative density D_r the sample will experience initial liquefaction if a certain amount of potential volumetric strain (referred as volume change during reconsolidation following the cyclic loading by Ishihara and Yoshimine, 1992) is developed in the sample, as shown in Fig. 2-4.

The potential plastic volumetric strains ε_v^p required to trigger initial liquefaction are plotted against the relative density D_r or $(N_1)_{60}$ of the sample in Fig. 2-5. The lower bound values of the potential volumetric strains in the original plot (Fig. 2-4) by Ishihara and Yoshimine (1992) have been adopted so that the assessment of liquefaction is on the conservative side. This relationship implies that the amount of volume change required to trigger initial liquefaction is much larger in a very loose sand than in a very dense sand. At initial liquefaction the volume change is about 1.5% for a sample with D_r = 40% but 0.5% for a sample with D_r = 80%.

The use of eqs. [3] and [5] leads to a closed form relationship between the pore water pressure u and the plastic volumetric strain ε_v^p as

[6] $$u = \sigma_{v0}' \cdot (1 - EXP(-M \cdot \varepsilon_v^P))$$

or

[7] $$PPR = 1 - EXP(-M \cdot \varepsilon_v^P)$$

where PPR = pore water pressure ratio, PPR = u/σ_{v0}'

The rebound modulus constant M is determined by assuming that initial liquefaction occurs at PPR = 0.95. The relationship between the rebound modulus constant M and $(N_1)_{60}$ is shown in Fig. 2-6. It can be seen that the rebound modulus constant M increases from 180 at $(N_1)_{60}$ = 6 to 510 at $(N_1)_{60}$ = 24.

The proposed volume-constant pore water pressure model has been verified against test data by Bhatia (1980) as shown in Fig. 2-7. For the experimental data points the plastic volumetric strains are measured from the drained tests, and the pore water pressure ratios are measured from the corresponding undrained tests subjected to the same shear strain histories as in the drained tests. For the model prediction the pore water pressure ratios are calculated from the amount of plastic volumetric strain using Eq. (7). The computed pore water pressure response agrees well with the experimental response for sample of Dr = 45% and Dr = 60%.

3.0 COMPARISON BETWEEN MODEL PREDICTIONS AND FIELD MEASUREMENTS

The proposed volumetric strain model has been applied to predict settlements at the ground surface for four blast projects. These projects are field tests of single charges by Kummeneje and Eide (1961), 4-hole multi-deck charges fired in Fraser River sand deposits, Richmond, B.C. (AGRA, 1991), explosive compaction using a large number of multiple charges at the SM-3 Dam in Quebec (AGRA, 1995), and deep explosive compaction performed at the Jebba dam (Solymar, 1984). These studies confirm the satisfactory performance of the volumetric strain model.

3.1 Tests by Kummeneje and Eide (1961)

TEST RESULTS

Kummeneje and Eide (1961) reported results of blasting conducted in a marine sand deposit on the West Coast of Norway. The blasting site is located in a large delta deposit at the mouth of the river Verdalselven. The site consists mainly of fine sand and coarse silt with occasional layers of coarse sand. Laboratory tests conducted on samples taken from the blasting site (5 m away from bore hole #3) showed that the mean grain size of the soil particle was in the range from D_{50} = 0.05 mm to 0.2 mm. The fines content (grain size less than 0.075 mm) in the upper 10 m is about 15 to 20 % but increases to over 50 % for depths greater than 10 m. The cone tip resistance Q_c measured by cone penetration sounding varied from 1 MPa to 3 MPa, i.e., 10 bars to 30 bars, just before blasting. The ground water table was at 1.0 m below the ground surface.

Seven charges (total 6.9 kg of Dynamite) were fired individually at a depth of 7 m below the ground surface. The first charge was 0.3 kg, the second charge 0.6 kg, followed by five charges of 1.2 kg. Ground surface settlements were measured following detonation of each single charge. The measured settlements are shown in Fig. 3-1. A total settlement of 40 cm at the surface directly above the blast point was caused by the series of detonations, and the settlements at the surface with a horizontal distance 15 m away from the blast point was about 0.5 cm. The total volume of the settlement dish around the blast point was 39 m^3.

Between each explosion, sufficient time was allowed for the residual pore water pressures to dissipate fully. The residual pore water pressures were measured by a specially made piezometer. The residual pore water pressures induced by explosion of the first 1.2 kg charge are shown in Fig. 3-2. At a

horizontal distance 5 m away from the blast point, the maximum residual pore water pressure was approximately 50 % of the effective overburden stress. The residual pore water pressure decreased rapidly with horizontal distance from the blast point. At a horizontal distance 15 m to 20 m away from the blast point, the residual pore water pressure was only 5 % of the effective overburden stress.

ANALYSIS RESULTS

The soil properties used in the analysis is given in Table 1. The resistance of sandy soil to cyclic loads is characterized by equivalent clean sand values of $(N_1)_{60}$. The $(N_1)_{60}$ profile of the blast site was established from the cone tip resistance Q_c with overburden stress correction and fines content correction. First the equivalent SPT N values were obtained from the cone tip resistance Q_c using the correlation chart by Robertson et al. (1983). Secondly, the SPT N values were corrected to $(N_1)_{60}$ according to the effective overburden stress using the relationship proposed by Liao and Whitman (1985). The last step is to obtain the $(N_1)_{60}$ values equivalent to those measured in clean sand by performing a fines content correction using the method described by Seed at al. (1985).

Other parameters used in the analysis were obtained according to the $(N_1)_{60}$ values using the charts presented in the previous section.

Table 1. Soil parameters used in the analysis

Depth (m)	V_S (m/s)	V_P (m/s)	K_η	τ_{max} (kPa)	B_1	B_2	$(N_1)_{60}$
0 to 1.0	100	560	50	15	above water table		
1 to 3.0	120	1520	55	30	4.9	0.040	10
3.0 to 6.0	150	1540	55	30	4.9	0.040	10
6.0 to 10.0	160	1560	63	50	3.6	0.056	14
over 10.0	170	1580	84	50	2.1	0.096	20

The computed surface settlements from detonation of each single charge are shown in Fig. 3-3. The computed settlement profiles at the blast point and at 5 m away from the blast point are shown in Fig. 3-4. A ground surface settlement of 41.0 cm was computed at the blast point, compared to a measured

settlement of 40 cm at the same location.

3.2 Field Blasting Trials at Richmond site, B.C.

TEST RESULTS

In October 1991, HBT AGRA Limited and Foundex Explorations Ltd. carried out field blasting trials on the southern part of Lulu Island, B.C.. Lulu Island is a part of the Fraser River Delta, situated between the North and South Arms of the Fraser River. The soil conditions typically consist of an upper layer of peat or silt over loose to medium dense Fraser River sand, which in turn overlies marine silts to great depth. The sands are generally fine to medium grained and tend to be uniformly graded.

The results of dynamic cone penetration tests (DCPTs) carried out at the site prior to blasting are shown in Fig. 3-5. The DCPTs were carried out using a 60.3 mm diameter cone with a 150 mm sleeve driven by an automatic hammer. No sampled holes were drilled at the site.

Four blast holes were drilled at the site using a hollow stem auger. PVC tubing was dropped into the hole and the augers were withdrawn. The relative position of the four blast holes are shown in Fig. 3-6. Blast holes 1 and 4 were 7 meters deep, and blast holes 2 and 3 were 14 m and 13.85 m deep, respectively. The size and distribution of the charges fired at the site are shown in Table 2. The blast holes were set off individually at the times and delays shown in Table 2. All charges were fired from the top down.

Wooden stakes were hammered into the ground at each corner, and at 1.5 m intervals along the perimeter of the rectangle to allow elevations to be monitored. Prior to each blast, the elevations of all settlement stakes were monitored. The blast hole was then detonated. Elevations were then monitored again. Between each blast, residual pore water pressures were allowed to dissipate fully prior to the next blast proceeding.

The distribution of settlements measured on the surface settlement pins are shown in Figs. 3-7(a)-(d) for sections AA, BB, CC and DD, respectively. Maximum settlements of about 35.8 cm at the north end (4 decks to a depth of 14 m) and 31.1 cm at the south end (2 decks to a depth of 7 m) were obtained between blast hole locations. The maximum radius of influence observed along section AA and CC was greater than 9.0 m as settlement was observed at all settlement points along the 18 m long sections.

Table 2 Charge size and distribution (Richmond site, oct. 1991)

	Charge Mass (kg)	Charge Length (m)	Depth to Mid-Point of Charge (m)	Time of Detonation	Time Delay (msec)
Blast Hole 1	1.000	0.6	3.30	12:17 p.m.	0
	1.000	0.6	6.70		500
Blast Hole 2	1.010	0.6	3.50	13:25 p.m.	25
	1.020	0.6	6.90		175
	1.030	0.6	10.30		325
	1.020	0.6	13.70		475
Blast Hole 3	2.070	1.2	3.65	15:09 p.m.	25
	2.040	1.2	6.85		175
	2.060	1.2	10.05		325
	2.050	1.2	13.25		475
Blast Hole 4	2.060	1.2	2.90	15:46 p.m.	0
	2.060	1.2	6.40		500

ANALYSIS RESULTS

Soil parameters used in the analysis are given in Table 3. The $(N_1)_{60}$ profile was estimated from the results of dynamic cone penetration tests carried out at the site. The computed settlement profiles at the four blast holes after all blasts are shown in Fig. 3-8. The computed surface settlements along section AA and CC are shown in Fig. 3-9(a) and Fig. 3-9(b), respectively, together with the measured surface settlement after all blasts. It can be seen that the numerical model works reasonably well in the near field, e.g., at a radial distance less than 6 m in this case; but it may overestimate the settlement in the far field.

Table 3. Soil parameters used in the analysis (Richmond site)

Depth (m)	V_S (m/s)	V_P (m/s)	K_η	τ_{max} (kPa)	B_1	B_2	$(N_1)_{60}$
0 to 1.25	100	560	50	15	above water table		
1.25 to 2.5	120	1520	55	15	4.0	0.044	11
2.5 to 4.2	150	1580	58	25	4.6	0.044	11
4.2 to 7.5	120	1550	50	35	6.0	0.033	8
7.0 to 9.0	150	1600	60	43	4.3	0.047	12
over 9.0	250	1660	100	118	1.3	0.154	25

3.3 Field Blasting Trials at SM-3 Site, Quebec

TEST RESULTS

From Feb. 23 to April 12, 1995, a blast densification program was carried out at the SM-3 site along the Ste. Marguerite River, Quebec (AGRA, 1995). The purpose of the blast densification was to reduce the risk of static liquefaction in the sand deposits at the site, and the consequent instability of an excavation adjacent to the cofferdam during the construction of the main dam. The volume of the densified zone was approximately 100 m by 100 m with a depth of up to 20 m. A typical cross section within the densified area is shown in Fig. 3-10. Site investigation showed that the sand deposit at the site consists of loose sand overlying a dense sand layer followed by loose sand overlying gravel and cobbles. Thicknesses of the sand layer varied from 4 to 20 meters across the site due to variable bedrock elevations. Typical gradation curves of the sand sampled at the site are shown in Fig. 3-11, which indicate D_{50} values in the range of 0.3 to 1.5 mm (average about 0.75 mm) and coefficients of uniformity C_u in the range of 0.9 to 4.5. The sand is quite clean with a fines content less than 5 % passing a U.S. no. 200 sieve size (0.075 mm).

The blast boreholes were advanced through an approximately 1.20 m thick ice sheet covering the Ste. Marguerite River into the underlying river bed. There was typically 1.0 to 2.0 m of river water underneath the ice sheet. The thick ice sheet was required to support the heavy drilling equipment working on the ice, as well as to withstand the hydrodynamic water pressures generated by the under-

ground blasting. Two series of test blasts were conducted prior to production blasting in order to fine tune the final blast design.

The measured surface settlements after completion of production blasting were in the range of 0.50 m to 1.0 m. Ground settlements occurred within 0.5 hour of the completion of blasting when the residual pore water pressures had dissipated. A relationship between the volume change (settlement/layer thickness) in percentage and the powder factor obtained from this site is shown in Fig. 3-12. The powder factor is defined as the charge weight per unit volume of soil treated. It can be seen that the same charge density expressed as the powder factor will produce larger volume change in a loose sand layer than in a dense sand layer.

While the settlement occurs immediately after blasting, the gain in CPT cone tip resistance usually shows a delayed time effect. The time effect on the increase of CPT cone tip resistance Q_c is shown in Fig. 3-13 which shows that Q_c values measured 2 days after blasting are not significantly higher than pre-blast values, and at some depths where initial Q_c values were higher a reduction in Q_c may occur. The reduction in Q_c is believed due to dilation (volumetric expansion) caused by the effects of the blast and initial destruction of the sand structure caused by the blast. Cone tip resistance measured 12 days after blasting are typically 2 to 3 times higher than the pre-blast values. The data also demonstrate that initially low cone tip resistances measured 12 days after blasting can show further increases of up to 200 % based on data measured 35 days after blasting.

ANALYSIS RESULTS

Ground surface settlements due to the first pass of blasting are computed in three areas where CPT tests prior to blasting were available. These areas were in the vicinity of test holes CPT95-5, CPT95-7, and CPT95-17. In the analysis equivalent $(N_1)_{60}$ values were computed from the cone tip resistance Q_c using the relationship proposed by Robertson et al. (1983). A correlation factor $Q_C/N_{SPT} = 5.70$ has been used for this purpose. Comparison with energy calibrated SPT N values measured at the site showed that this correlation factor is appropriate.

In the vicinity of CPT95-5

The locations of the blast holes and the total charge weight in each blast hole are shown in Fig. 3-14.

The total charge weight varied from 9 kg to 21.5 kg per blast hole and was distributed among two to four decks over depth. The blast holes were spaced at 6 m in one direction and 10 m in the perpendicular direction.

The distribution of cone tip resistance with depth for CPT95-5 is shown in Fig. 3-15. The corresponding soil parameters used in the analysis are given in Table 4. The computed settlements at point A and point B with depth are shown in Fig. 3-16, which shows a surface settlement of 0.36 m at point A and 0.44 m at point B. Surface settlements in the order of 0.50 m were measured at both point A and point B after this blasting.

Table 4. Soil parameters used for CPT95-5 (SM-3 site, Quebec)

Depth (m)	V_S (m/s)	V_P (m/s)	K_η	τ_{max} (kPa)	B_1	B_2	$(N_1)_{60}$
0 to 4.00	100	1525	46	15	7.0	0.028	6
4.0 - 10.0	120	1580	57	36.5	4.68	0.043	11
10.0 - 13.0	200	1640	87	62	1.82	0.110	22
13.0 - 17.0	150	1600	70	68.5	3.00	0.067	16
> 17.0	150	1600	70	82	0.0	0.0	rock

In the vicinity of CPT95-7

The locations of blast holes and the total charge weight in each blast hole are shown in Fig. 3-17 The total charge weight varied from 12.5 kg to 19.0 kg per blast hole and was distributed among two to four decks over depth. The blast holes were spaced at 6 m in one direction and 10 m in the perpendicular direction.

The distribution of cone tip resistance with depth for CPT95-7 is shown in Fig. 3-18. The corresponding soil parameters used in the analysis are given in Table 5. The computed settlements at point A and point B with depth are shown in Fig. 3-19, which shows a surface settlement of 0.47 m at point A and 0.48 m at point B. Surface settlements of 0.50 m at both point A and point B were measured after this blasting.

Table 5. Soil parameters used for CPT95-7 (SM-3 site, Quebec)

Depth (m)	V_S (m/s)	V_P (m/s)	K_η	τ_{max} (kPa)	B_1	B_2	$(N_1)_{60}$
0 - 2.50	100	1525	46	15	7.0	0.028	6
2.5 - 5.0	110	1560	55	20	4.94	0.04	10
5.0 - 8.2	130	1570	60	30	4.29	0.047	12
8.2 - 10.0	120	1550	50	36	5.96	0.033	8
10.0 - 13.0	140	1570	60	62	4.29	0.047	12
13.0 - 19.0	150	1600	70	82	2.99	0.067	16
> 19.0	150	1600	70	82	0.0	0.0	rock

In the vicinity of CPT95-17

The locations of blast holes and the total charge weight in each blast hole are shown in Fig. 3-20. The total charge weight varied from 19.0 kg to 20.5 kg per blast hole and was distributed among four decks over depth. The blast holes were distributed in one direction at a spacing of 6 m.

The distribution of cone tip resistance with depth for CPT95-17 is shown in Fig. 3-21. The corresponding soil parameters used in the analysis are given in Table 6. The computed settlements at point A and point B with depth are shown in Fig. 3-22, which shows a surface settlement of 0.38 m at point A and 0.28 m at point B. Surface settlements of 0.46 m at point A and 0.30 m at point B were measured after this blasting.

Table 6. Soil parameters used for CPT95-17 (SM-3 site, Quebec)

Depth (m)	V_S (m/s)	V_P (m/s)	K_η	τ_{max} (kPa)	B_1	B_2	$(N_1)_{60}$
0 - 3.00	100	1525	46	15	7.0	0.028	6
3.0 - 4.2	130	1590	62.5	18	3.51	0.057	14
4.2 - 5.6	170	1610	84	24.5	2.08	0.096	20
5.6 - 7.6	140	1590	62.5	32	3.51	0.057	14
7.6 - 9.0	120	1550	50	36	5.98	0.033	8
9.0 - 10.0	180	1610	84	41	2.08	0.096	20
10.0 - 11.0	130	1570	60	46	4.29	0.047	12
11.0 - 12.2	180	1610	84	55	2.08	0.096	20
12.2 - 13.0	140	1570	60	57	4.29	0.047	12
13.0 - 15.0	190	1610	84	64	2.08	0.096	20
15.0 - 16.0	150	1570	60	68	4.29	0.047	12
16.0 - 19.0	190	1610	84	82	2.08	0.096	20
> 19.0	150	1610	84	82	0.0	0.0	rock

3.4 Deep blasting at Jebba dam

Solymar (1984) reported results of deep blasting for a hydroelectric development at Jebba in Nigeria. The main dam is a 42 m high zoned rockfill embankment constructed partially on river alluvial deposits up to 70 m in depth as shown in Fig. 3-23. The figure shows the zones of foundation densified by deep blasting. The foundation design required that the river alluvium should have a minimum relative density of 70 % for the upper layer 20 m below the natural riverbed, 60 % for the layer between 20 m to 30 m in depth and 50 % for the layer below 30 m in depth. Vibrocompaction was used for densification of sands in the top 25 m, and deep blasting was used for densification of sand between 25 m and 40 m in depth.

The alluvial deposits consisted of fine to coarse grained, quartzitic sands with trace of gravel. The initial relative densities of the sands varied from loose to dense and showed appreciable variations in both the vertical and horizontal directions. The typical gradation curves of sands for depths where blasting was performed are shown in Fig. 3-24, which indicate D_{50} values in the range of 0.2 to 1.5 mm (average about 0.50 mm) for the testing area, and 0.5 mm to 3.0 mm (average about 1.5 mm) in the blast zone 4. The coefficients of uniformity C_u varied between 1.51 and 8.83 with an average value of 2.94. The sand is very clean with percentage fines (passing a U.S. no. 200 sieve size or 0.075 mm) less than 3 % for the testing section and zero percentage fine for the sands in blast zone 4.

Test Blasting

The results of test blasting (test blast 3) are shown in Fig. 3-25. In this test three blast coverages or passes were detonated, using 3 kg charges for the first pass, 2 kg charges for the second pass and 1 kg charges for the third pass. Surface settlements in the order of 0.17 m were caused by the first pass of blasting. Additional settlements of 0.1 m and 0.05 m were induced by the second and the third pass of blasting, respectively. It was reported that in spite of immediate surface settlements, an initial reduction in cone tip resistance was observed due to either dissolved gas in the water or to rearrangement of soil structure. Excess pore water pressures dissipated fully within 2 hours after the blast.

This test blasting was simulated using the proposed numerical model. The cone tip resistance Q_c at the test location prior to blasting was used to establish the input parameters required in the analysis. In the analysis $(N_1)_{60}$ values were obtained from the cone tip resistance Q_C using the correction factor $Q_C / N_{SPT} = 7.5$ according to (Solymar, 1984). Other parameters were obtained from the corresponding values of $(N_1)_{60}$ as given in Table 7.

The computed settlement profiles at point A and B after each pass of blasting are shown in Fig. 3-26. After the first pass, ground surface settlements of 0.23 m at point A and 0.24 m at point B are predicted by the model, compared to measured settlements of 0.16 m and 0.17, respectively. The corresponding computed settlements are 0.30 m and 0.31 m after the second coverage, compared to measured settlements of 0.25 m and 0.27 m, respectively. The computed surface settlements at point A and B after three coverages of blasting are 0.30 m and 0.30 m, respectively, which agree well with the measured final surface settlements of 0.30 m and 0.32 m at point A and B, respectively.

Table 7. Soil parameters used for deep test blasting at Jebba dam

Depth (m)	V_S (m/s)	V_P (m/s)	K_η	τ_{max} (kPa)	B_1	B_2	$(N_1)_{60}$
0 to 10.0	120	1580	65	50	0.0	0.0	14
10.0 - 25.0	140	1630	84	108	0.0	0.0	20
25.0 - 30.0	200	1650	95	154	1.30	0.154	25
30.0 - 35.0	160	1610	77	170	2.47	0.081	18
35.0 - 36.5	160	1560	55	180	5.0	0.04	10
36.5 - 38.0	170	1590	69	190	3.25	0.061	15
38.0 - 44.0	180	1560	58	215	4.68	0.043	11
> 44.0	190	1620	80	285	2.34	0.085	19

Production Blasting in Zone 1

The charge pattern used in the first pass of production blasting for zone 1 is shown in Fig. 3-27. Charge weights from 8.3 kg to 10 kg were placed in each blast hole between Elevations 31 m and 40 m. In the vicinity of the CPT hole CP138, surface settlements of 0.52 m to 0.57 m (average 0.53 m) were measured. The CPT data for CP138 before and after blasting are shown in Fig. 3-28. The cone tip resistance Q_C measured before blasting (CP138-1 in Fig. 3-28) has been used for determining the $(N_1)_{60}$ profile in the vicinity of the blast holes. The $(N_1)_{60}$ values and other soil parameters used in the numerical analysis are given in Table 8.

The settlement at CP138 was computed by considering 12 charges of 8.3 kg (7.0 kg TNT equivalent) arranged within a 14 m radius. Charges located outside the 14 m radius were considered to have a small contribution to the settlement at CP138. The charge used in the blasting was about 6.9 m long, calculated using a charge distribution of 1.2 kg/m for an 8.3 kg charge (Solymar, 1984). In the numerical simulation the long charge was divided into two subcharges to simulate approximately the effect of charge length on ground response when the spherical model is used for the simulation of blast loads.

The computed settlement profile at CP138 is shown in Fig. 3-29. Surface settlement of 0.51 m was

predicted by the model, compared to a measured surface settlement of 0.53 m.

Table 8. Soil parameters used for deep test blasting at Jebba dam

Depth (m)	V_S (m/s)	V_P (m/s)	K_η	τ_{max} (kPa)	B_1	B_2	$(N_1)_{60}$
0 - 10.0	120	1580	65	50	0.0	0.0	14
10.0 - 28.0	140	1580	65	108	0.0	0.0	14
28.0 - 32.0	140	1560	57	154	4.68	0.043	11
32.0 - 34.0	150	1570	60	170	4.29	0.047	12
34.0 - 38.0	190	1620	80	185	2.34	0.085	19
38.0 - 40.0	160	1570	48	200	6.50	0.031	7
40.0 - 43.0	160	1560	55	213	5.00	0.040	10
43.0 - 46.0	170	1570	60	228	4.29	0.047	12
46.0 - 48.0	180	1580	65	241	3.58	0.056	14
> 48.0	190	1620	80	285	2.34	0.085	19

4.4 Summary

The proposed numerical model has been used to predict surface settlements caused by blasting. The computed settlements for all blasting trials investigated in the section are compared with the corresponding measured settlements in Fig. 3-30.

It can be seen that, in general, the numerical model predicts settlements in good agreement with the measured settlements. The model simulation may overestimate the surface settlements at relatively far distance from the blast holes. This fact implies that the model may overestimate plastic volumetric strains in the far field, thus overestimating residual pore water pressures in the far field.

4.0 PREDICTIONS OF VOLUME CHANGE AND RESIDUAL PORE WATER PRESSURES

Efforts were made to establish the relationships between the plastic volumetric strain, residual pore water pressures and the charge intensity for the case of a single charge placed in a saturated sand. The charge intensity is represented by the commonly used scaled distance, $R/W^{0.333}$, where R is the distance away from the charge, and W is the charge weight per delay. The plastic volumetric strain caused by multiple charges can be obtained by accumulating the volumetric strain from each individual charge using eq. [1].

It has been found that the SPT $(N_1)_{60}$ values of sand have great influence on the response of saturated sand to blast loads. In this study $(N_1)_{60}$ values of 8, 12, 16, 20 and 25 have been used for simulating the response of sands with different liquefaction resistance to blast loads. The influence of charge weight on the response has been investigated by varying the charge weight from 1.0, 3.0 to 8.0 kg. The effects of charge depth on response have also been studied.

4.1 Response of Clean Sands to Single Charges

The studies were carried out to investigate the response of clean sands subjected to 3.0 kg single charges detonated under an effective vertical stress of 100 kPa. $(N_1)_{60}$ values of 8, 12, 16, 20 and 25 have been used for simulating the response of sands with different liquefaction resistance to blast loads. The sands were assumed to have a saturated unit weight of 20 kN/m^3 and a friction angle of 35°. Other parameters required by the analysis such as compression wave velocity V_P, viscosity number K_η, volumetric strain constants B_1 and B_2 and the rebound modulus constant M were determined using the formulation and charts presented in section 2. These parameters are functions of $(N_1)_{60}$ of the sand. In all studies, the water level was assigned at the ground surface.

The computed peak dynamic and plastic volumetric strains at the depth of detonation are plotted as a function of the scaled distance $R/W^{0.333}$ in Fig. 4-1 and Fig. 4-2, respectively. The results clearly show that the volumetric strains decrease rapidly with the radial distance R away from the charge. For $(N_1)_{60}$ = 8 the plastic volumetric strain is 2.2 % at R = 2.88 m but decreases to 0.20 % at R = 14.42 m for the 3 kg charge. On the other hand, the plastic volumetric strain decreases significantly when the same charge is placed in a denser sand. The corresponding plastic volumetric strains at R = 2.88 m are 0.70 % for $(N_1)_{60}$ = 16 and 0.20 % for $(N_1)_{60}$ = 25.

The established relationship (Fig. 4-2) between the plastic volumetric strain and the scaled distance $R/W^{0.333}$ can be used to estimate the degree of volume compaction achieved by blasting densification and to estimate the residual pore water pressures.

The computed residual pore water pressures are presented using the pore water pressure ratio, PPR, which is defined as the ratio of the residual pore water pressure to the initial effective overburden stress. The computed PPR - $R/W^{0.333}$ curves for $(N_1)_{60}$ = 8, 12, 16, 20 and 25 are shown in Fig. 4-3. The results show that 100 % pore water pressure occurs within a scaled radial distance $R/W^{0.333}$ = 2.0 for $(N_1)_{60}$ = 8, but 93% and 65 % pore water pressures within the same distance for $(N_1)_{60}$ = 16 and $(N_1)_{60}$ = 25, respectively.

The computed pore water pressure ratios, PPR, agree reasonably well with these measured in the field as shown in Fig. 4-4. In general, there is a satisfactory agreement between the measured PPR (for example, Charlie et al., 1992; Kok and Trense, 1979, Klohn et al., 1981; Kummeneje and Eide, 1961) and the PPR predicted by the model. However the PPR values at scaled distances measured by Schure (1990) seem to be much higher than those given by others. The reason for this difference is not clear to the author at the present time.

4.2 Response of Clean Sand to Single Charges: Effect of Charge Weight

Analyses were carried out to study the effect of charge weight W on the response of saturated clean sand having a $(N_1)_{60}$ = 12. The charge weight W of single charges was varied between 1.0 kg, 3.0 kg and 8.0 kg. The computed plastic volumetric strains and the residual pore water pressure ratios corresponding to these charges are shown in Fig. 4-5 and Fig. 4-6, respectively. It is seen that the size of charge has a minor effect on the proposed relationships between plastic volumetric strain, residual pore water pressures and the scaled distance.

4.3 Response of Clean Sand to Single Charges: Effect of Effective Overburden Pressure

Analyses were next carried out to study the effect of charge depth using a 3.0 kg charge weight on the response of saturated clean sand having a $(N_1)_{60}$ = 12. The single charges were placed at different depths of 10.0 m, 20 m and 40 m, which gave effective vertical stresses of 100 kPa, 200 kPa and 400 kPa, respectively. The computed plastic volumetric strains and the residual pore water pressure ratios are

shown in Fig. 4-7 and Fig. 4-8, respectively. It is seen that increasing effective overburden pressure will increase the liquefaction resistance of sand to blast loads. When other conditions remain the same, the plastic volumetric strains and the residual pore water pressures are less at a high overburden pressure than at a low overburden pressure. This observation may imply that the effectiveness of deep blasting can be reduced by high effective overburden pressure unless charge weights are correspondingly increased.

Measurements supporting the above observation is very limited at the present time. This result is obtained solely based on deep blasting data from the Jebba dam project (Solymar, 1984). Further field data are required to study the effect of overburden pressure on the plastic volumetric strain and the residual pore water pressure induced by blast loads.

5.0 CONCLUSIONS

An empirical formulation has been proposed for computing the plastic volumetric strains of saturated granular soils to blast loads. The dynamic volumetric strain rather than the dynamic shear strain has been used in the formulation. All soil parameters in the model have been determined from back-analysis of field blasting data, and they are presented as a function of $(N_1)_{60}$. It has been shown that the soil settlement predicted by the numerical model agrees well with the measured settlements based on the $(N_1)_{60}$ correlations obtained.

A constant-volume pore water pressure model has been developed for the calculation of residual pore water pressures. The model uses a very simple parameter, the rebound modulus constant M, which can be determined from the SPT $(N_1)_{60}$. The numerical model predicts pore water pressure ratios in reasonable agreement with pore water pressure ratios measured in field blasting trials for single charge detonations.

The theory has been implemented in a computer program BLAST which has been used for generating curves describing the relationship between the plastic volumetric strain, residual pore water pressure and the scaled distance $R/W^{0.333}$ for sands having different $(N_1)_{60}$ values. These curves may be used in a preliminary design of controlled blasting for soil densification.

REFERENCE

1. AGRA Earth and Environmental Ltd. (1991). Internal file
2. AGRA Earth and Environmental Ltd. (1995). Internal report
3. Bhatia, S.K. (1980), " The verification of relationships for effective stress method to evaluate liquefaction potential of saturated sands," Ph.D thesis, Department of Civil Engineering, the University of British Columbia, Vancouver, B.C., Canada
4. Byrne, P.M. (1981). " A cyclic shear-volume coupling and pore pressure model for sand," Proceedings, 2nd international conference on Recent Advances in Geotechnical Earthquake and Soil Dynamics, St. Louis, Missouri, U.S.A.
5 Charlie, W.A., Jacobs, P.J. and Doehring E.O. (1992) "Blasting induced liquefaction of an alluvial sand deposit", Geotechnical Testing Journal, Vol. 15, No. 1, pp.14-23.
6. Ishihara K. and Yoshimine M. (1992) "Evaluation of settlements in sand deposits following liquefaction during earthquakes", Soils and Foundations, Vol. 32, No. 1, pp. 173 - 188
7. Kok, L. and Trense, R.W., (1979) " Blast-induced liquefaction, state-of-the-art", Proceedings , 6th International Symposium. Military Application of Blasting Simulations, Cahors, France
8. Kummeneje, O. and Eide, O. (1961) " investigation of loose sand deposits by blasting", Proceedings, 5th International Conference on Soil Mechanics and Foundation Engineering, Vol. 1, pp. 4910-497
9. Klohn, E.J., Garga, V.K., and Shukin, W. (1981), "Densification of Loose Sand Deposits by Blasting," Proc. of 10th International Conf. on Soil Mechanics and Foundation Engineering, Vol.3, pp.725-730
10. Liao, S.C., and Whitman, R.V. (1985). " Overburden correction factors for SPT in sand", Journal of the Geotechnical Engineering Division, ASCE, Vol. 112, NO.3, pp. 373 - 377
11. Martin, G.R., Finn, W.D.Liam and Seed, H.B. (1975) " Fundamentals of liquefaction under cyclic loading", Journal of the Geotechnical Engineering Division, ASCE, Vol. 101, GT5
12. Robertson, P. K., Campanella, R.G and Wightman A. (1983). "SPT-CPT correlations", Journal of the Geotechnical Engineering Division, ASCE, Vol. 109, NO.11, pp. 1449-1459.
13. Schure, L.A. (1990) "Pore water pressure increases resulting from blast-induced spherical stress waves", thesis for the degree of Master of Science, Colorado State University.
14. Seed, R.B. and Harder L.F. (1990). " SPT-based analysis of cyclic pore pressure generation and undrained residual strength", Proceedings of H. Bolton Seed Memorial Symposium, May, 1990
15. Seed, H.B., Tokimatsu, K., Harder, L.F., and Chung, R. (1985). " Influence of SPT procedures

in soil liquefaction resistance evaluations", Journal of the Geotechnical Engineering Division, ASCE, Vol. 111, NO.12

16. Seed, H.B., Idriss, I.M., and Aarango, I. (1983). " Evaluation of liquefaction potential using field performance data", Journal of the Geotechnical Engineering Division, ASCE, Vol. 102, NO.4, pp. 246 - 270.

17. Solymar, Z. V. (1984)," Compaction of Alluvial Sands by Deep Blasting," Canadian Geotechnical Journal, Vol. 21, pp. 305-321

18. Tokimatsu, K and Seed, H.B. (1987) " Evaluation of settlements in sands due to earthquake shaking", Journal of the Geotechnical Engineering Division, ASCE, Vol. 113, No. 8

19. United States Army Corps of Engineers (1972), " Systematic Drilling and Blasting for Surface Excavation, " Engineering Manual, EM 1110-2-3800, Office of the Chief, United States Army Corps of Engineers, Washington, D.C., 119 pages

20. Wu, Guoxi (1995) " Dynamic response analysis of saturated granular soils to blast loads using a single phase model", A research report submitted to Natural Sciences and Engineering Research Council of Canada.

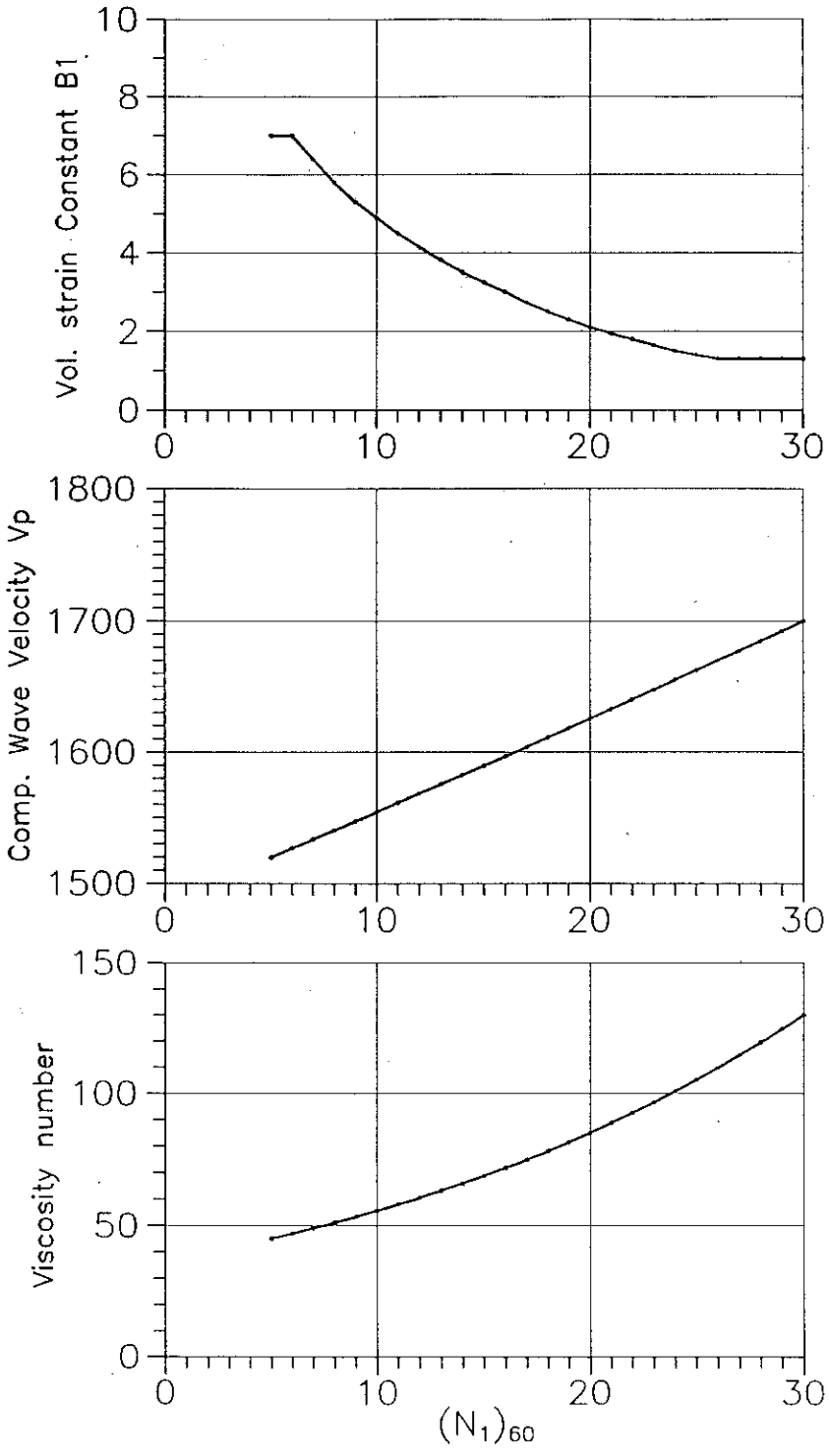

Fig. 2-1 Correlations with $(N_1)_{60}$ of (a) volume strain constant B_1, (b) compressive shear wave velocity V_P and (c) viscosity number K_η

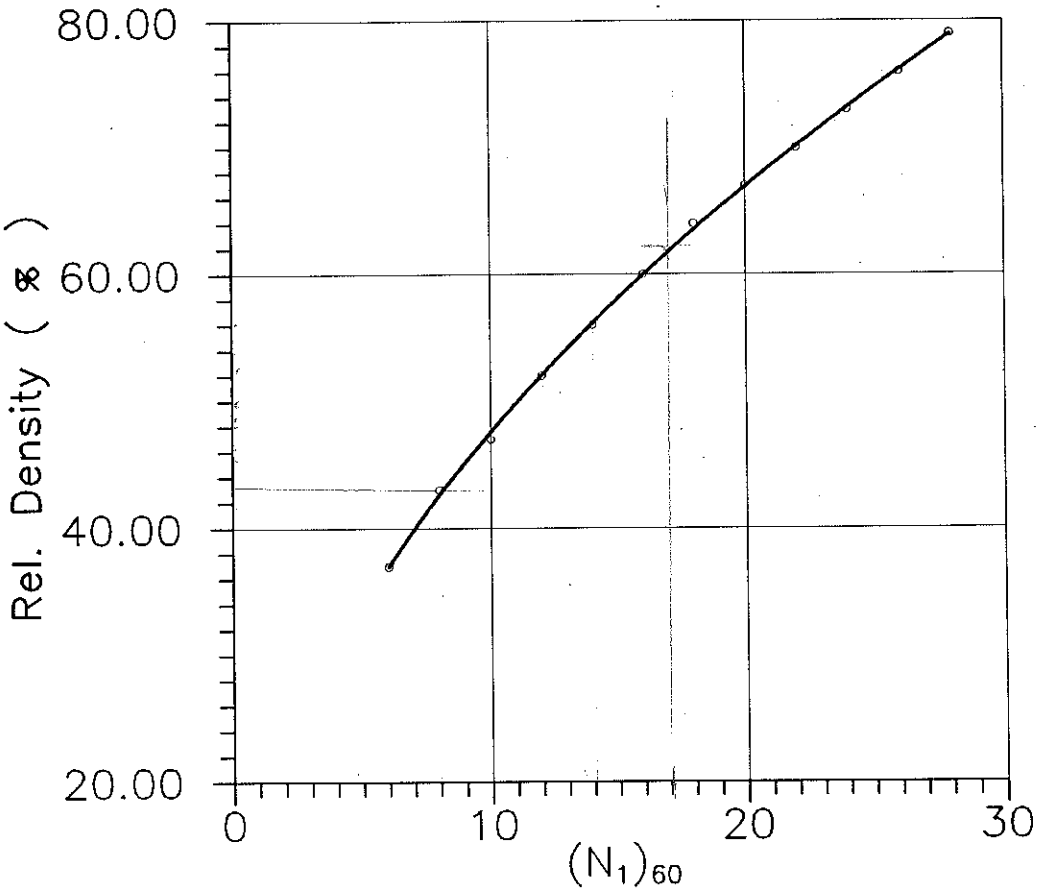

Fig. 2-2 SPT $(N_1)_{60}$ and the relative density D_r of sand (after Tokimatsu and Seed, 1987)

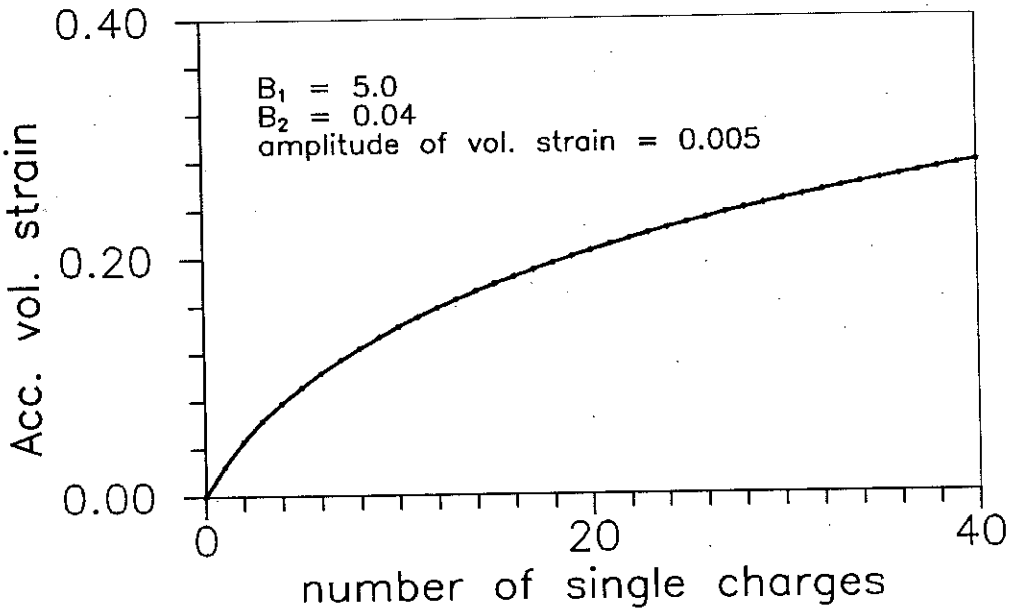

Fig. 2-3 A schematic drawing show the relationship between the plastic volumetric strain and the number of single charges

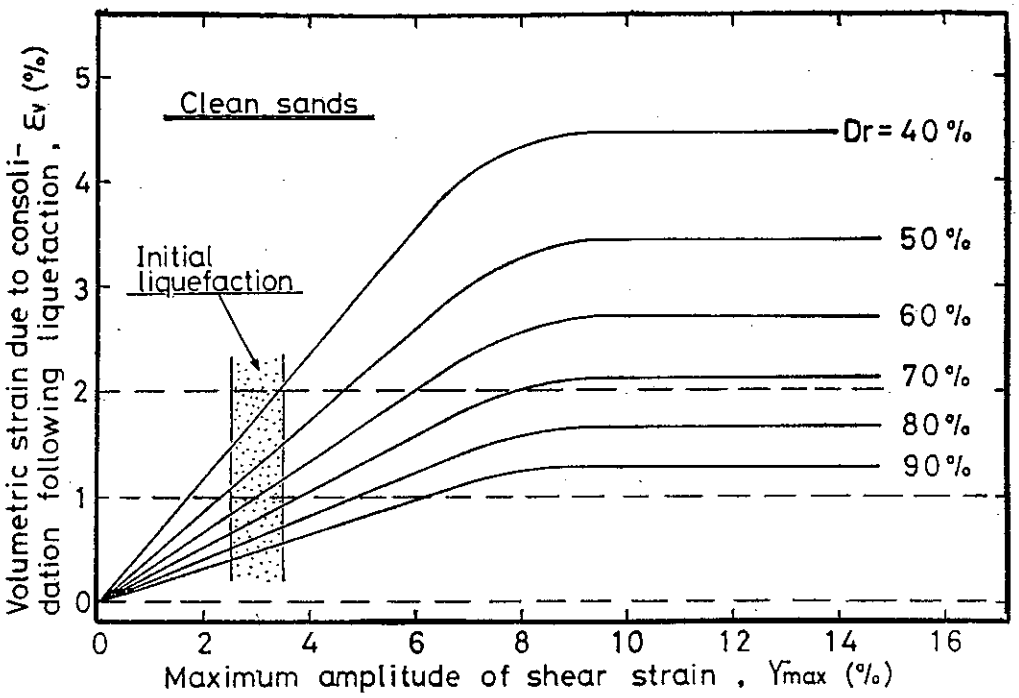

Fig. 2-4 Relationship between the plastic volumetric strain and level of strain (after Ishihara and Yoshimine, 1992).

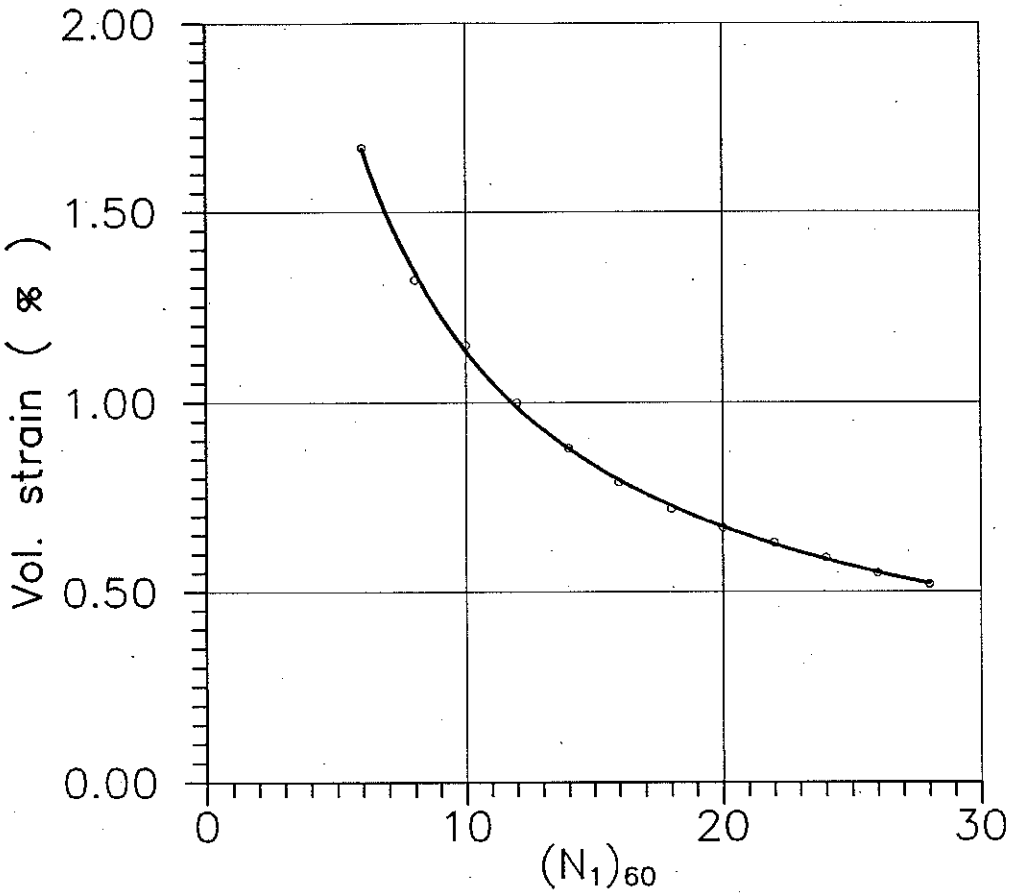

Fig. 2-5 Plastic Volumetric strain required to trigger initial liquefaction

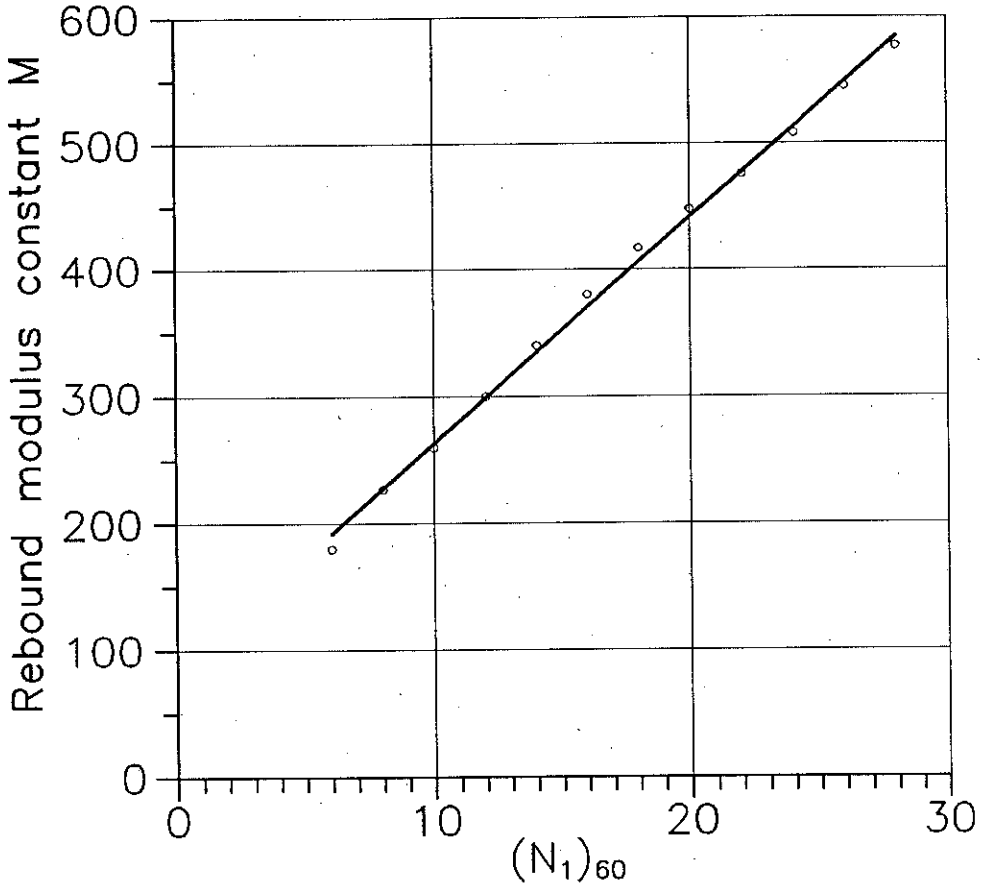

Fig. 2-6 A relationship between the rebound modulus constant M and $(N_1)_{60}$

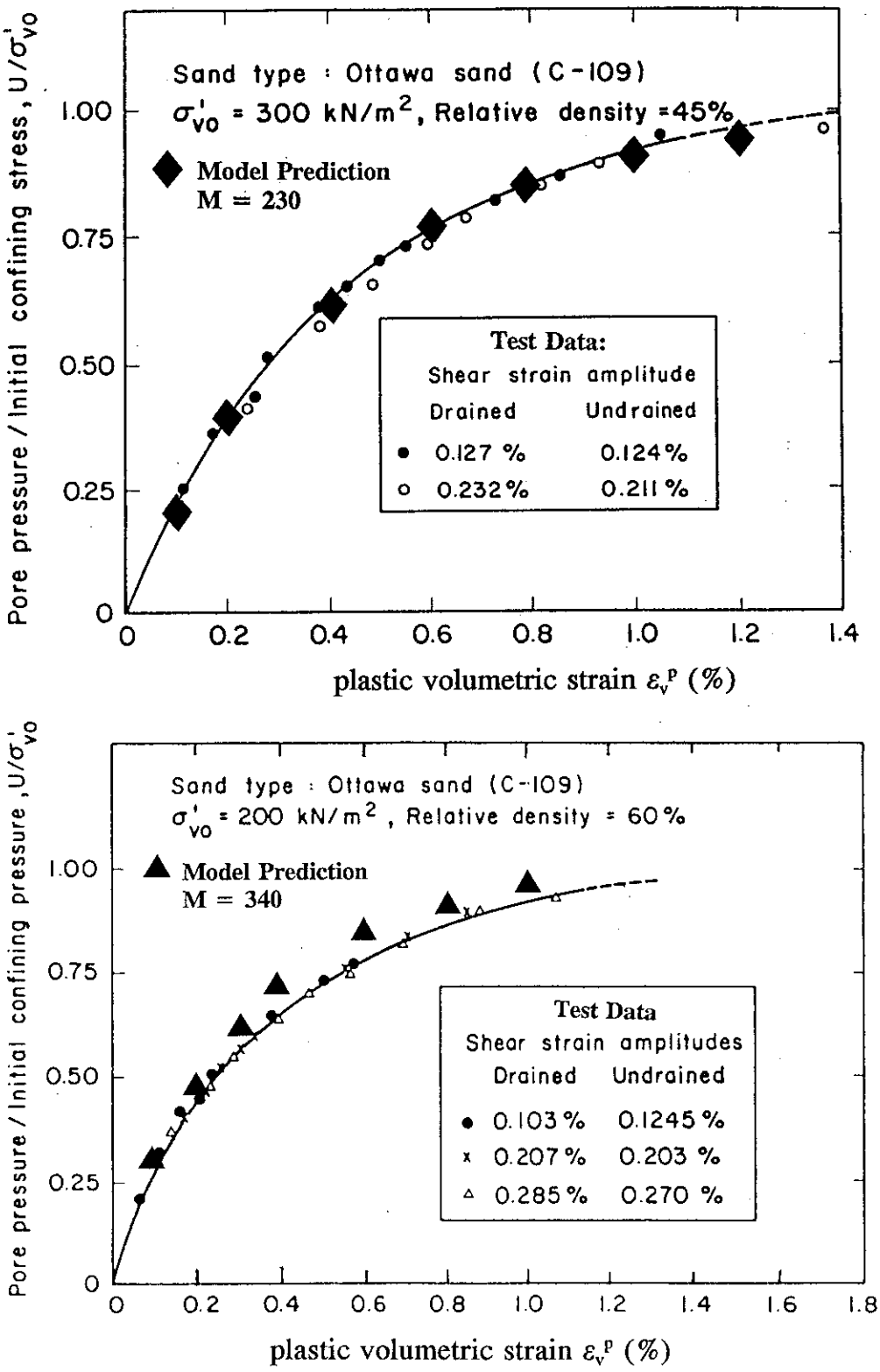

Fig. 2-7 Computed pore water pressure response compared with the measured response (a) D_r = 45 % (b) D_r = 60 % (experimental data from Bhatia, 1980)

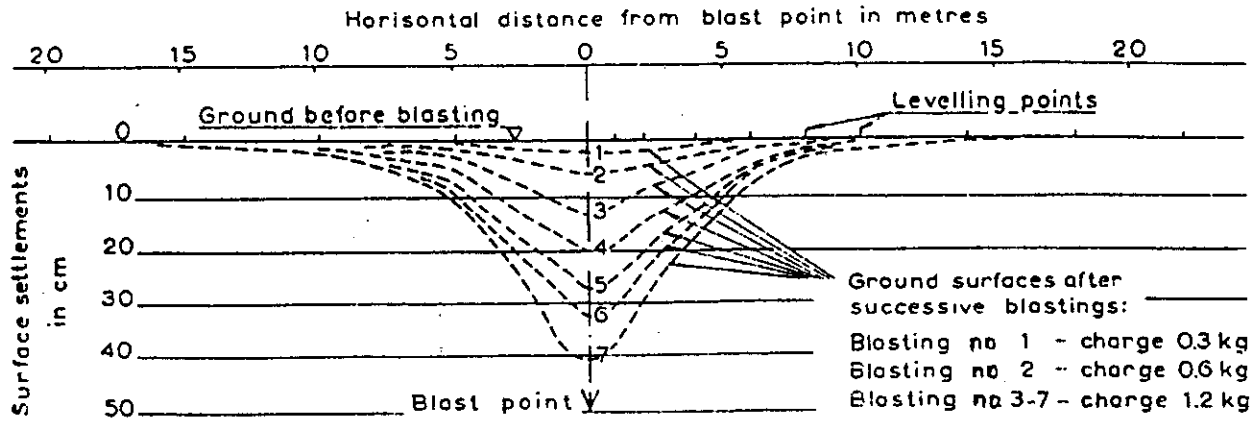

Fig. 3-1 Measured settlement in a marine sand deposit (after Kummeneje and Eide, 1961)

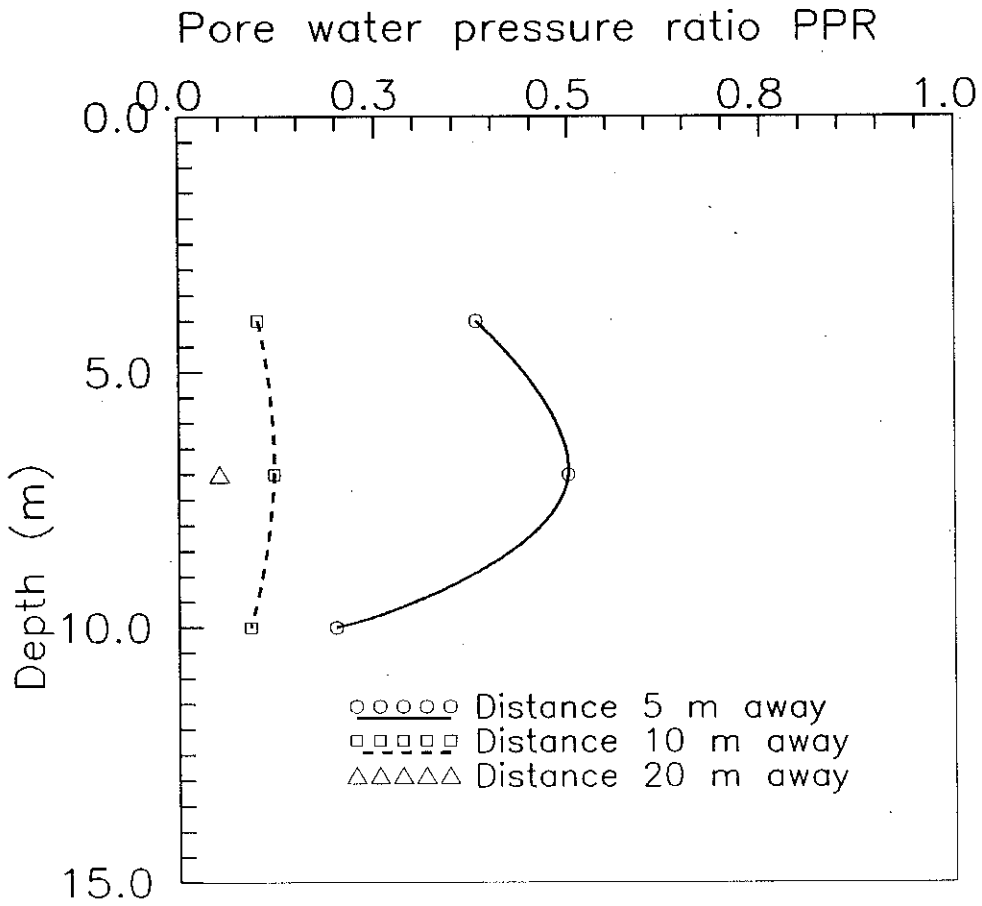

Fig. 3-2 Measured residual pore water pressure ratios from the first 1.2 kg charge (after Kummeneje and Eide, 1961)

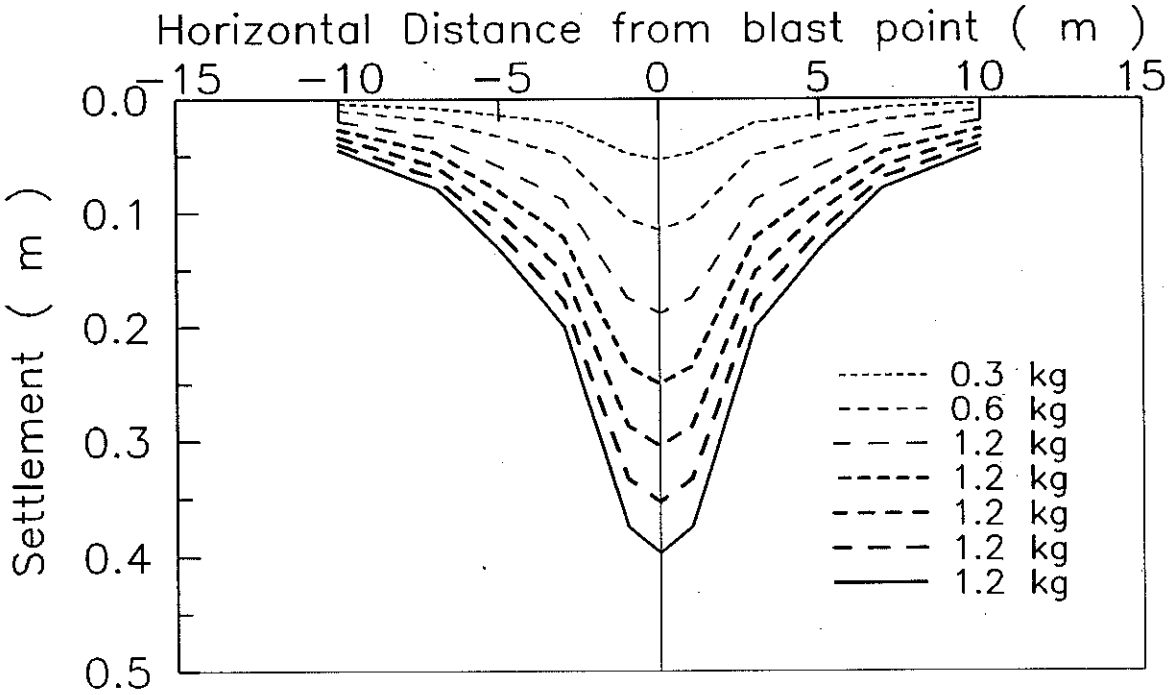

Fig. 3-3. Computed settlement distribution after detonation of each single charge for Verdalselven River site (Kummeneje and Eide, 1961)

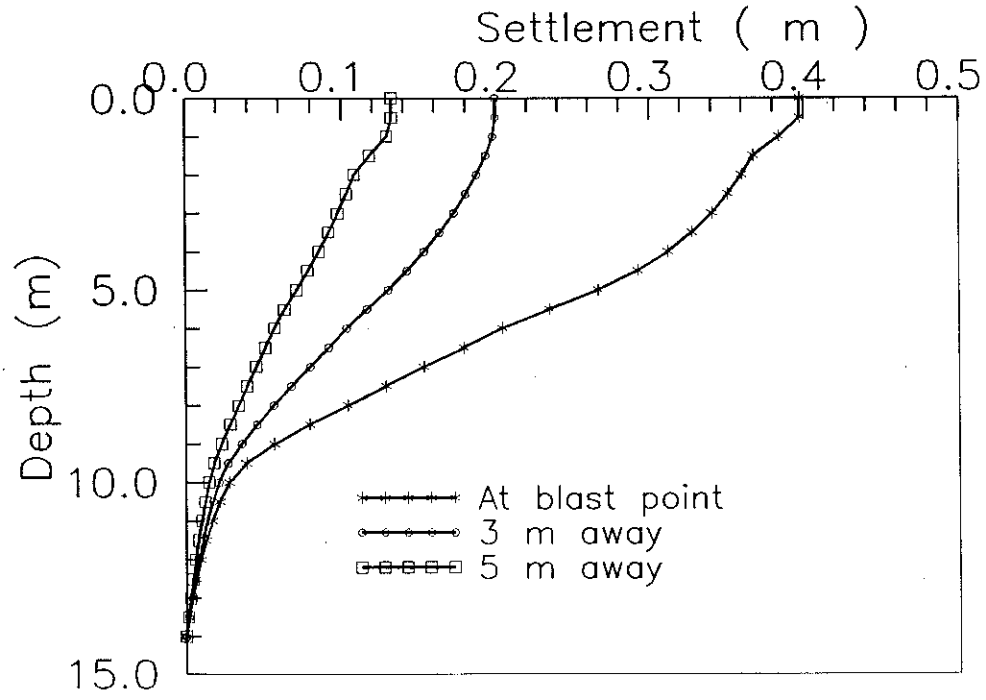

Fig. 3-4 Computed settlement distributions with depth after all blasts for Verdalselven River site (Kummeneje and Eide, 1961)

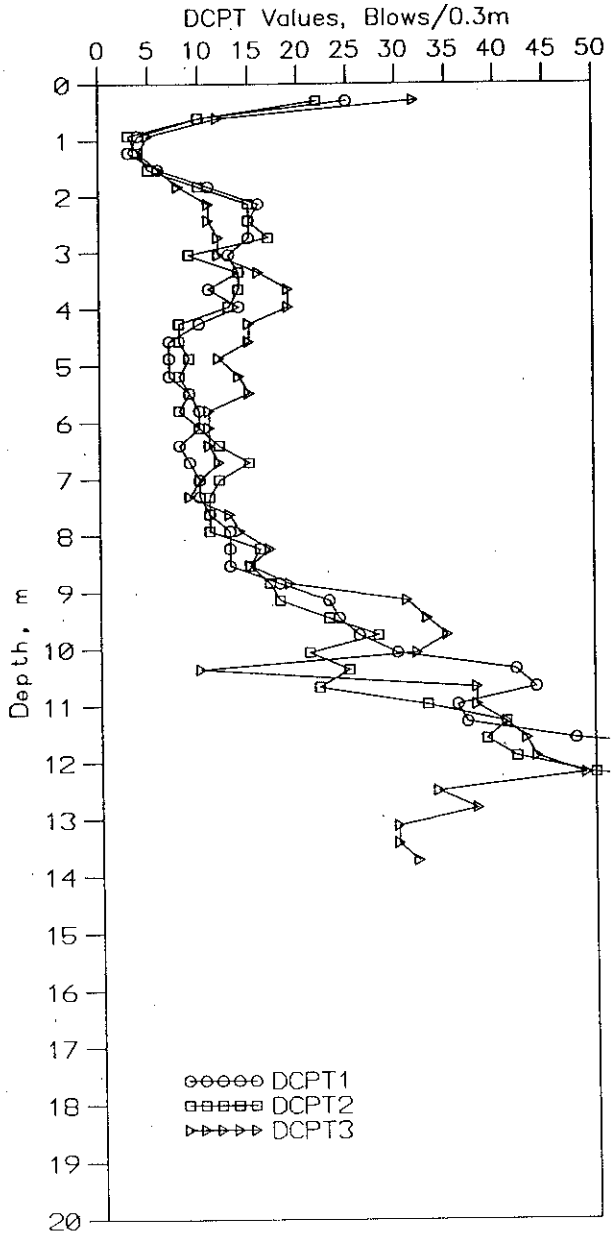

Fig. 3-5 Results of dynamic cone penetration tests at Richmond site

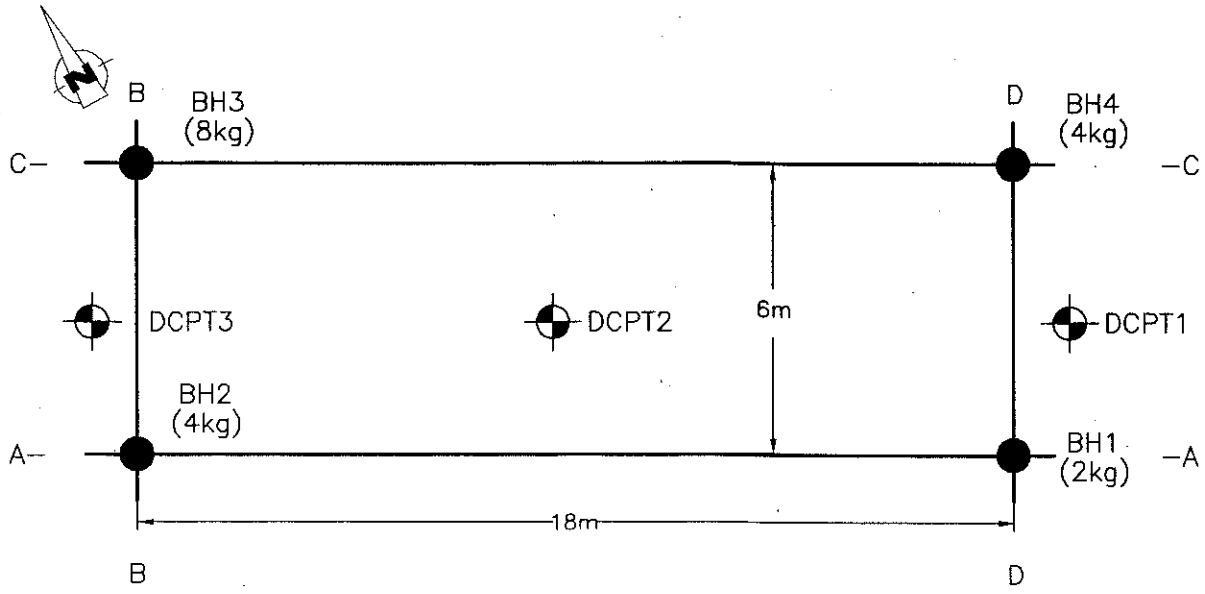

Fig. 3-6 Locations of the four blast holes at Richmond site

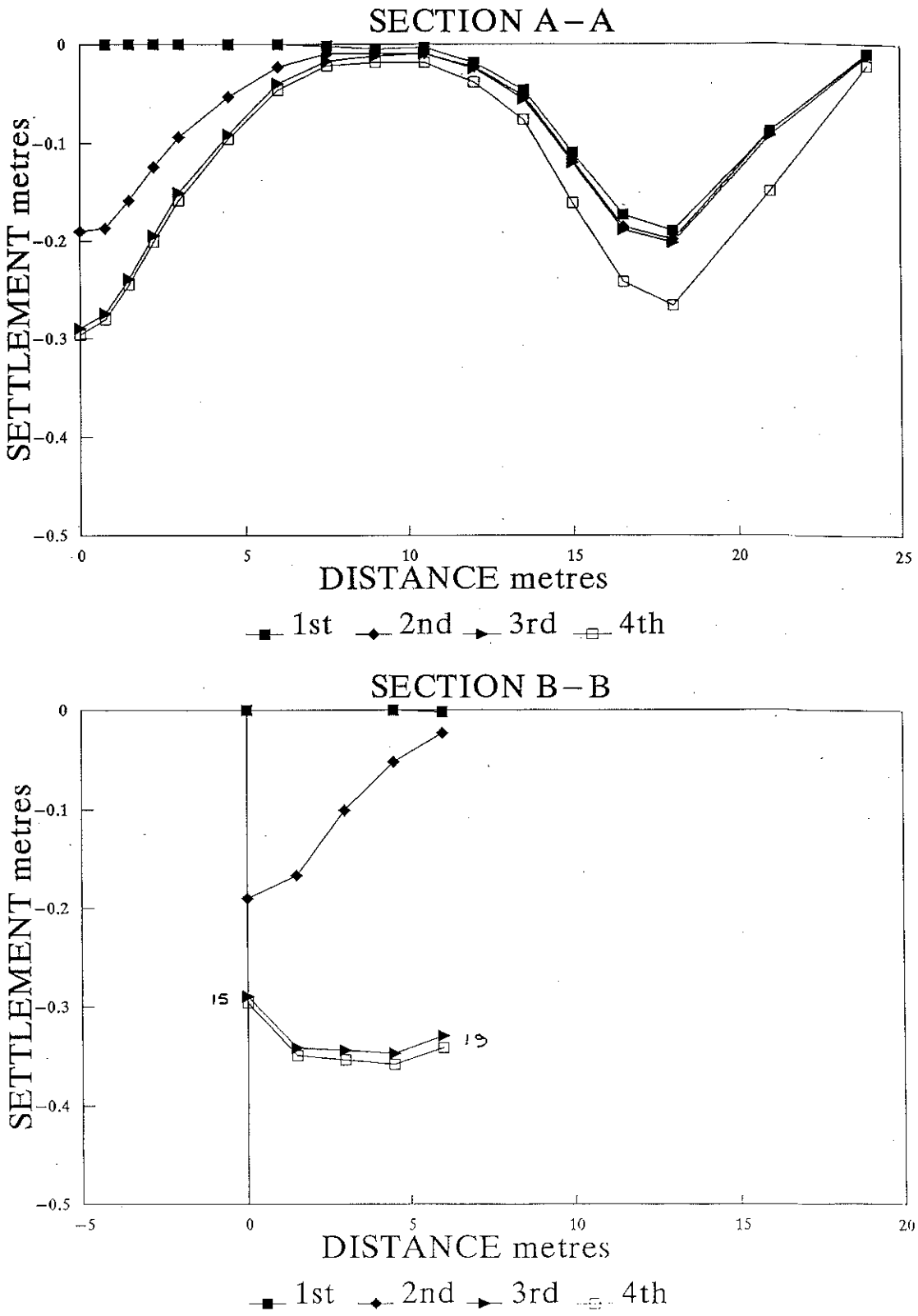

Fig. 3-7 Measured settlement along sections (a) A-A (b) B-B (c) C-C and (d) D-D, Richmond site

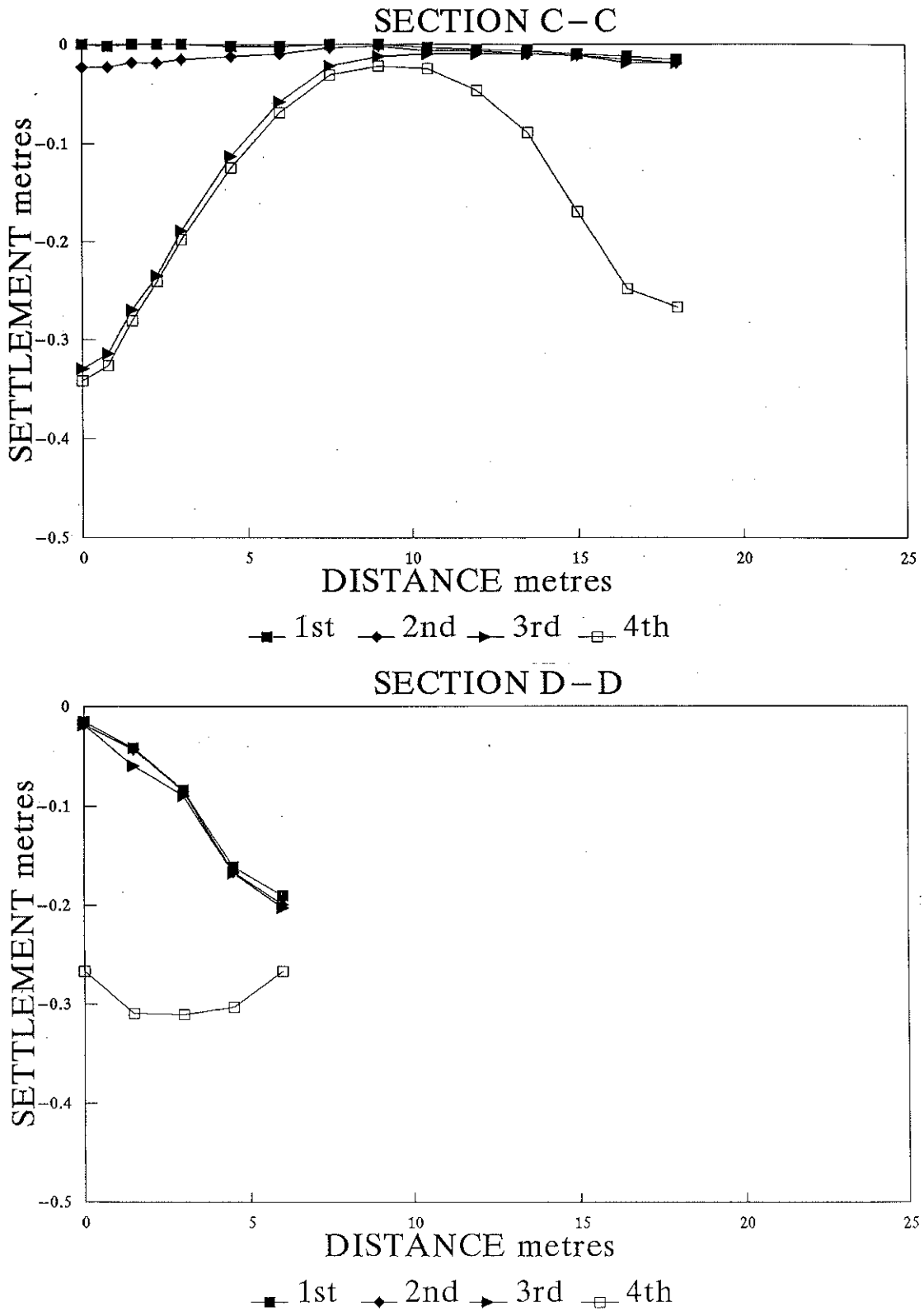

Fig. 3-7(cont.) Measured settlement along sections (a) A-A (b) B-B (c) C-C and (d) D-D, Richmond site

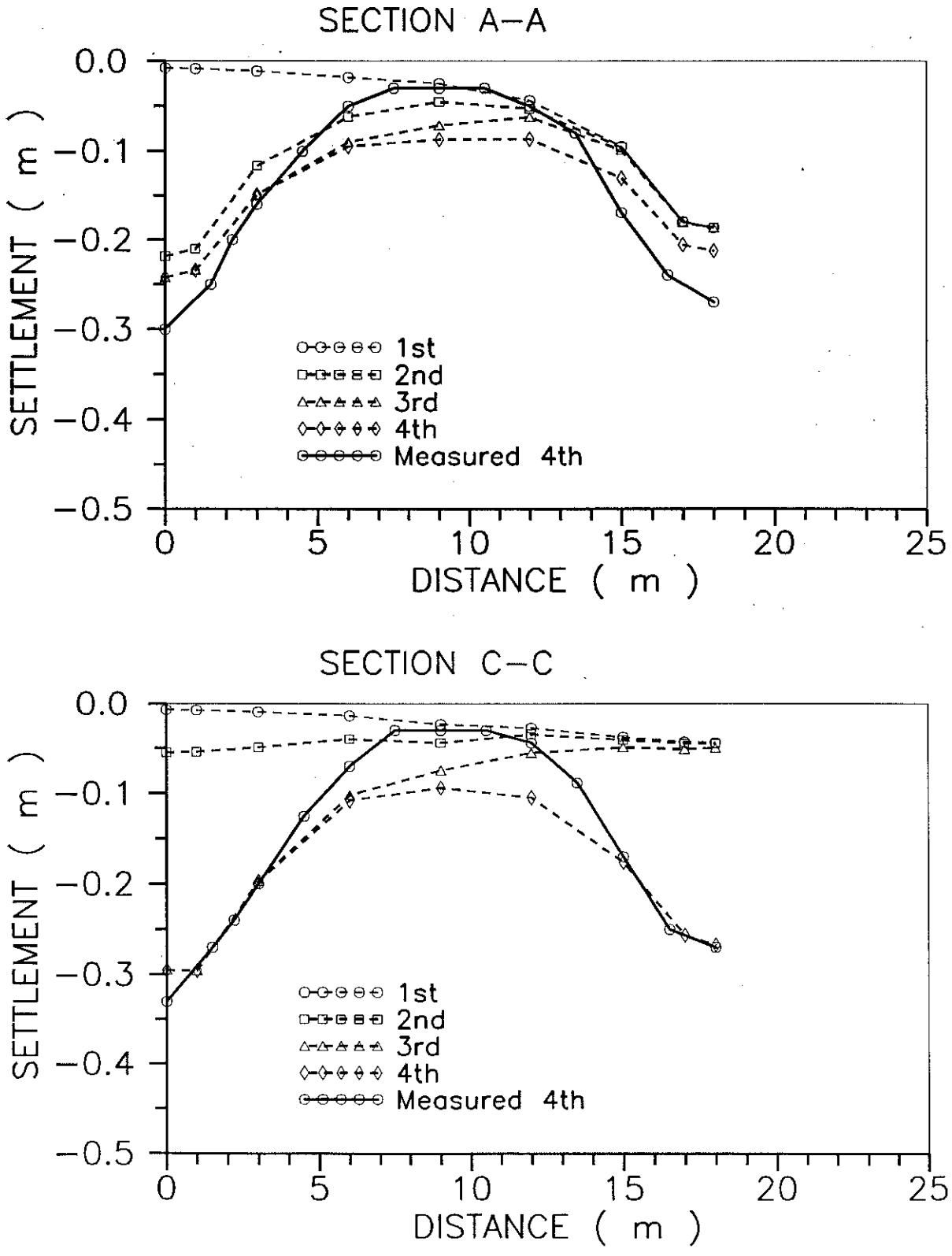

Fig. 3-8 Comparison of measured and computed surface settlements along (a) section A-A and (b) section C-C at Richmond, B.C. site

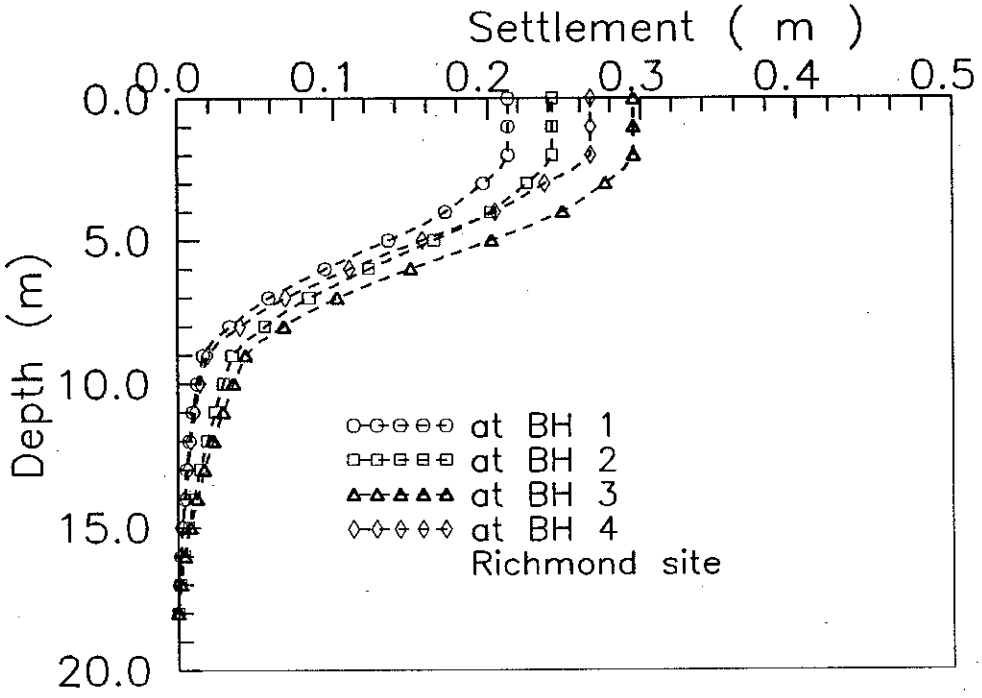

Fig. 3-9 Computed settlement distributions with depth at the four blast holes after all blasts, Richmond, B.C. site

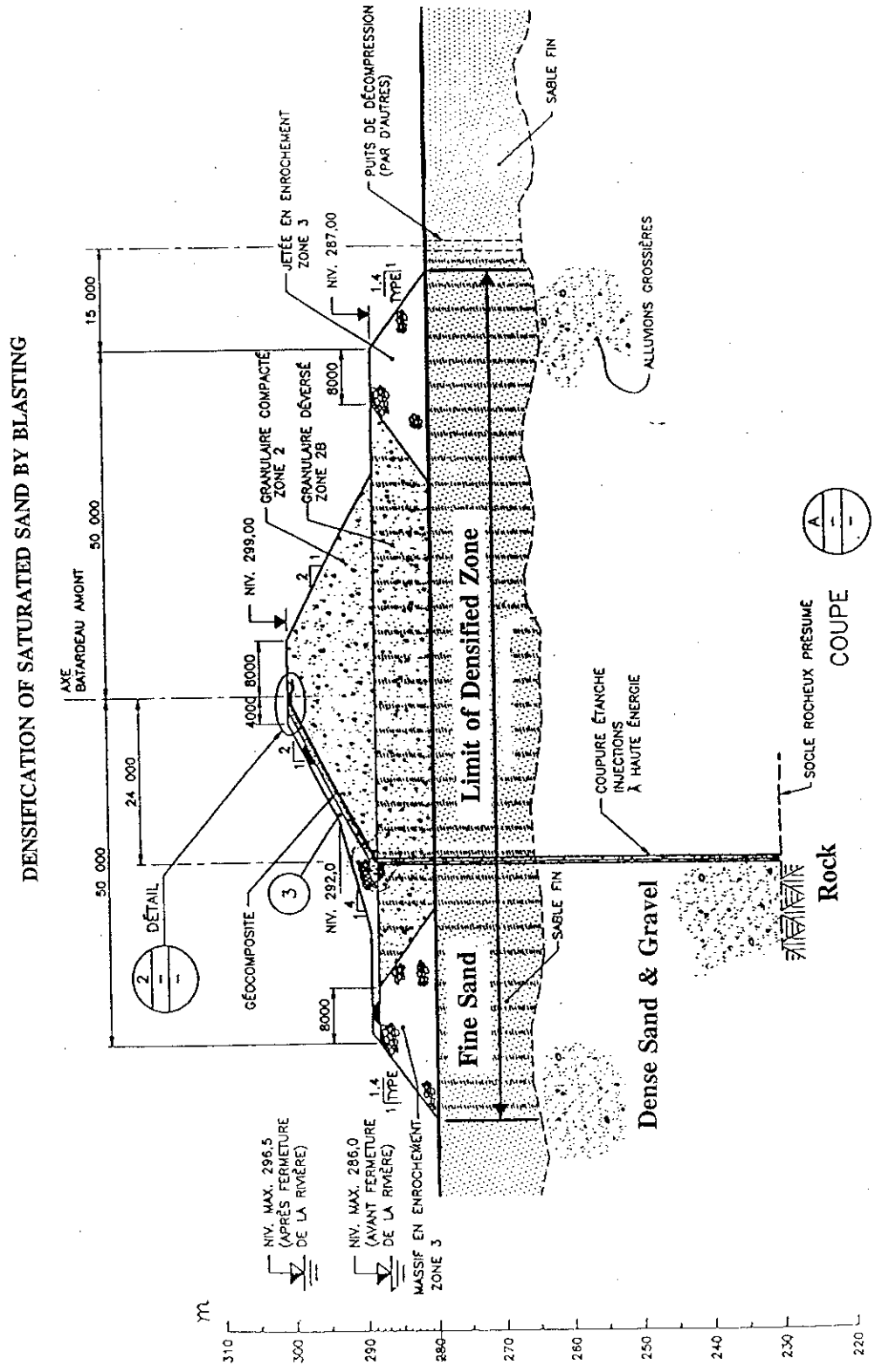

Fig. 3-10 Cross Section -- Sainte Marguerite 3 Site, Quebec

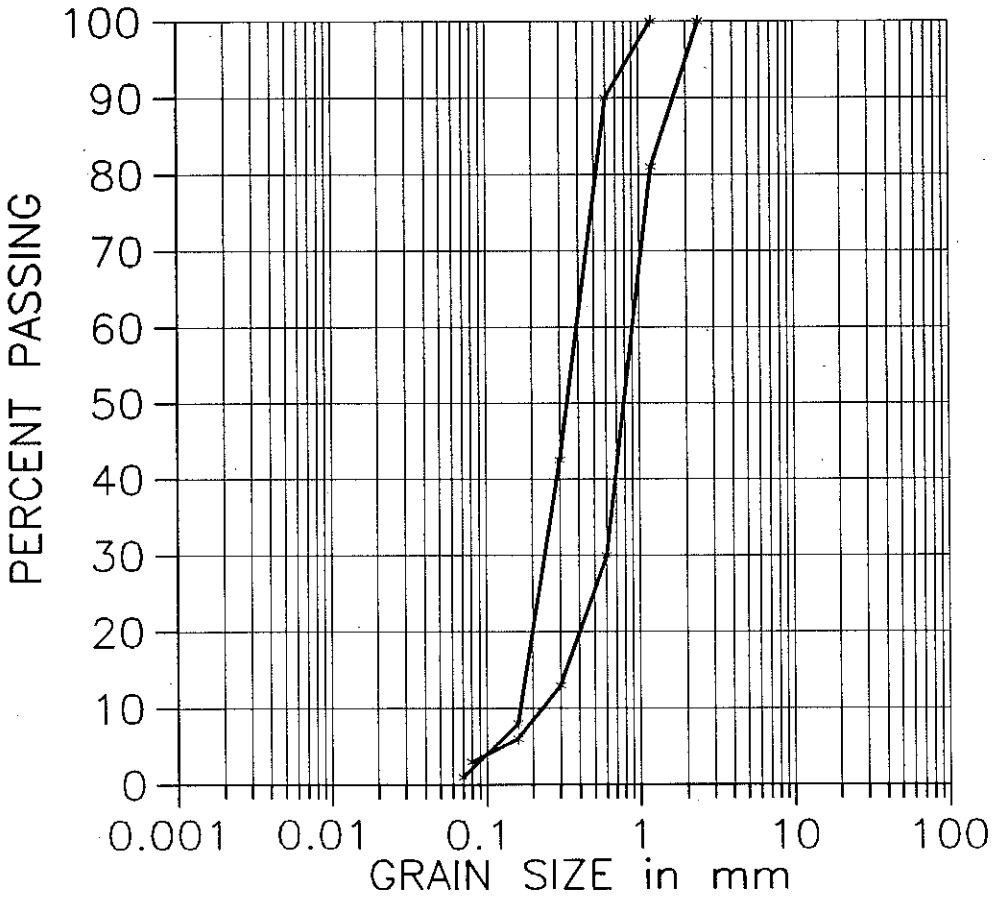

Fig. 3-11 Gradation curves of sands sampled at the SM-3 site, Quebec

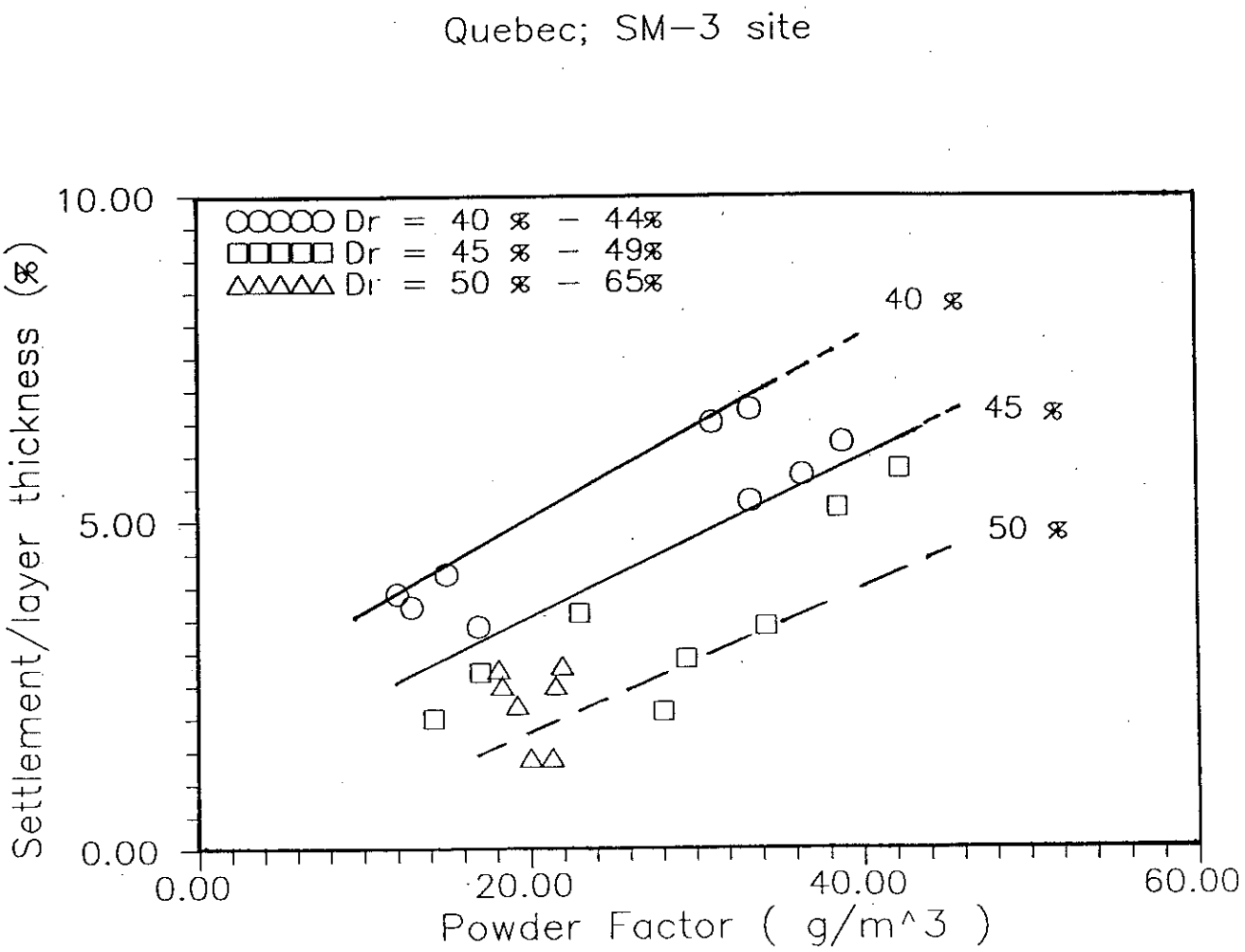

Fig. 3-12 A relationship between volume change, powder factor and sand relative density at the SM-3 site, Quebec (powder factor = charge weight per unit volume of soil treated)

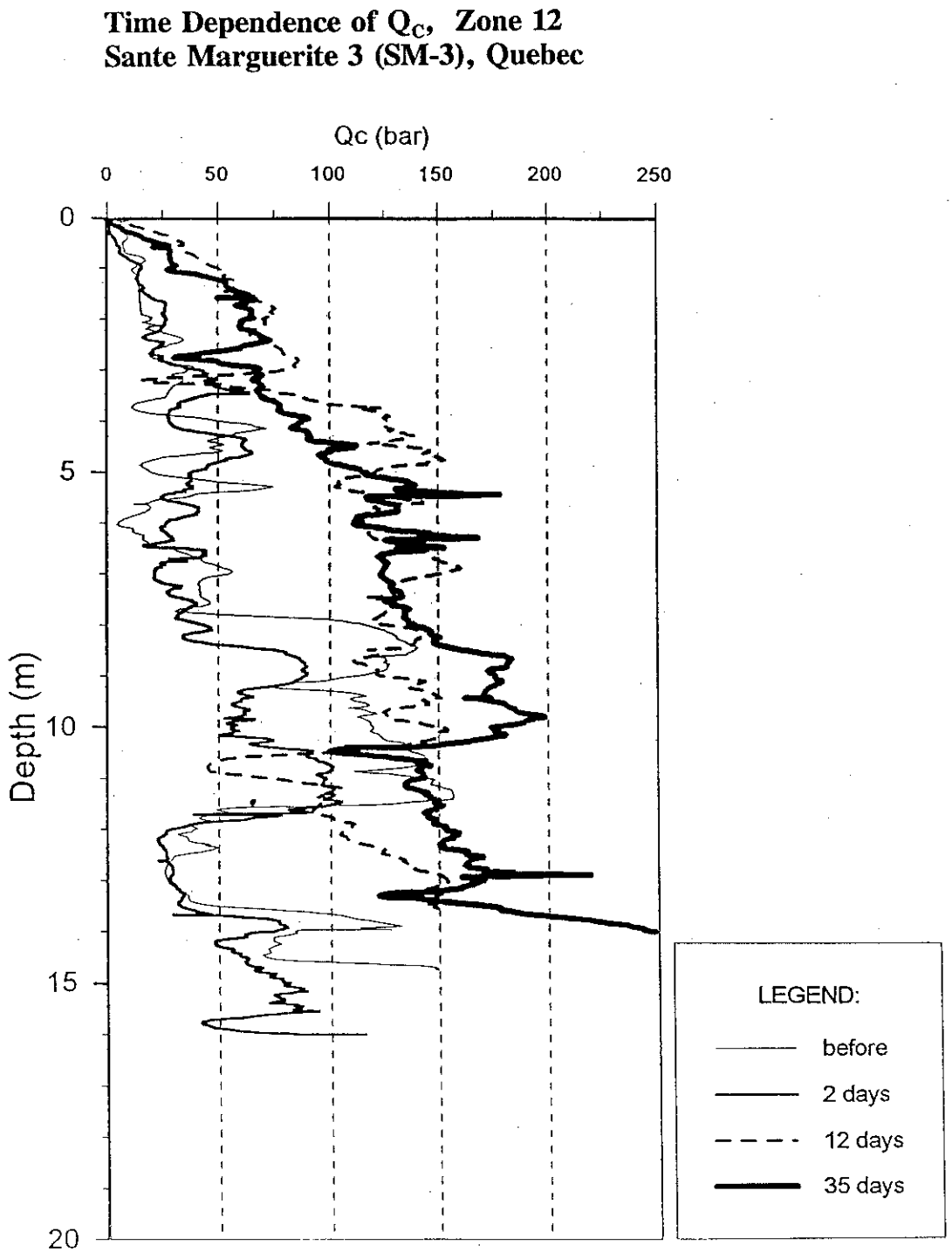

Fig. 3-13 Time dependency of CPT cone tip resistance Q_c at the SM-3 site, Quebec

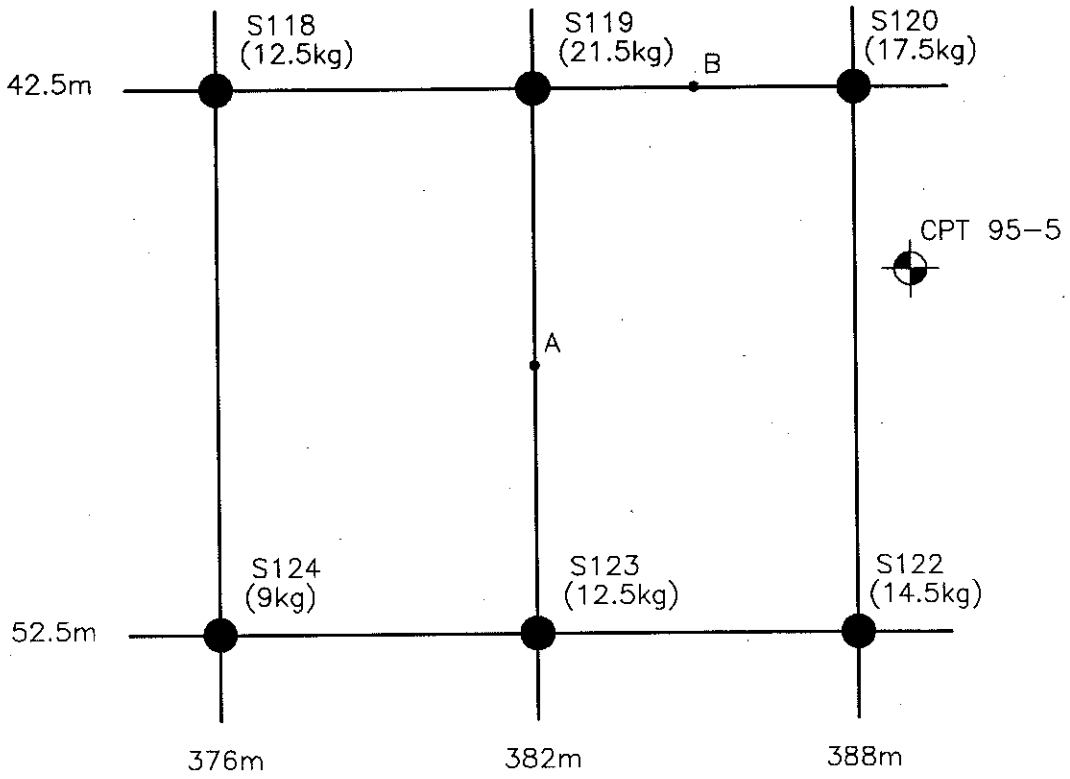

Fig. 3-14 Locations of blast holes and charge in the vicinity of CPT95-5 at SM-3 site, Quebec

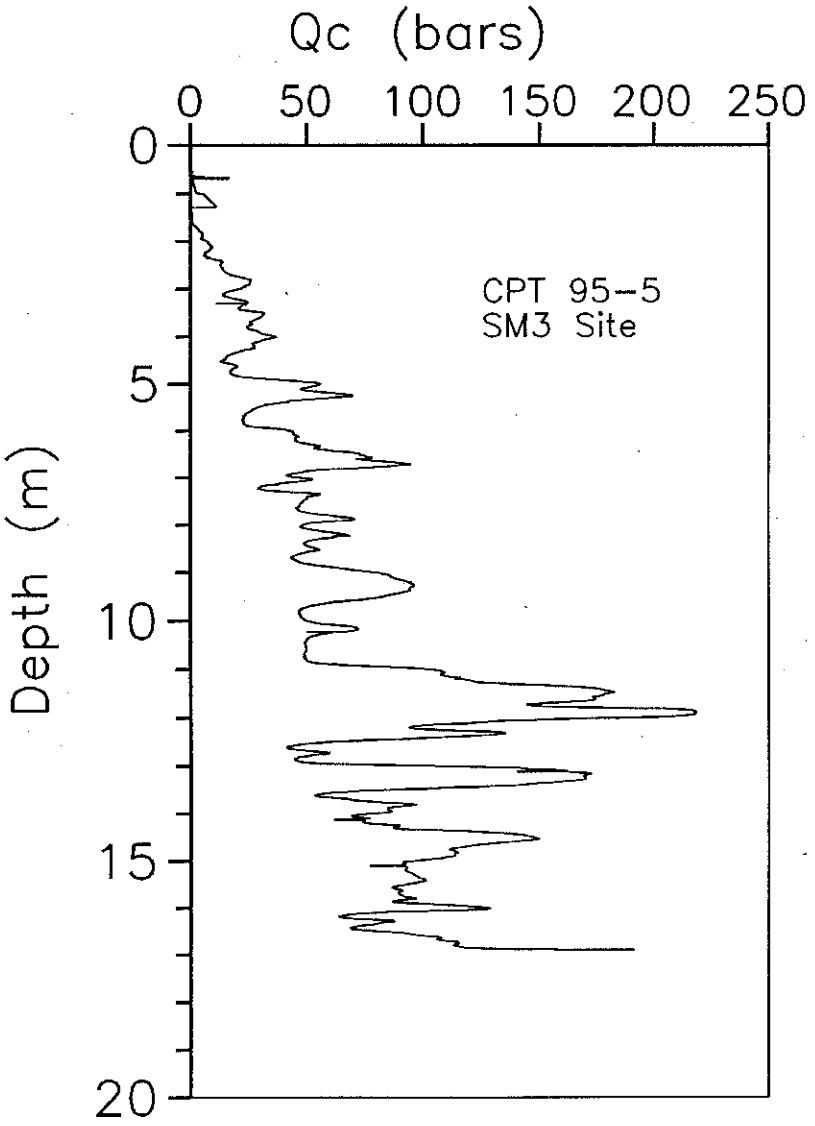

Fig. 3-15 Cone tip resistance Q_c versus depth for CPT95-5 at SM-3 site, Quebec

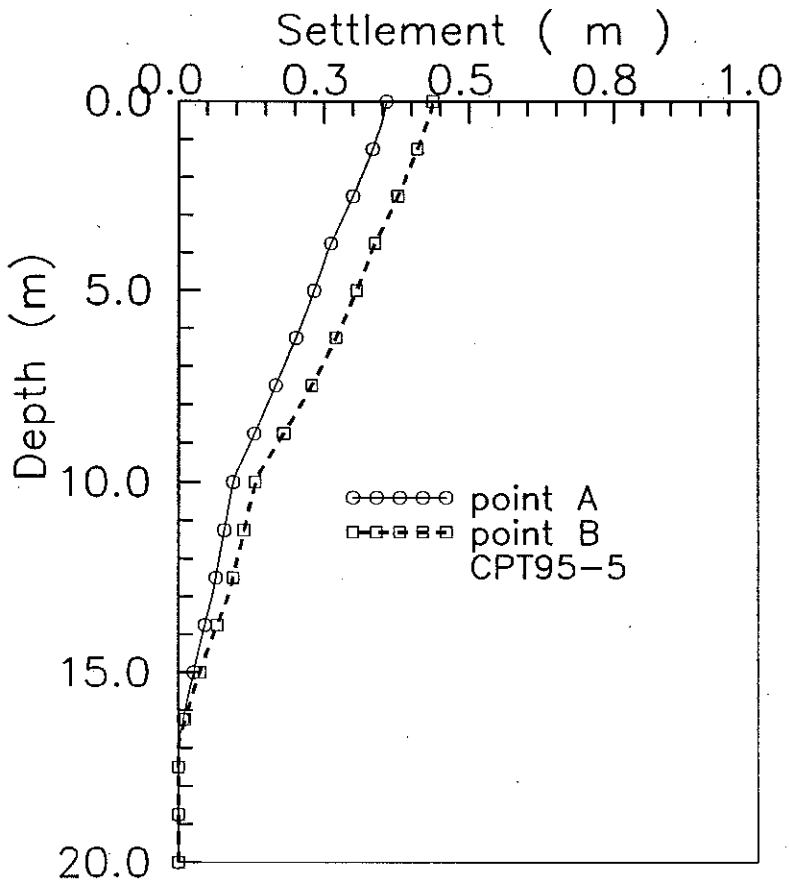

Fig. 3-16 Computed settlements with depth in the vicinity of CPT95-5 at SM-3 site, Quebec

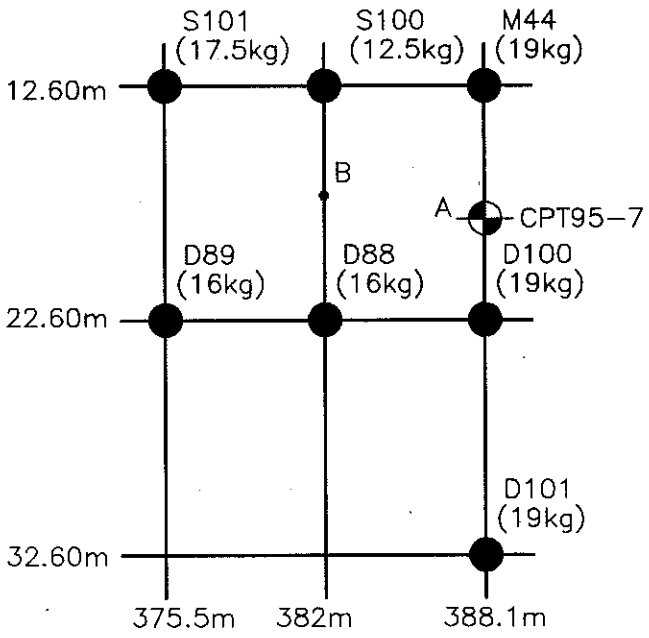

Fig. 3-17 Locations of blast holes and charge in the vicinity of CPT95-7 at SM-3 site, Quebec

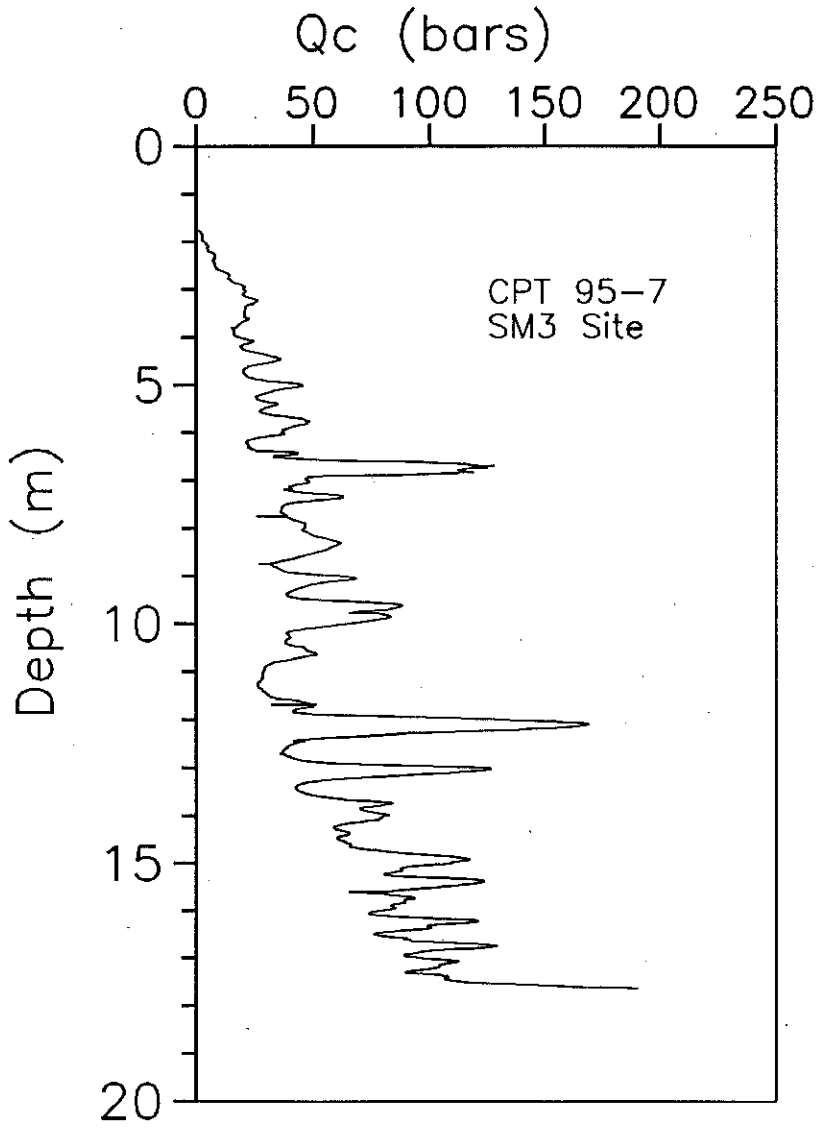

Fig. 3-18 Cone tip resistance Q_c versus depth for CPT95-7 at SM-3 site, Quebec

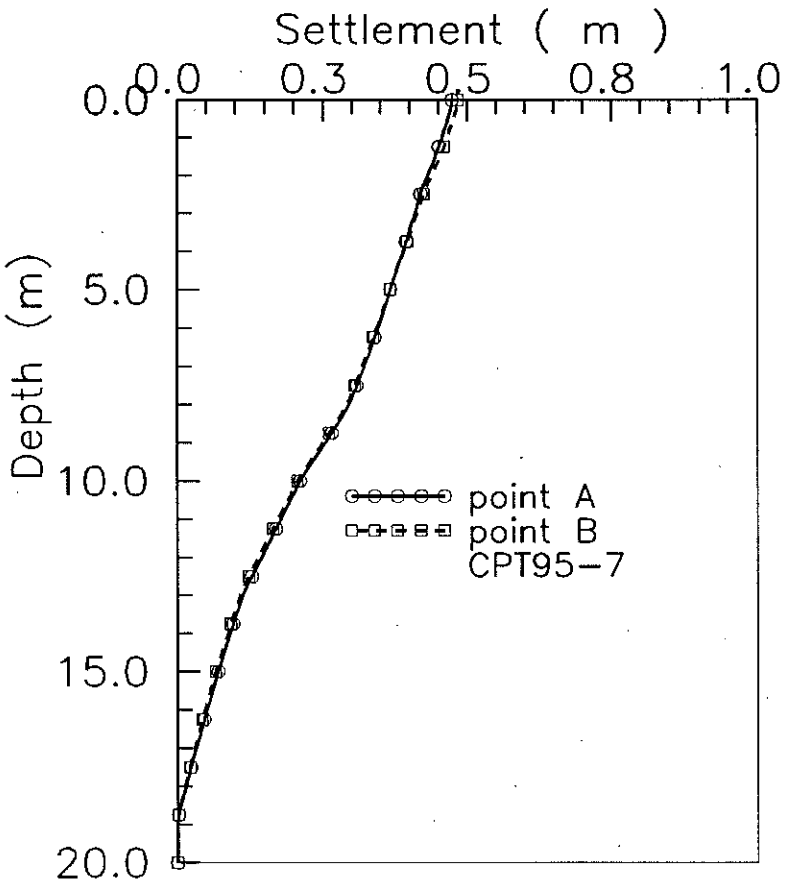

Fig. 3-19 Computed settlements with depth in the vicinity of CPT95-7 at SM-3 site, Quebec

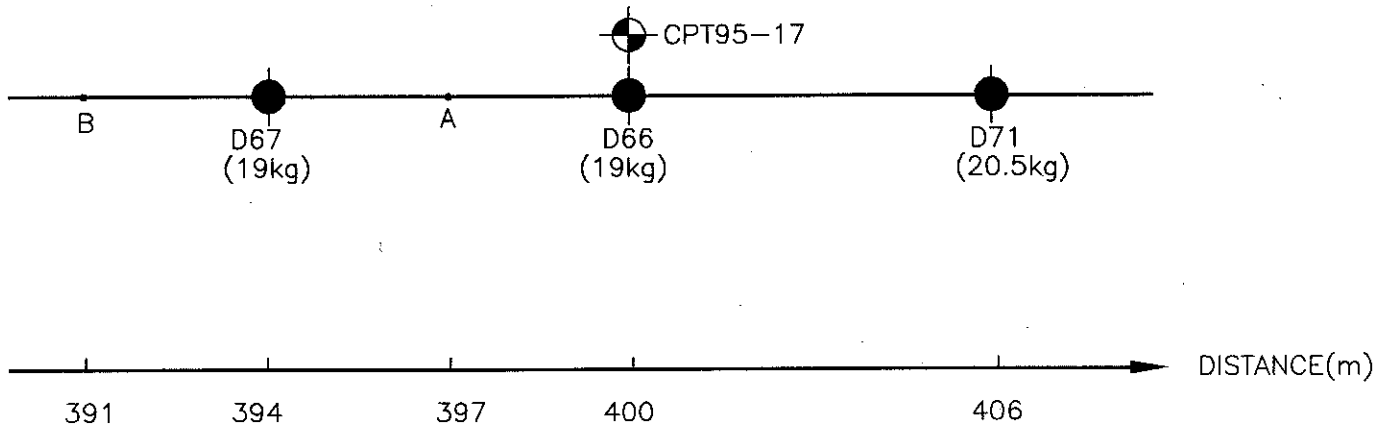

Fig. 3-20 Locations of blast holes and charge in the vicinity of CPT95-17 at SM-3 site, Quebec

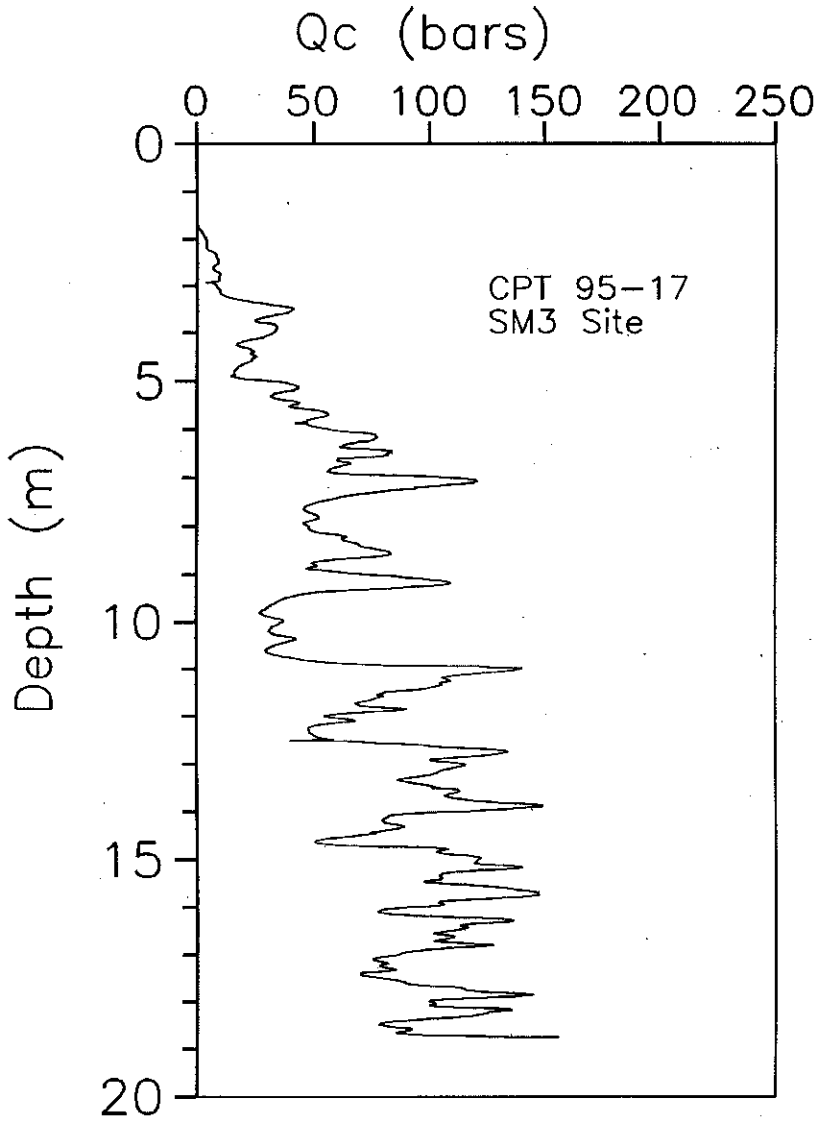

Fig. 3-21 Cone tip resistance Q_c versus depth for CPT95-17 at SM-3 site, Quebec

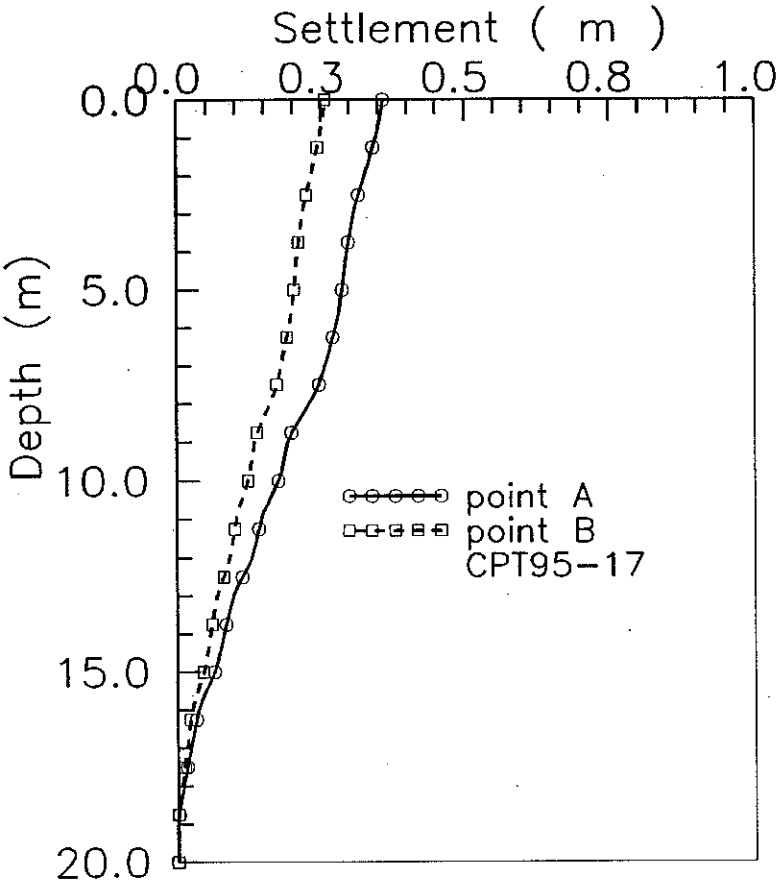

Fig. 3-22 Computed settlements with depth in the vicinity of CPT95-17 at SM-3 site, Quebec

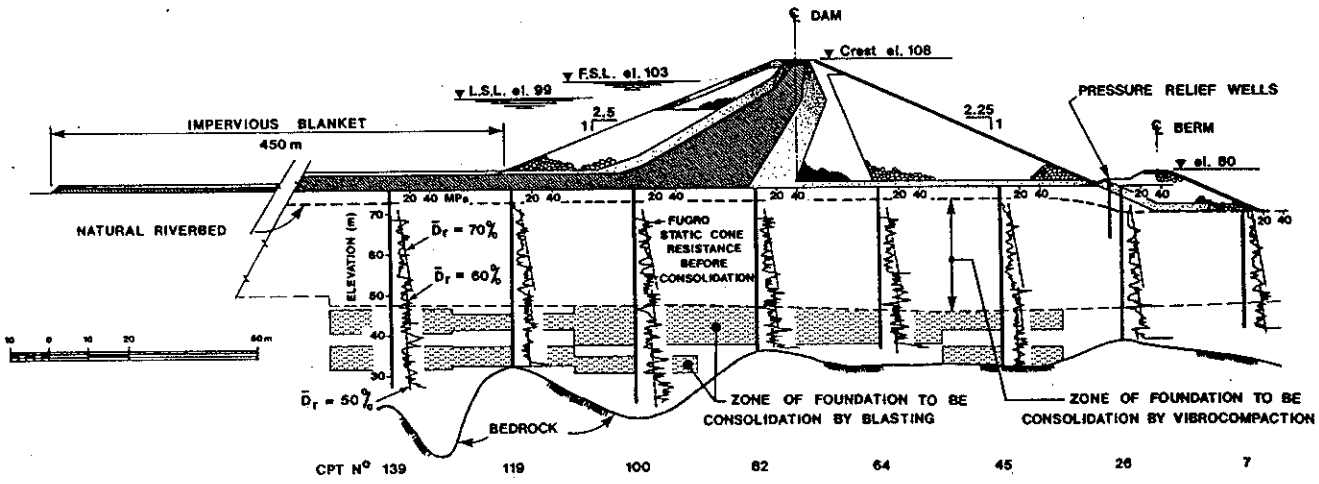

Fig. 3-23 Main dam cross section showing zones of foundation densified by blasting (after solymar, 1984)

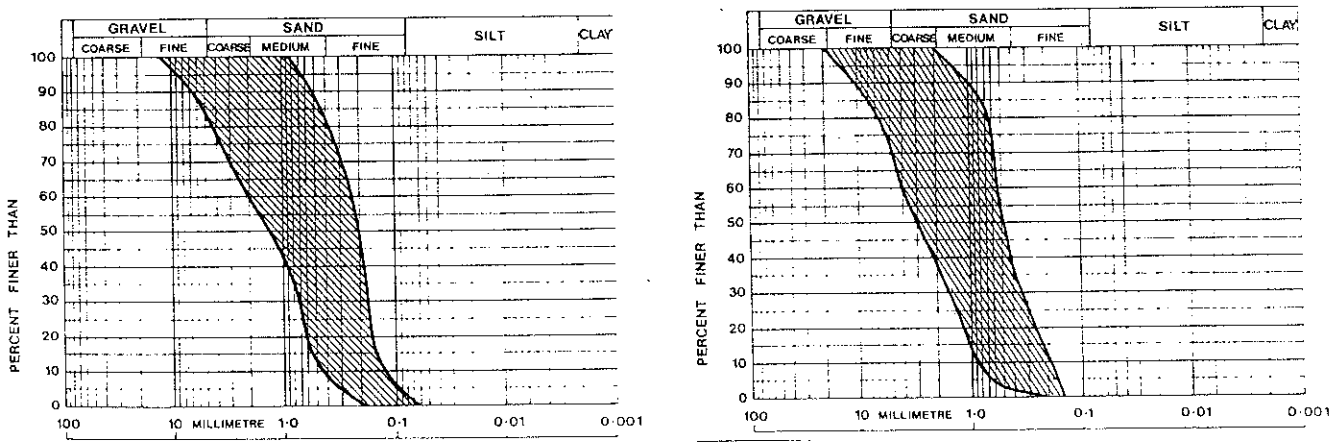

Fig. 3-24 Grain size envelopes for (a) test area and (b) blast zone 4 (after Solymar, 1984)

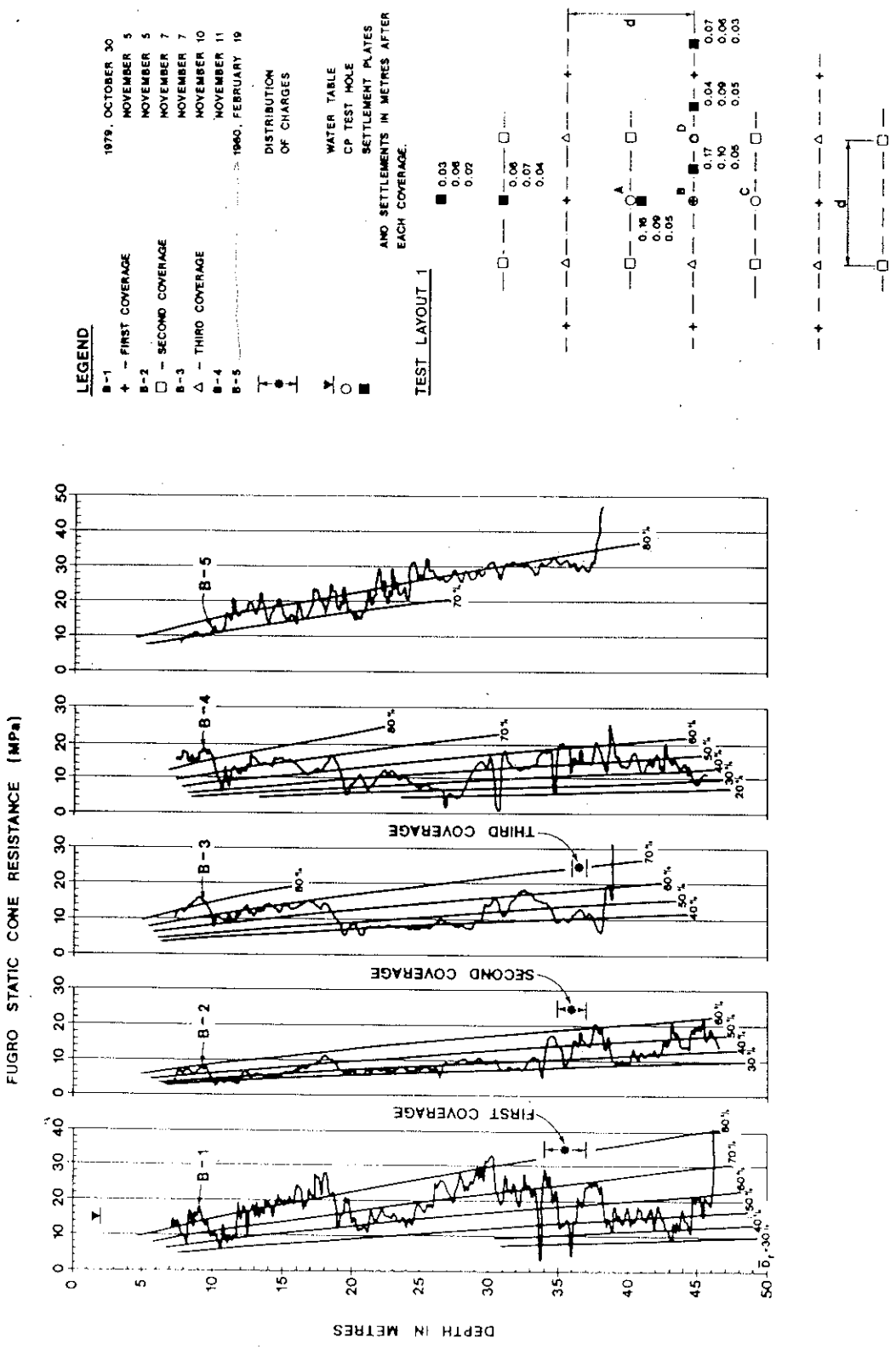

Fig. 3-25 CPT data and blast layout for test blast 3 at Jebba dam (after Solymar, 1984)

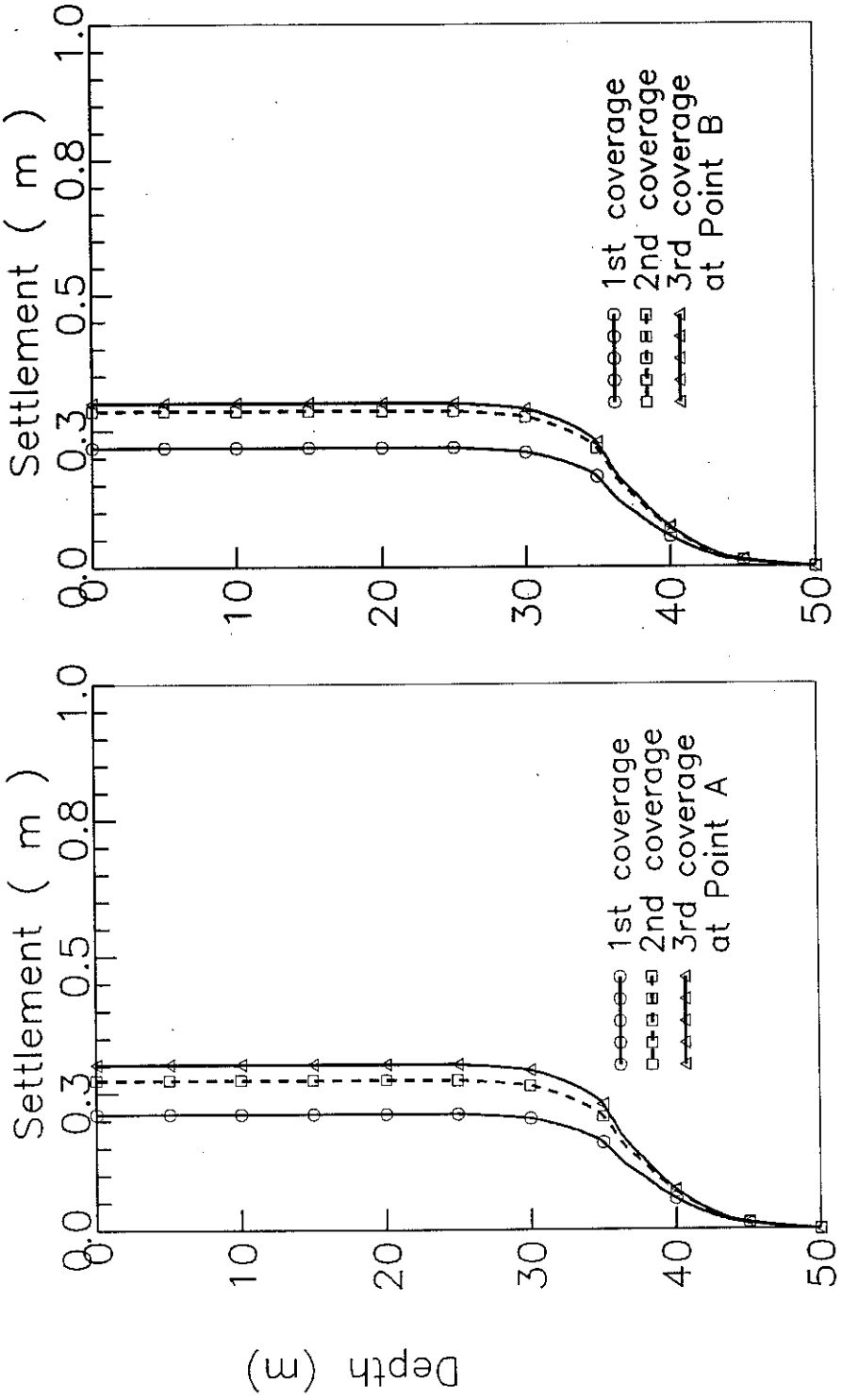

Fig. 3-26 Computed settlements at (a) point A and (b) point B for test blast 3, Jebba dam

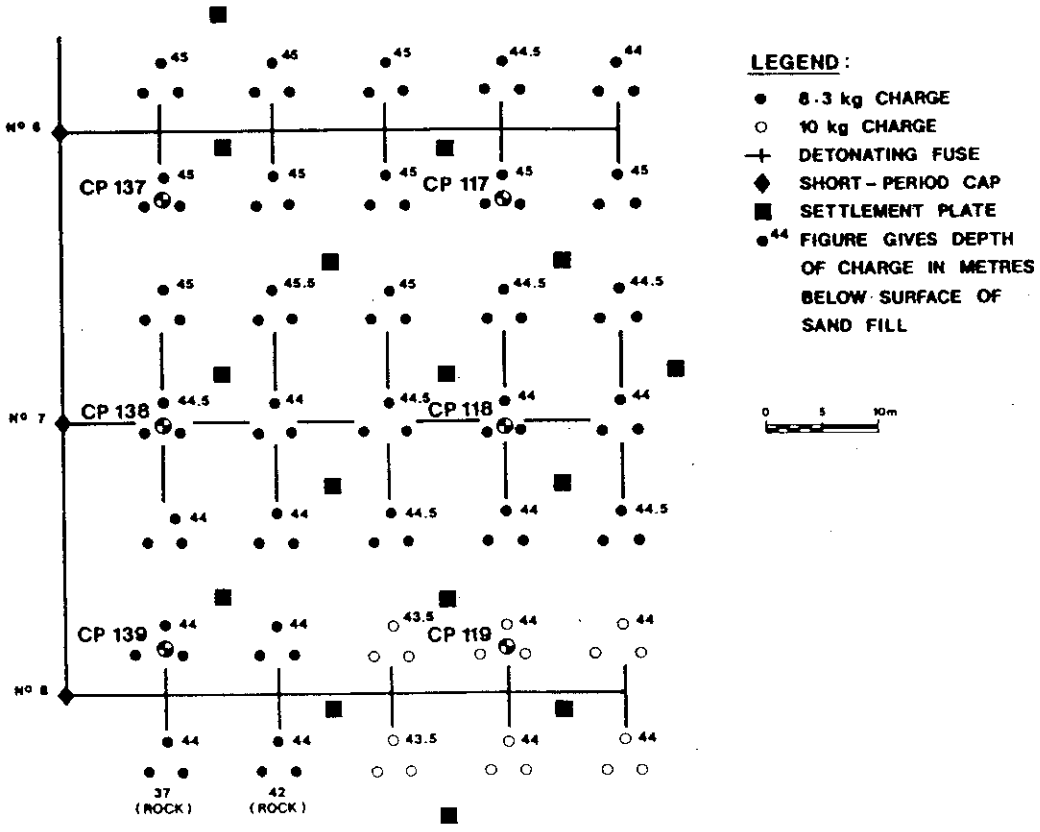

Fig. 3-27 Charge layout for the first coverage in production blasting zone 1, Jebba dam (after Solymar, 1984)

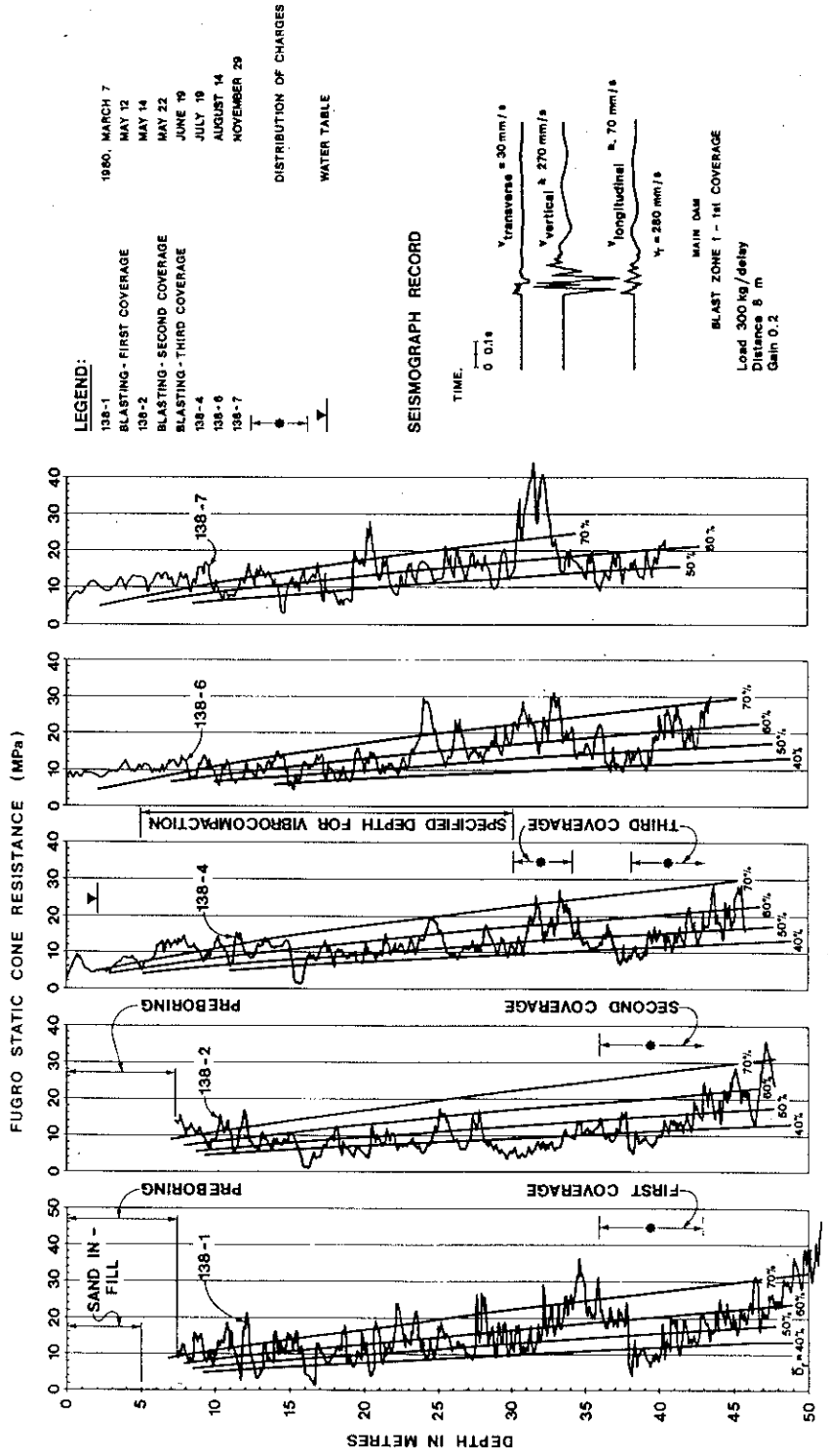

Fig. 3-28 CPT results for hole CP138, Jebba dam (after Solymar, 1984)

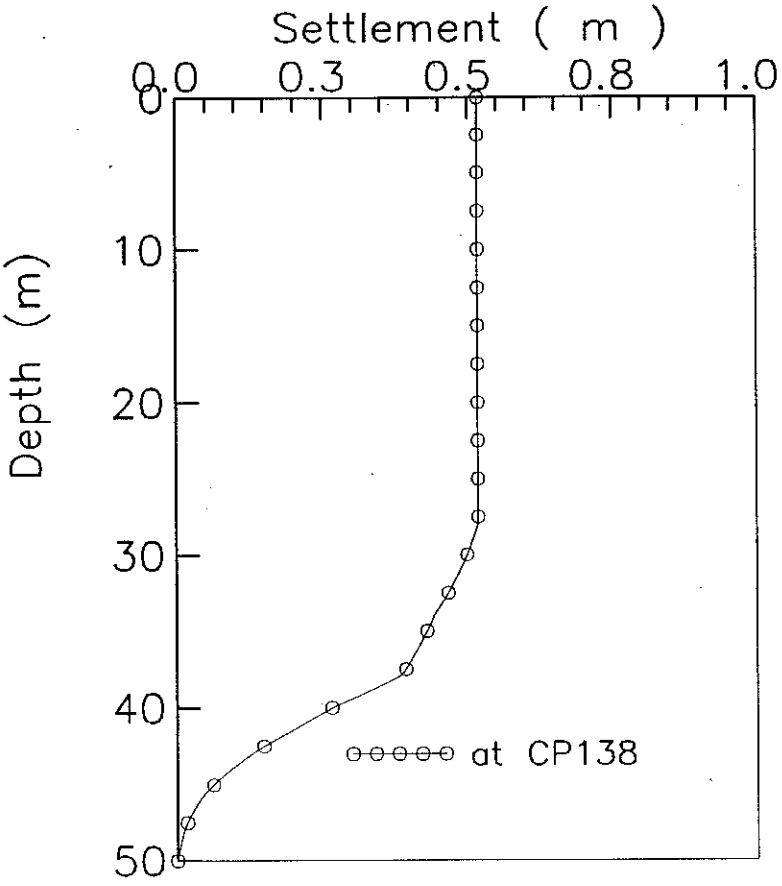

Fig. 3-29 Computed settlement profile at CP138 after first coverage of zone 1 production blasting, Jebba dam.

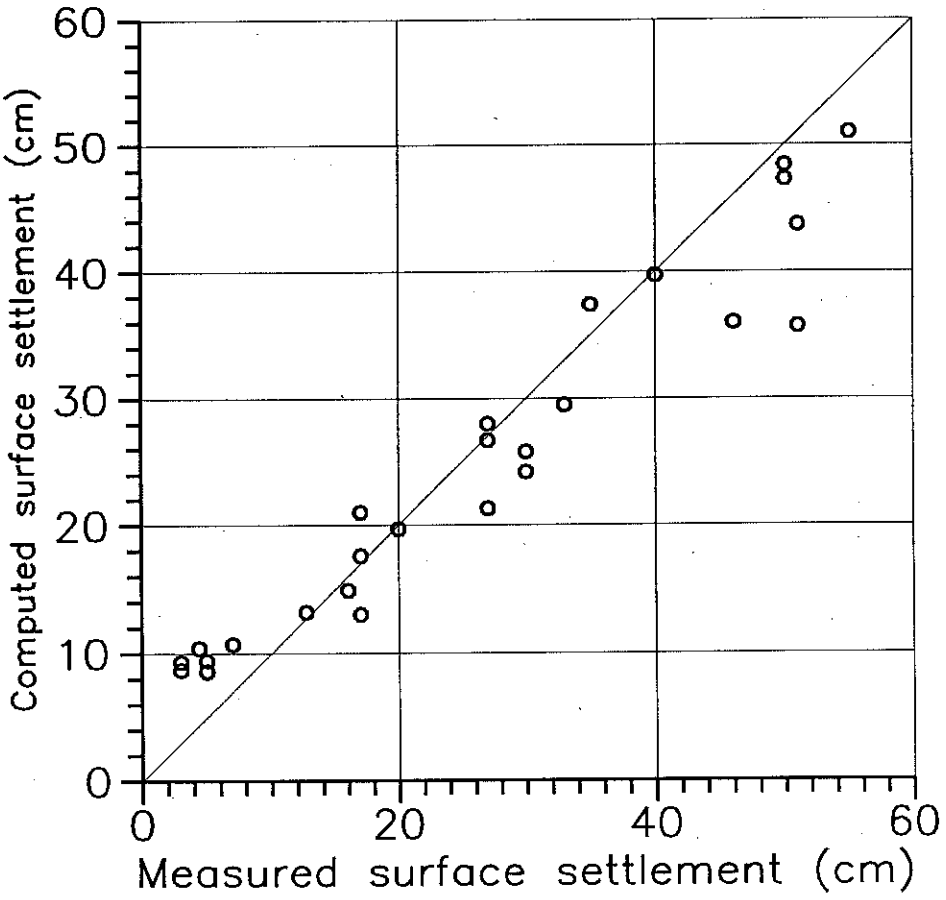

Meaured settlements are from the following sites:
1. Verdalsora – single hole (Kummeneje and Eide, 1961)
2. Richmond site, B.C. (AGRA Earth & Environmental, 1991)
3. SM–3 site, Quebec (AGRA Earth & Environmental, 1995)
4. Jebba project, Nigeria (Solymar, 1984)

Fig. 3-30 Comparison of computed and measured surface settlements for all blasting trials

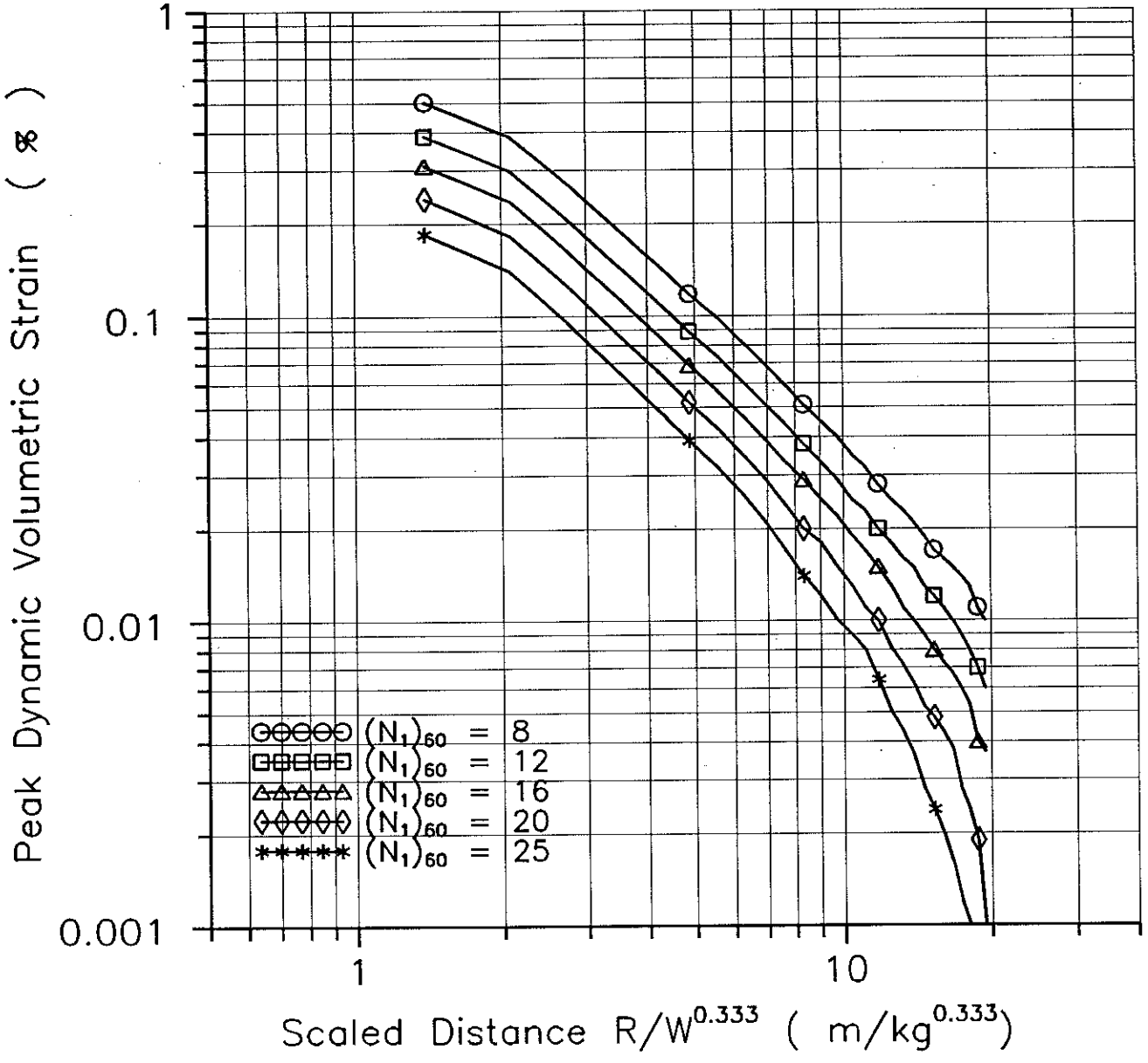

Fig. 4-1 Computed relationships between the peak dynamic volumetric strain and the scaled distance $R/W^{0.333}$ for different $(N_1)_{60}$ values at a constant effective overburden pressure of 100 kPa

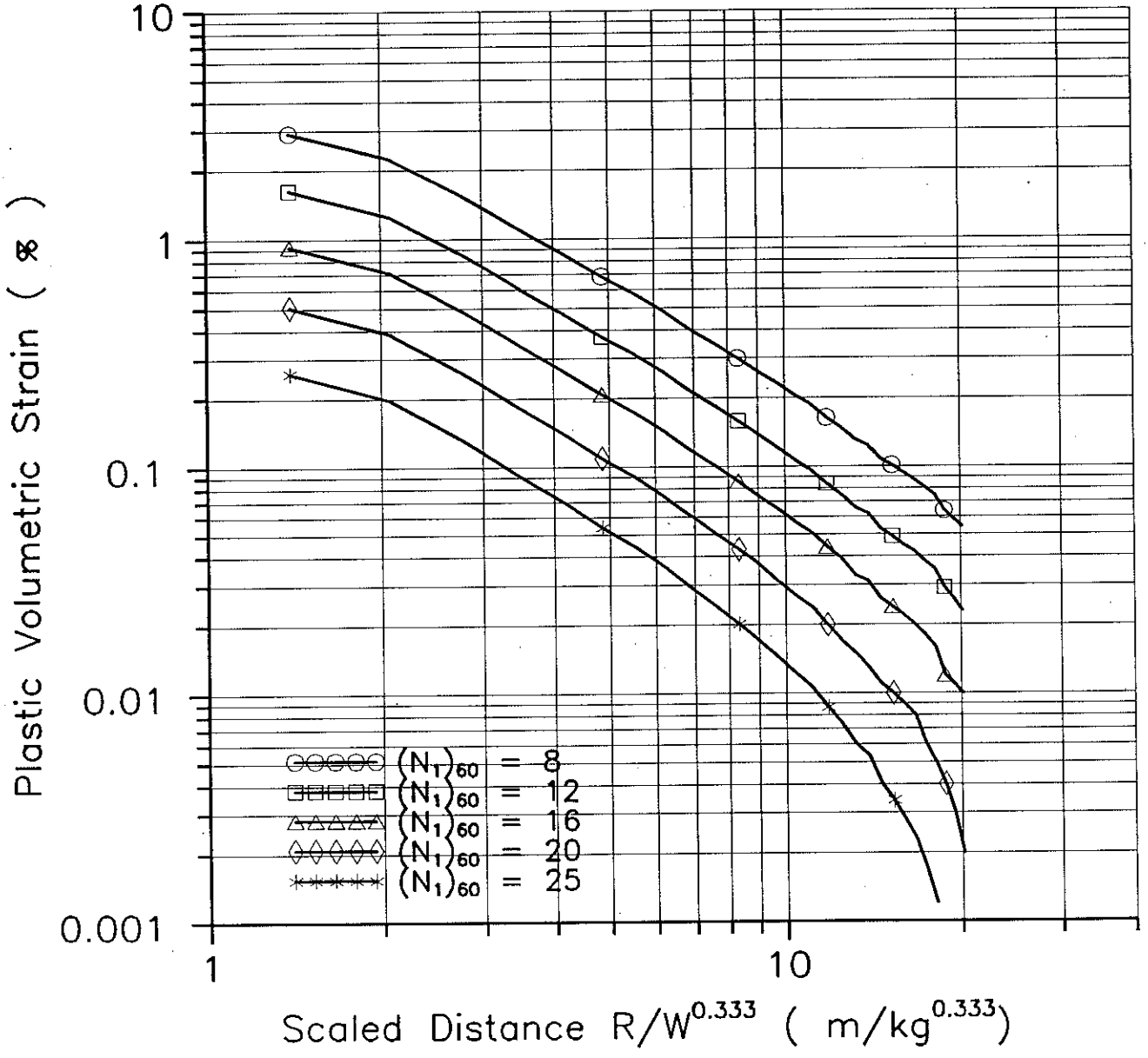

Fig. 4-2 Computed relationships between the plastic volumetric strain and the scaled distance $R/W^{0.333}$ for different $(N_1)_{60}$ values at a constant effective overburden pressure of 100 kPa

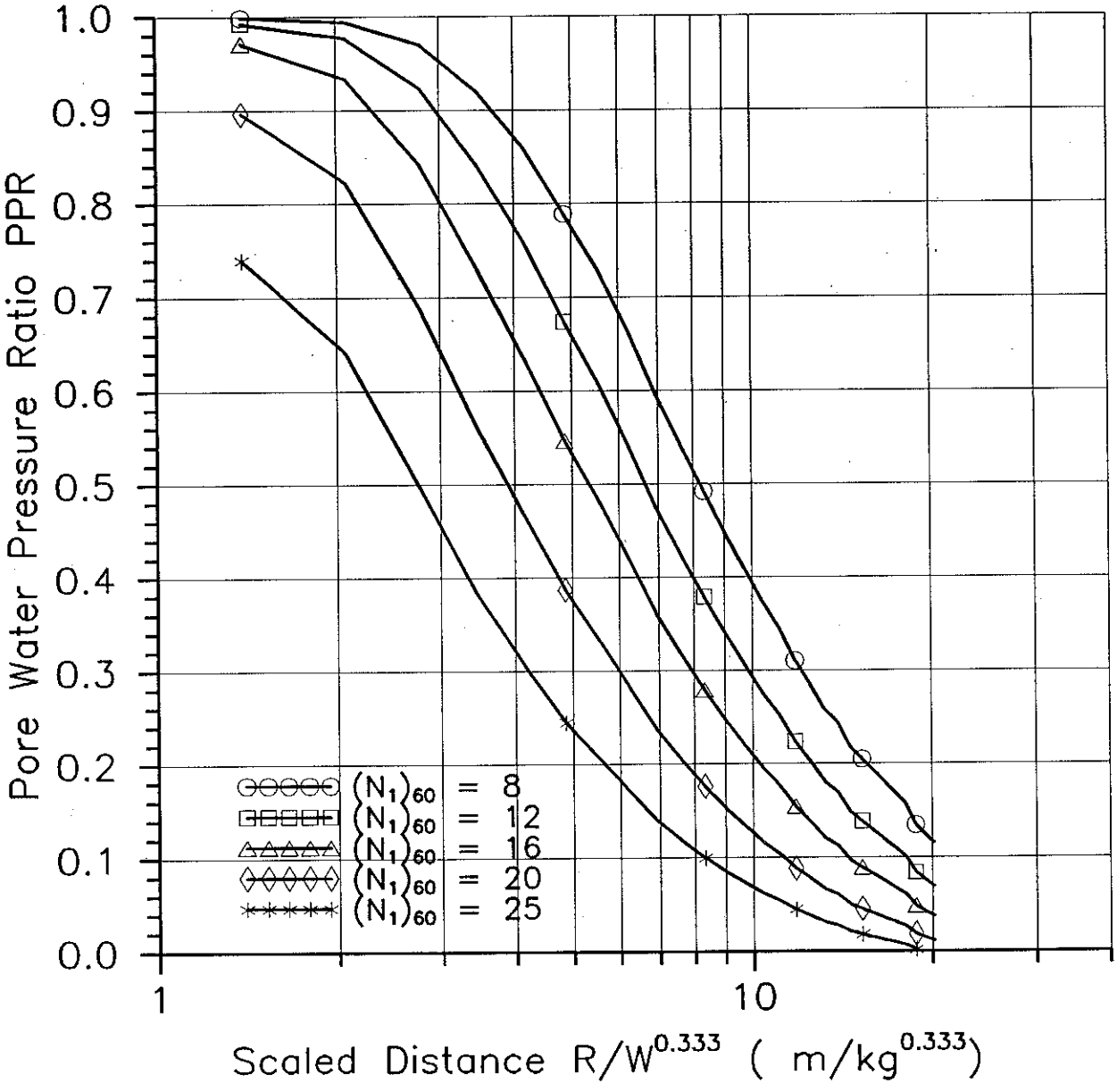

Fig. 4-3 Computed relationships between the pore water pressure ratio PPR and the scaled distance $R/W^{0.333}$ for different $(N_1)_{60}$ values at a constant effective overburden pressure of 100 kPa

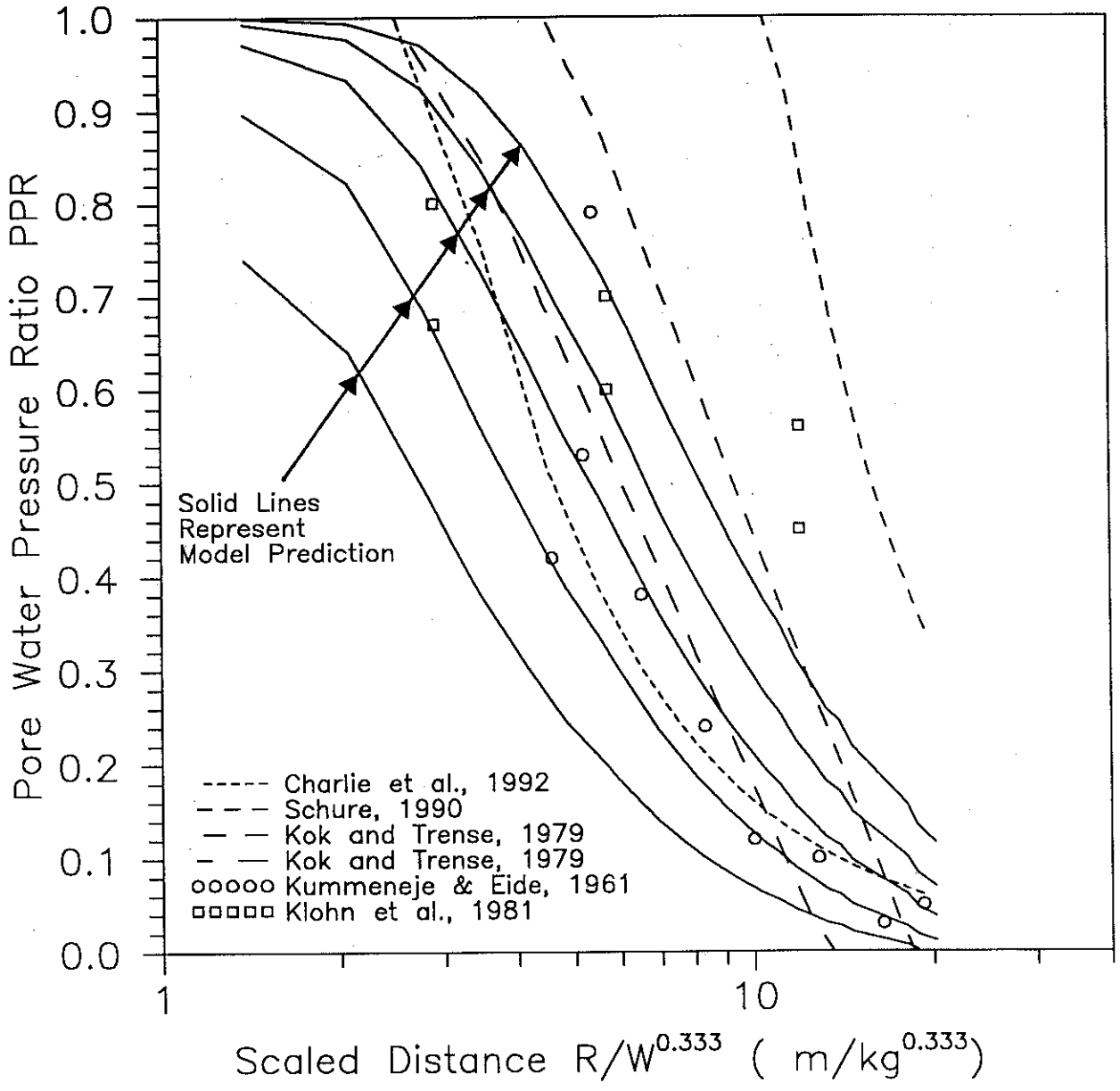

Fig. 4-4 A comparison of empirical relationships between the pore water pressure ratio PPR and the scaled distance $R/W^{0.333}$

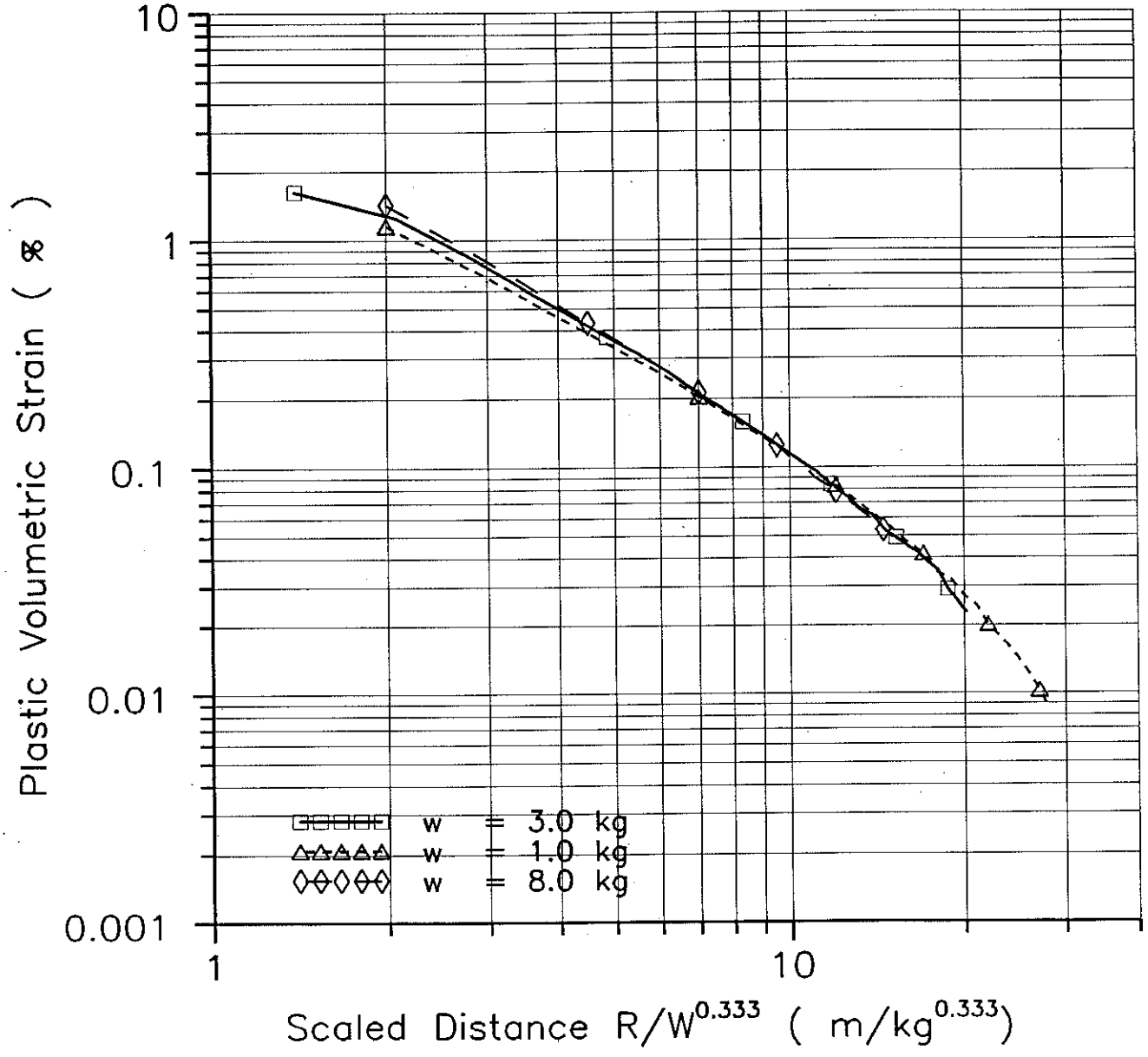

Fig. 4-5 Relationship between plastic volumetric strain and the scaled distance $R/W^{0.333}$: effect of charge weight

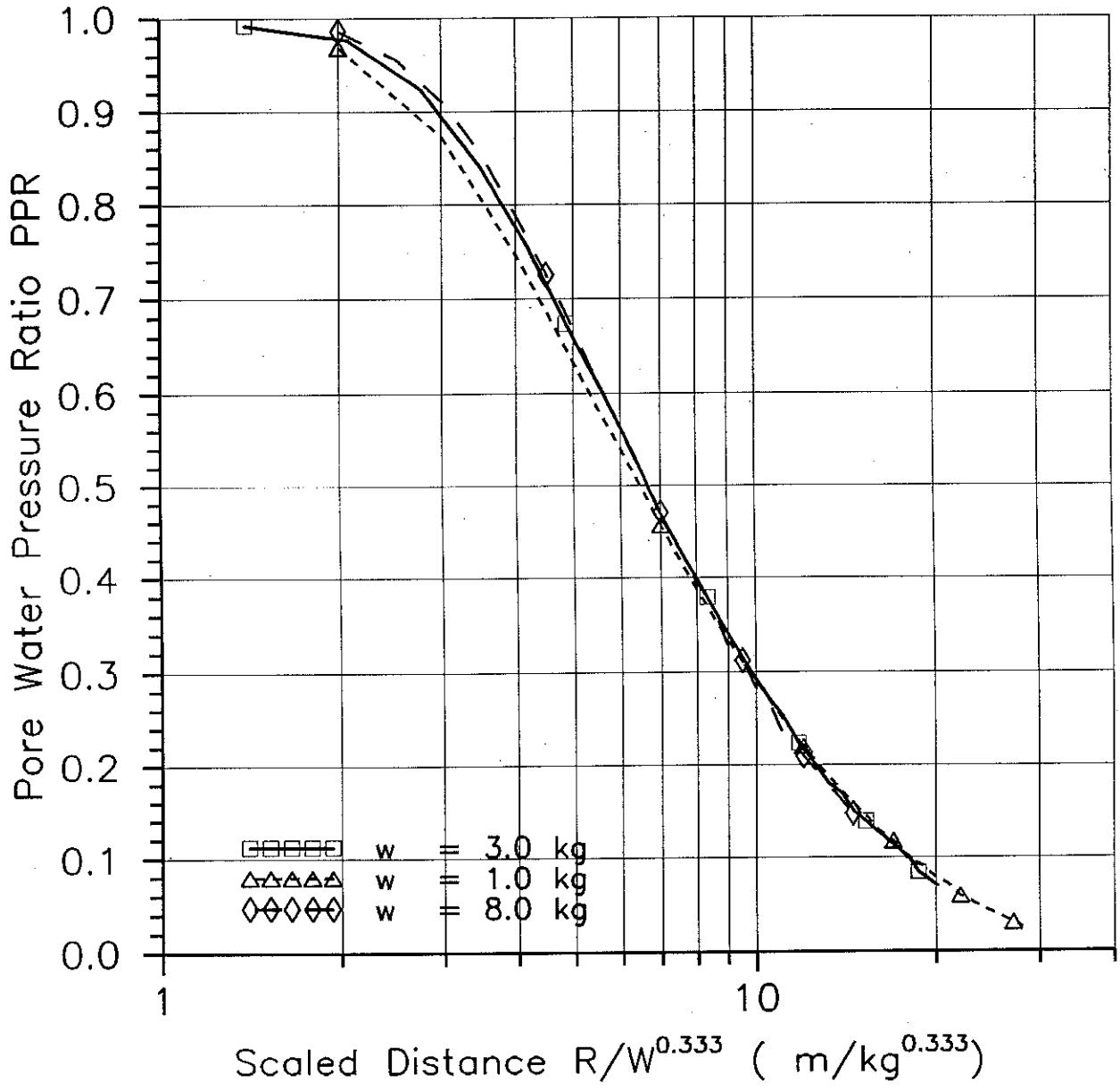

Fig. 4-6 Relationship between pore water pressure ratio and the scaled distance $R/W^{0.333}$: effect of charge weight

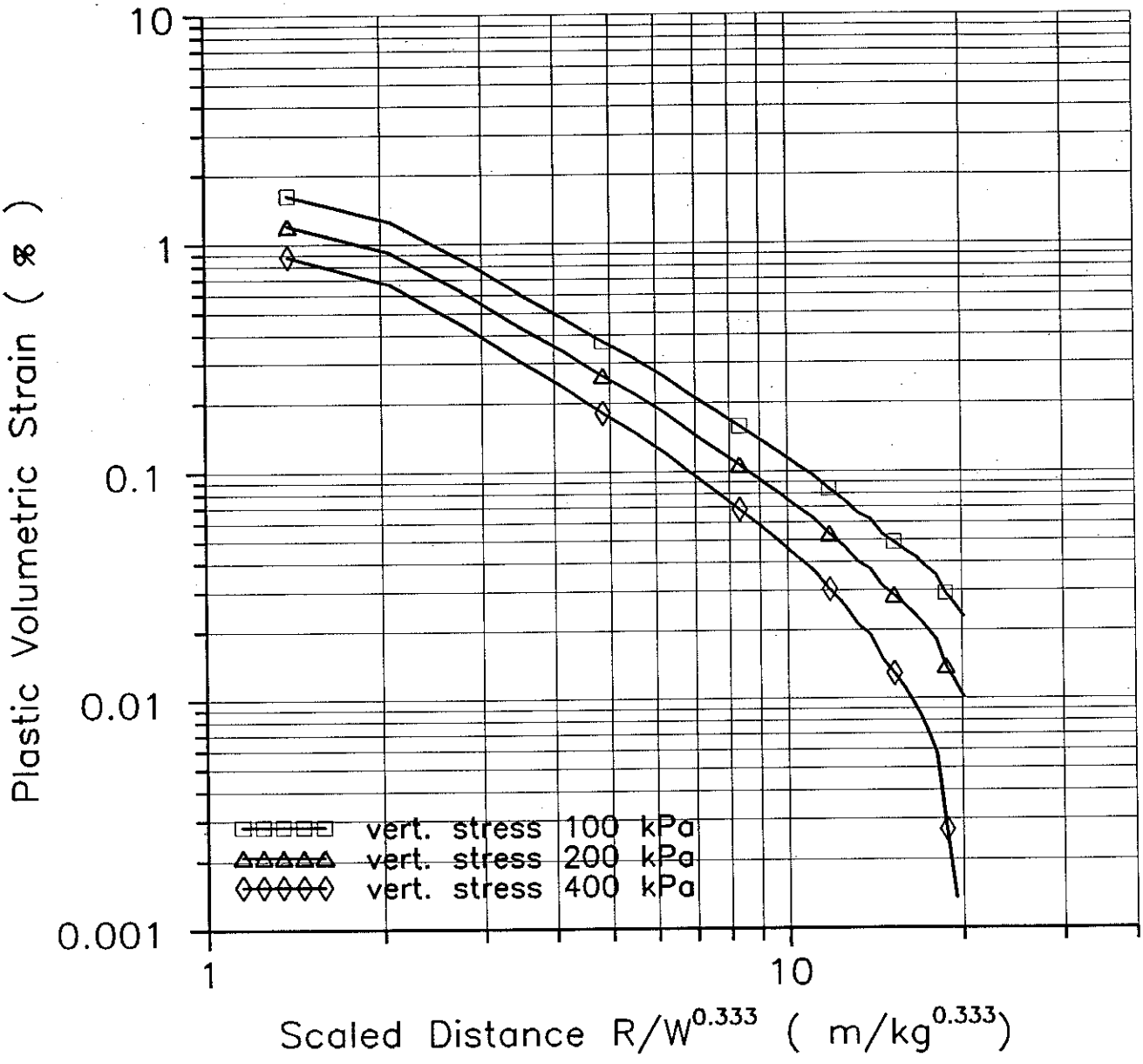

Fig. 4-7 Relationship between plastic volumetric strain and the scaled distance $R/W^{0.333}$: effect of effective overburden pressure

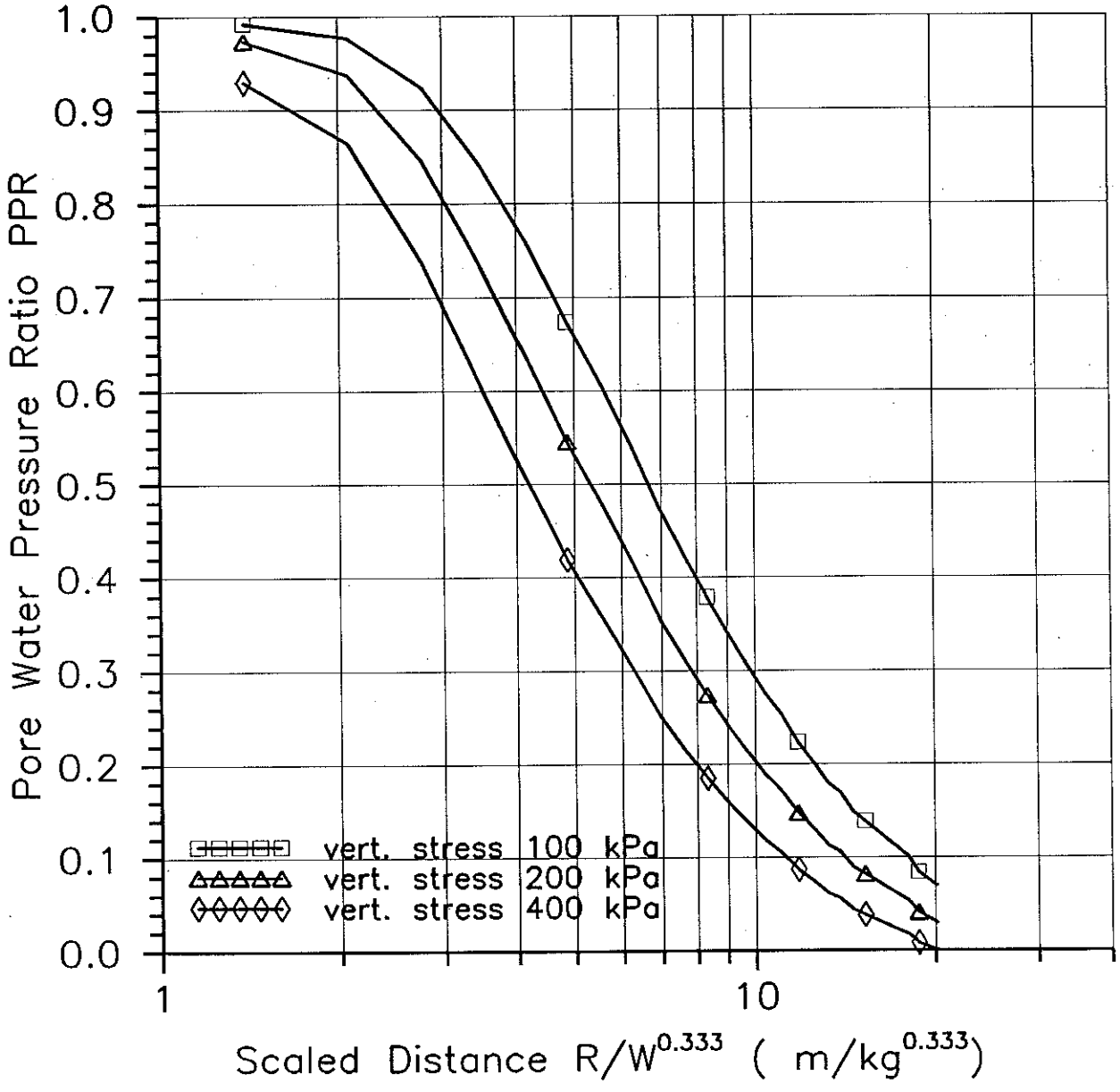

Fig. 4-8 Relationship between pore water pressure ratio and the scaled distance $R/W^{0.333}$: effect of effective overburden pressure

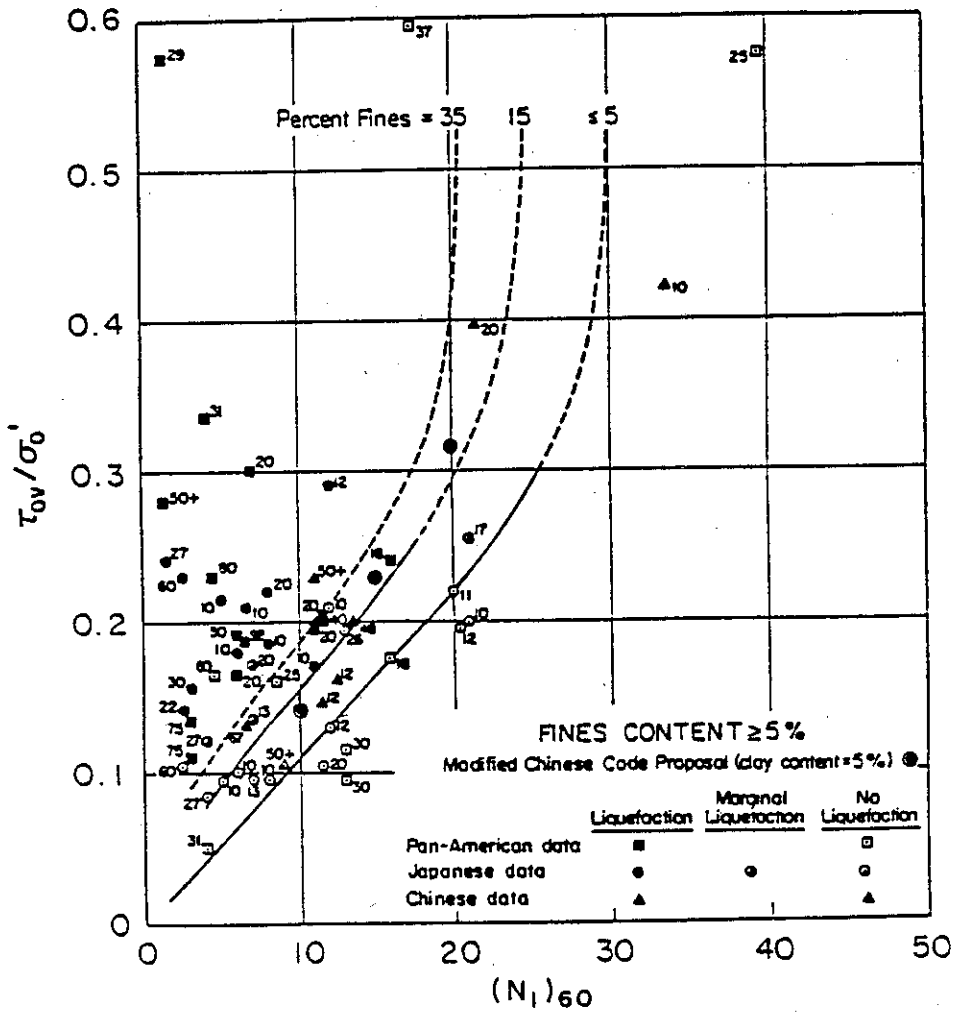

Fig. A-1 Relationship between stress ratio causing liquefaction and $(N_1)_{60}$ values for silty sands for earthquakes of magnitude M = 7.5 (after Seed et al., 1985)

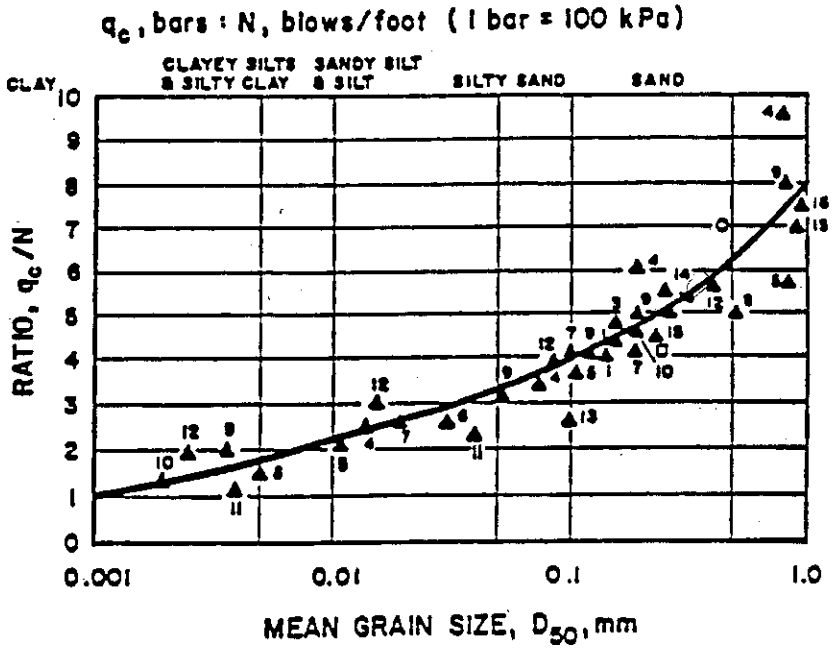

Fig. A-2 Relationship between q_c/N_{SPT} and mean grain size D_{50} (after Robertson et al., 1983)

APPENDIX A

Current Practice for Evaluation of Liquefaction

One of the most commonly used methods to characterize the soil in the ground is the standard penetration test, SPT method. Seed and his colleagues (Seed et al., 1983 and Seed et al., 1985) developed engineering charts for determining the cyclic shear stress ratio (CSR_{liq}) required to cause liquefaction according to the SPT-N value during earthquakes of magnitude M = 7.5. The correlations between CSR_{liq} and $(N_1)_{60}$ which are presented in Fig. A-1 were established based on observed response of sites during earthquake loading. Liquefaction is defined in terms of surface effects such as sand boils, lateral spreading, cracks and settlements. Lower bound curves separating liquefied from non-liquefied sites are shown in Fig. A-1 corresponding to various fines contents of the sands.

To compare the ground conditions at one site with those at another, it is necessary to standardize the measured penetration values to a standard driving energy and effective stress. Seed et al. (1985) normalized the SPT to an energy level of 60 % of the free-fall potential energy of the hammer and an effective vertical stress of 100 kPa (1 tsf). Hence the correlations illustrated in Fig. A-1 show the normalized SPT N value, $(N_1)_{60}$.

The correction for energy level may be made using the data in Table A-1 or by direct measurement of the energy delivered to the rods. The correction factors C_N for effective vertical stress may be determined using the simple equation (Liao and Whitman, 1985),

$$C_N = \frac{1}{\sqrt{\sigma'_{vo}}} \quad (1)$$

where σ_{vo}' = effective vertical stress in **tsf**, 1 tsf = 100 kPa.

Judgement is required in limiting the maximum value of the correction factor C_N. Generally the upper limit is taken as 2.0.

The correlations shown in Fig. A-1 are representative of earthquakes with a magnitude M = 7.5, sites under level ground conditions with no initial static shear stresses on horizontal planes and to effective vertical stress less than 150 kPa. The detailed procedures for making corrections when these conditions are violated can be found in Seed and Harder (1990).

The correlation relationship between cone resistance and standard penetration resistance by Robertson et al. (1983) is useful for estimating the equivalent $(N_1)_{60}$ of sands when CPT data are available. This relationship is shown in Fig. A-2, which indicates that the ratio of cone resistance to blow count increases with increasing mean grain diameter.

Table A-1 Summary of energy ratios for SPT procedures (after Seed et al., 1985)

Country	Hammer Type	Hammer Release	Est. Rod Energy (%)	Correction Factor for 60% Rod Energy
Japan[a]	Donut Donut	Free - Fall Rope & Pulley with Special Throw Release	78 67	78 / 60 = 1.30 67 / 60 = 1.12
U.S.	Safety Donut[b]	Rope & Pulley Rope & Pulley	60 45	60 / 60 = 1.0 45 / 60 = 0.75
Argentina	Donut	Rope & Pulley	45	45 / 60 = 0.75
China	Donut Donut	Free-Fall[c] Donut	60 50	60 / 60 = 1.0 50 / 60 = 0.83

[a] Japanese SPT results have additional corrections for borehole diameter and frequency effects.

[b] Prevalent method in the United States today.

[c] Pilcon-type hammers develop an energy ratio of about 60 %.

Appendix B

Description of the Computer Program BLAST
October 1996

The computer program BLAST is developed for simulating response of saturated granular soil to blast loads. The blast loads are high pressure impulses caused by detonation of explosives within the ground. Surface explosions of explosives can not be modelled at present. Single charges or multiple charges of explosives can be arranged at any points within the 3-dimensional ground. The response of saturated soil includes the dynamic transient response and the residual response. The dynamic response represents acceleration, particle velocity, normal strains and stresses as well as dynamic pore water pressures. The residual response represents the residual pore water pressures at the end of blast and the permanent ground deformation caused by the blast. These quantities are the primary output of this analysis.

Some important aspects of the program are described below.

1. The theory used in BLAST for computing the dynamic transient response of saturated soil has been described in a technical report by Wu (1995). The theory uses a 3D spherically symmetric model to simplify the 3D geometry of soil mass. The shear stress - strain behaviour of soil has been modelled to be nonlinear and hysteretic. Heavy viscosity has been implemented in the model to simulate the attenuation of dynamic response with distance.

2. Dynamic response analysis is performed separately for each individual charge. Peak dynamic response at a specified point within the ground is obtained by comparing the peak dynamic response at this point for all charges being analyzed. Dynamic response for multiple charges are not superimposed considering the fact that blast waves usually elapse less than 15 msec within a distance of 20 m from the charge point, and the fact that delays longer than 15 msec are commonly used between charges in a blast trial.

3. Residual response at a specified point within the ground for multiple charges are superimposed through the accumulation of plastic volumetric strain from each charge. Residual pore water pressures are related to the plastic volumetric strain according to the rebound characteristics of the sand. The theory for this simulation has been presented in section 2 of this report.

4. The layered soil profiles are used to simulate the variation of soil conditions within the ground. The variation of soil properties is confined to the change of depth. Variation

of soil properties in the horizontal direction at a specific depth can not be simulated.

5. In BLAST the 3-dimensional half-space is divided into six conical soil zones radiating out from each individual charge point. For each soil zone dynamic response analysis is performed using soil properties in this soil zone. The 1-D spherically symmetric finite element mesh for this analysis is automatically generated by the program. Free displacement condition is applied at the surface of the 3-dimensional half-space. The effect of soil condition on dynamic response at a specified point within the ground depends on the relative position of the point to the charge point, i.e., depends on the zone in which the point is allocated.

6. The travelling time t for the P-wave to propagate a distance R is

$$t = \frac{R}{V_P}$$

where V_P = the P-wave velocity of the saturated soil.

Sufficient time duration must be used so that the P-wave can reach the reaction point from the charge point.

For example 7 msec (0.007 sec) or longer duration must be used in order to determine the dynamic response at 10 m away from the charge point, assuming V_P = 1430 m/s. However 14 msec and 21 msec must be used for response at 20 m and 30 m away from the charge point, respectively. In BLAST the time duration is calculated by NPOINT * DT, in which NPOINT is the total number of integration points and DT is the time increment for integration. A time increment DT = 0.00004 sec is appropriate in most practical cases.

7. The high-pressure impulse acting on the inner surface of the explosion cavity is computed using the following equation

$$P(t) = A(e^{-\alpha t} - e^{-\beta t})$$

with the peak value of p(t) determined by the following formulation (U.S. Army Corps of Engineers, 1972)

$$P_0 = 450.0\times10^{-3}\left(\frac{\rho_e V_d^2}{1+0.8\rho_e}\right)$$

where P_0 = peak detonation pressure (kPa)
V_d = detonation velocity of the explosive (m/sec)
ρ_e = specific gravity of the explosive (g/cm^3)

The radius a_0 of the cavity is determined by the charge weight W and the density ρ_e as

$$W = \frac{4}{3}\pi a^3 \rho_e \qquad or \qquad a_0 = \left(\frac{3W}{4\pi\rho_e}\right)^{0.3333}$$

The charge can be modelled by using the actual V_d, ρ_e, and W of the explosive or by using the charge weight W equivalent to TNT and using the V_d, ρ_e of TNT. However the computed response from the two approaches are different. It may be preferable to use the later approach.

8. In the determination of peak dynamic response a cut-off distance R_0 equal to 30 times the radius of cavity a_0, typically R_0 = 2.9 m for a 5 kg TNT charge and 2.2 m for a 2 kg TNT charge, has been used. This is to reduce the unrealistically too high dynamic response within this distance computed by the 1D spherically symmetric model.

For points within this distance the peak dynamic response at this distance is retained. This rule also applies to the determination of peak dynamic volumetric strain used in the calculation of plastic volumetric strain.

A threshold dynamic volumetric strain equal to 0.005% is used in the calculation of plastic volumetric strain.

9. The viscosity coefficient η is calculated by the following equation

$$\eta = K_\eta \cdot W^{0.333} \cdot (\sigma'_{v0})^{0.333}$$

in which η = viscosity coefficient in kPa.s
W = TNT equivalent charge weight in kg
K_η = viscosity number
σ_{v0}' = effective overburden stress in tsf (1 tsf = 100 kPa)

10. The increment of rebound modulus constant M due to the fully consolidated volumetric strain $\Delta\varepsilon_v^p$ can be estimated using the equation

$$\Delta M = \alpha_M \cdot \Delta\varepsilon_v^p$$

The increment ΔM is added to the initial rebound modulus constant M_0 prior to consolidation of $\Delta\varepsilon_v^p$. The constant α_M may be determined from

$$\alpha_M = \frac{\alpha_1}{\alpha_2} \cdot \frac{1+e_0}{e_{max}-e_{min}} \cdot 100$$

in which e_0 = void ratio of the sand
e_{max} = maximum void ratio of the sand
e_{min} = minimum void ratio of the sand
α_1 = the tangential slope in the M - $(N_1)_{60}$ curve; i.e., $\Delta M = \alpha_1 \Delta(N_1)_{60}$
α_2 = the tangential slope in the D_r (%)-$(N_1)_{60}$ curve; i.e., $\Delta D_r = \alpha_2 \Delta(N_1)_{60}$
D_r = relative density of sand in percentage, $D_r = 100*(e_{max}-e_0)/(e_{max}-e_{min})$

11. A vertical line of points having the same x, y coordinates but decreasing z coordinates (depth) must be specified for the calculation of settlement. The settlement at a point on this line is calculated from the bottom up using

$$s = \Sigma\ \varepsilon_v^p(i) \cdot h(i)$$

where $\varepsilon_v^p(i)$ = plastic volumetric strain at the point i
h(i) = thickness of the layer between the point i and the point just above i

Therefore sufficient number of points must be used to compute the settlement at a reasonable accuracy. Normally an interval of 0.5 m in depth is used by the author. The supporting program **XYZ.EXE** may be used for generating the points where output is required.

12. Prediction of surface response is less satisfactory than prediction of response within the ground because the model is not a fully 3D model and simplification is used in modelling the free surface.

INPUT MANUAL FOR BLAST

[XYZ.EXE can be used to generate 3D nodes where output is required]

1. TITLE
   Title of the problem

2. GACCE, UNITWW, PA, AMETER, WTBL,IMSH (5F10.0,I5)
   GACCE = gravity acceleration (e.g., 9.81 m/s/s; 32.2 ft/s/s etc)
   UNITWW= unit weight of water (9.81 kN/m^3 ...)
   PA = atmospheric pressure (101. kPa...)
   AMETER= (1 meter=AMETER*unit of length); 3.28 if foot is used.
   WTBL = depth to water table
   IMSH = index for grid of mesh
   0 = regular
   1 = finer mesh
   -1 = coarser mesh

3. NPOINT, NRVSUB, DTIME, FAMPL, THETA (2I5, 3F10.0)
   NPOINT = number of integration points to be analyzed
   NRVSUB = 1
   DTIME = time increment for integration (sec), 0.00004 is recommended
   FAMPL = 0.0 not used
   THETA = 1.42
   ** time of duration = NPOINT * DTIME

4. ND3D, NCHARG, NM, NDIR, IPRINT (5I5)
   ND3D = number of points in the 3D half space where response is required
   NCHARG= number of charges arranged in the 3D half space
   NM = number of soil layers
   NDIR = direction number along which dynamic analysis is performed
   0 = regular analysis. conducting analysis in all six directions
   4 = conducting dynamic analysis in the horizontal plane only
   IPRINT= 0 do not print peak dynamic response after each charge
   1 do print

5. NNPOUT
   NNPOUT = total number of nodes and elements where time histories are required

6. (NPOUT(J), J=1, NNPOUT)
   NPOUT = node number or element number (if negative value is specified)

7. NM cards must be input for this section
   (materials must be defined from the top down)

7.1 MGROUP(I), DZMG(I) (I5,F10.0)

MGROUP = material number
DZMG = depth to which the material ends
** one of DZMG values must be equal to WTBL unless WTBL = 0.0

7.2 EMAT(I,J), J =1, 6 (6F10.0)
EMAT(I,1) = shear wave velocity
EMAT(I,2) = compressive wave velocity
EMAT(I,3) = total unit weight
EMAT(I,4) = shear strength
EMAT(I,5) = 0.0 not used
EMAT(I,6) = viscosity number $K\eta$

7.3 EMAT(I,J), J =7, 12 (6F10.0)
EMAT(I,7) = average σ_{v0}' of the layer in tsf; use $\sigma_{v0}'=1.0$ if $\sigma_{v0}' < 1.0$
EMAT(I,8) = $(N_1)_{60}$
EMAT(I,9) = volumetric strain constant B_2
EMAT(I,10) = volumetric strain constant B_1
EMAT(I,11) = rebound modulus constant M
EMAT(I,12) = the constant α_M

continued on 7.1 until NM cards are specified

8. ND3D cards must be input for this segment (use XYZ.exe to generate)
I, X(I), Y(I), Z(I), EPV0(I) (I5,3 F10.0)
I = point number
X(I) = x-coordinate of the point
Y(I) = y-coordinate of the point
Z(I) = z-coordinate of the point
EPV0(I) = volumetric strain at this point prior to this analysis (%)

9. NCHARG cards must be input for this section

9.1 ICHARG(I), XCHG(I), YCHG(I), ZCHG(I) (I5,3F10.0)
ICHARG = charge number
XCHG(I) = x-coordinate of the charge in the 3D half space
YCHG(I) = y-coordinate
ZCHG(I) = z-coordinate

9.2 WTCHG,RHOCHG,VELCHG,ALPHA, BETA (6F10.0)
(It is recommended that the equivalent TNT charge weight be used)
WTCHG = charge weight in kg
RHOCHG = density of the explosive
VELCHG = detonation velocity of the explosive, 5800.0 m/s for TNT
ALPHA = α constant, usually 1000.0
BETA = β constant, usually 2000.0

Continued 9.1 until NCHARG cards are specified

USER MANUAL FOR XYZ.EXE

1.0 NLINE (I5)
NLINE = number of lines where settlement and other response are required

2.0 X0, Y0, DEPTH2, DEPTH1, DTH (5F10.0)
X0 = x-coordinate of the line
Y0 = y-coordinate of the line
DEPTH2 = z-coordinate of the deep end of the line
DEPTH1 = z-coordinate of the shallow end of the line
DTH = uniform interval at which the line is divided

USER MANUAL FOR RETRV.EXE

Input Card 1: NDATA

NDATA = total number of time histories to be retrieved

Input Cards 2:

(ND(J), J =1, NDATA) (16I5)

list of codes indicating specific response to be retrieved from the file TH.DAT. The codes associated with the element and node number can be found in the file OUT.DAT.

Appendix C

A Listing of the Source Code for BLAST

A example input

A example output

Test5, K. & Edie; 7th charge; BLAST5
9.81,9.81,100.0,1.0,1.0,1,
250,0,4.0E-5,1.0,1.42,
203,1,5,0,0,
5,
228,-114,
1,1.0,
100.1,560.0,18.0,15.0,0.40,50.0, dry coarse sand
1.0,0.00,0.40,0.00,0.032,0.0,
2,3.0,
120.1,1520.0,18.0,30.0,0.40,55.0, sat. loose coarse sand N1= 10
1.0,0.00,0.040,4.94,260.0,4770.0,
3,6.0,
150.1,1540.0,17.0,50.0,0.40,55.5, loose fine sand N1=10
1.0,0.00,0.040,4.94,260.0,4770.0,
4,10.0,
160.1,1560.0,17.0,50.0,0.40,63.0, loose fine sand N1 = 14
1.0,0.00,0.056,3.58,340.0,4770.0,
5,100.0,
170.1,1580.0,17.0,50.0,0.40,84.0, loose fine sand N1 = 20
1.0,0.00,0.096,2.08,448.0,4770.0,

1	0.000	0.000	14.000	0.3190
2	0.000	0.000	13.500	0.3640
3	0.000	0.000	13.000	0.4150
4	0.000	0.000	12.500	0.4730
5	0.000	0.000	12.000	0.5520
6	0.000	0.000	11.500	0.6460
7	0.000	0.000	11.000	0.7750
8	0.000	0.000	10.500	0.9510
9	0.000	0.000	10.000	1.2030
10	0.000	0.000	9.500	2.7110
11	0.000	0.000	9.000	3.6320
12	0.000	0.000	8.500	4.3040
13	0.000	0.000	8.000	4.4650
14	0.000	0.000	7.500	4.4650
15	0.000	0.000	7.000	4.4650
16	0.000	0.000	6.500	4.6230
17	0.000	0.000	6.000	4.6230
18	0.000	0.000	5.500	6.1780
19	0.000	0.000	5.000	5.2210
20	0.000	0.000	4.500	3.9050
21	0.000	0.000	4.000	3.0700
22	0.000	0.000	3.500	2.4740
23	0.000	0.000	3.000	2.0270
24	0.000	0.000	2.500	1.7150
25	0.000	0.000	2.000	1.4780
26	0.000	0.000	1.500	1.1990
27	0.000	0.000	1.000	4.6240
28	0.000	0.000	0.500	0.0000
29	0.000	0.000	0.000	0.0000
30	0.000	1.000	14.000	0.3100
31	0.000	1.000	13.500	0.3540
32	0.000	1.000	13.000	0.4030
33	0.000	1.000	12.500	0.4590
34	0.000	1.000	12.000	0.5340
35	0.000	1.000	11.500	0.6270
36	0.000	1.000	11.000	0.7490
37	0.000	1.000	10.500	0.8970
38	0.000	1.000	10.000	1.1080

39	0.000	1.000	9.500	2.4580
40	0.000	1.000	9.000	3.1730
41	0.000	1.000	8.500	4.1280
42	0.000	1.000	8.000	4.3560
43	0.000	1.000	7.500	4.4650
44	0.000	1.000	7.000	4.4650
45	0.000	1.000	6.500	4.4410
46	0.000	1.000	6.000	4.3320
47	0.000	1.000	5.500	5.9130
48	0.000	1.000	5.000	4.5490
49	0.000	1.000	4.500	3.5120
50	0.000	1.000	4.000	2.8380
51	0.000	1.000	3.500	2.3380
52	0.000	1.000	3.000	1.9630
53	0.000	1.000	2.500	1.6660
54	0.000	1.000	2.000	1.4360
55	0.000	1.000	1.500	1.0770
56	0.000	1.000	1.000	4.1800
57	0.000	1.000	0.500	0.0000
58	0.000	1.000	0.000	0.0000
59	9.000	2.000	14.000	0.1290
60	9.000	2.000	13.500	0.1380
61	9.000	2.000	13.000	0.1430
62	9.000	2.000	12.500	0.1490
63	9.000	2.000	12.000	0.1600
64	9.000	2.000	11.500	0.1660
65	9.000	2.000	11.000	0.1720
66	9.000	2.000	10.500	0.2000
67	9.000	2.000	10.000	0.2070
68	9.000	2.000	9.500	0.3580
69	9.000	2.000	9.000	0.3680
70	9.000	2.000	8.500	0.3700
71	9.000	2.000	8.000	0.3810
72	9.000	2.000	7.500	0.3820
73	9.000	2.000	7.000	0.3830
74	9.000	2.000	6.500	0.3820
75	9.000	2.000	6.000	0.3810
76	9.000	2.000	5.500	0.5130
77	9.000	2.000	5.000	0.5100
78	9.000	2.000	4.500	0.5250
79	9.000	2.000	4.000	0.5220
80	9.000	2.000	3.500	0.5050
81	9.000	2.000	3.000	0.4880
82	9.000	2.000	2.500	0.4710
83	9.000	2.000	2.000	0.4550
84	9.000	2.000	1.500	0.4280
85	9.000	2.000	1.000	0.4090
86	9.000	2.000	0.500	0.0000
87	9.000	2.000	0.000	0.0000
88	0.000	3.000	14.000	0.2850
89	0.000	3.000	13.500	0.3150
90	0.000	3.000	13.000	0.3510
91	0.000	3.000	12.500	0.3990
92	0.000	3.000	12.000	0.4420
93	0.000	3.000	11.500	0.5010
94	0.000	3.000	11.000	0.5670
95	0.000	3.000	10.500	0.6450
96	0.000	3.000	10.000	0.7320
97	0.000	3.000	9.500	1.4520

98	0.000	3.000	9.000	1.6160
99	0.000	3.000	8.500	1.8090
100	0.000	3.000	8.000	1.9650
101	0.000	3.000	7.500	2.0760
102	0.000	3.000	7.000	2.1240
103	0.000	3.000	6.500	2.0760
104	0.000	3.000	6.000	2.0310
105	0.000	3.000	5.500	2.5910
106	0.000	3.000	5.000	2.3240
107	0.000	3.000	4.500	2.0800
108	0.000	3.000	4.000	1.8590
109	0.000	3.000	3.500	1.6690
110	0.000	3.000	3.000	1.4720
111	0.000	3.000	2.500	1.3150
112	0.000	3.000	2.000	1.1720
113	0.000	3.000	1.500	1.0440
114	0.000	3.000	1.000	0.5910
115	0.000	3.000	0.500	0.0000
116	0.000	3.000	0.000	0.0000
117	0.000	5.000	14.000	0.2310
118	0.000	5.000	13.500	0.2480
119	0.000	5.000	13.000	0.2670
120	0.000	5.000	12.500	0.2950
121	0.000	5.000	12.000	0.3170
122	0.000	5.000	11.500	0.3490
123	0.000	5.000	11.000	0.3750
124	0.000	5.000	10.500	0.4120
125	0.000	5.000	10.000	0.4420
126	0.000	5.000	9.500	0.8090
127	0.000	5.000	9.000	0.9070
128	0.000	5.000	8.500	0.9580
129	0.000	5.000	8.000	0.9870
130	0.000	5.000	7.500	1.0160
131	0.000	5.000	7.000	1.0160
132	0.000	5.000	6.500	1.0160
133	0.000	5.000	6.000	0.9870
134	0.000	5.000	5.500	1.3870
135	0.000	5.000	5.000	1.3160
136	0.000	5.000	4.500	1.2380
137	0.000	5.000	4.000	1.1680
138	0.000	5.000	3.500	1.0950
139	0.000	5.000	3.000	1.0050
140	0.000	5.000	2.500	0.9390
141	0.000	5.000	2.000	0.8610
142	0.000	5.000	1.500	2.7760
143	0.000	5.000	1.000	1.1260
144	0.000	5.000	0.500	0.0000
145	0.000	5.000	0.000	0.0000
146	0.000	7.000	14.000	0.1730
147	0.000	7.000	13.500	0.1870
148	0.000	7.000	13.000	0.2010
149	0.000	7.000	12.500	0.2150
150	0.000	7.000	12.000	0.2310
151	0.000	7.000	11.500	0.2410
152	0.000	7.000	11.000	0.2570
153	0.000	7.000	10.500	0.2670
154	0.000	7.000	10.000	0.2850
155	0.000	7.000	9.500	0.5500
156	0.000	7.000	9.000	0.5680

157	0.000	7.000	8.500	0.5860
158	0.000	7.000	8.000	0.5890
159	0.000	7.000	7.500	0.6050
160	0.000	7.000	7.000	0.6050
161	0.000	7.000	6.500	0.6050
162	0.000	7.000	6.000	0.5890
163	0.000	7.000	5.500	0.8120
164	0.000	7.000	5.000	0.8320
165	0.000	7.000	4.500	0.8070
166	0.000	7.000	4.000	0.7850
167	0.000	7.000	3.500	0.7520
168	0.000	7.000	3.000	0.7020
169	0.000	7.000	2.500	0.6620
170	0.000	7.000	2.000	0.6370
171	0.000	7.000	1.500	0.5970
172	0.000	7.000	1.000	0.5610
173	0.000	7.000	0.500	0.0000
174	0.000	7.000	0.000	0.0000
175	0.000	10.000	14.000	0.1160
176	0.000	10.000	13.500	0.1200
177	0.000	10.000	13.000	0.1280
178	0.000	10.000	12.500	0.1330
179	0.000	10.000	12.000	0.1390
180	0.000	10.000	11.500	0.1440
181	0.000	10.000	11.000	0.1690
182	0.000	10.000	10.500	0.1730
183	0.000	10.000	10.000	0.1790
184	0.000	10.000	9.500	0.3100
185	0.000	10.000	9.000	0.3200
186	0.000	10.000	8.500	0.3220
187	0.000	10.000	8.000	0.3310
188	0.000	10.000	7.500	0.3310
189	0.000	10.000	7.000	0.3310
190	0.000	10.000	6.500	0.3310
191	0.000	10.000	6.000	0.3310
192	0.000	10.000	5.500	0.4460
193	0.000	10.000	5.000	0.4430
194	0.000	10.000	4.500	0.4300
195	0.000	10.000	4.000	0.4550
196	0.000	10.000	3.500	0.4400
197	0.000	10.000	3.000	0.4280
198	0.000	10.000	2.500	0.4120
199	0.000	10.000	2.000	0.3900
200	0.000	10.000	1.500	0.3490
201	0.000	10.000	1.000	0.2850
202	0.000	10.000	0.500	0.0000
203	0.000	10.000	0.000	0.0000

1,0.0,0.0,7.0,

1.20,1.30,5800.0,1000.0,2000.0,

```
**************************************************
|                                                |
|     >>>>>  BLAST  <<<<<                        |
|                                                |
|    Simulation of the Response of Saturated Soil |
|    to Blast Loads                              |
|                                                |
|    Coded by:  Dr. Guoxi Wu, October, 1996      |
**************************************************
```

INPUT:inp.dat; OUTPUT: out.dat,charges,vol.dat,th.dat

Test5, K. & Edie; 7th charge; BLAST5

TYPE OF ANALYSIS = NON-LINEAR ANALYSIS: BLAST5
TOTAL NUMBER OF INTEGRATION 250
TOTAL NO. OF TIME HISTORY OUTPUT 5
TIME INCREMENT FOR INTEGRATION 0.00004000
UNIT WEIGHT OF WATER 9.81
GRAVITY ACCELERATION 9.81
AMPLIFACTION OF ACCELERATION 1.00
ATMOSPHERIC PRESSURE 100.00

ND3D	NCHARG	NM	NRVSUB	THETA	AMETER	WTBL	IMSH
203	1	5	0	1.420	1.000	1.000	0

NDIR = 0 IPRINT = 0

	Vs	Vp	Unit.W	TAUmax	Porosity	Visc.	(soil)
	SIGV0		U_B1	U_B2	M	ALPHA	DzMat (soil)
1 soil	100.1	560.0	18.00	15.0	0.4	50.00	
	1.000	0.000	0.400	0.000	0.032	0.000	1.00
2 soil	120.1	1520.0	18.00	30.0	0.4	55.00	
	1.000	0.000	0.040	4.940	260.000	4770.000	3.00
3 soil	150.1	1540.0	17.00	50.0	0.4	55.50	
	1.000	0.000	0.040	4.940	260.000	4770.000	6.00
4 soil	160.1	1560.0	17.00	50.0	0.4	63.00	
	1.000	0.000	0.056	3.580	340.000	4770.000	10.00
5 soil	170.1	1580.0	17.00	50.0	0.4	84.00	
	1.000	0.000	0.096	2.080	448.000	4770.000	100.00

NODE	MAT NO.	X-CORD	Y-CORD	Z-CORD	EPV0.(%)	EFFEC. OVER. STRESS

(EPV0 = volumetric strain prior to this analysis)

1	5	0.00	0.00	14.00	0.32	113.47
2	5	0.00	0.00	13.50	0.36	109.87
3	5	0.00	0.00	13.00	0.41	106.28
4	5	0.00	0.00	12.50	0.47	102.68
5	5	0.00	0.00	12.00	0.55	99.09
6	5	0.00	0.00	11.50	0.65	95.49

7	5	0.00	0.00	11.00	0.78	91.90
8	5	0.00	0.00	10.50	0.95	88.30
9	5	0.00	0.00	10.00	1.20	84.71
10	4	0.00	0.00	9.50	2.71	81.11
11	4	0.00	0.00	9.00	3.63	77.52
12	4	0.00	0.00	8.50	4.30	73.92
13	4	0.00	0.00	8.00	4.46	70.33
14	4	0.00	0.00	7.50	4.46	66.73
15	4	0.00	0.00	7.00	4.46	63.14
16	4	0.00	0.00	6.50	4.62	59.54
17	4	0.00	0.00	6.00	4.62	55.95
18	3	0.00	0.00	5.50	6.18	52.35
19	3	0.00	0.00	5.00	5.22	48.76
20	3	0.00	0.00	4.50	3.90	45.16
21	3	0.00	0.00	4.00	3.07	41.57
22	3	0.00	0.00	3.50	2.47	37.97
23	3	0.00	0.00	3.00	2.03	34.38
24	2	0.00	0.00	2.50	1.72	30.29
25	2	0.00	0.00	2.00	1.48	26.19
26	2	0.00	0.00	1.50	1.20	22.09
27	2	0.00	0.00	1.00	4.62	18.00
28	1	0.00	0.00	0.50	0.00	9.00
29	1	0.00	0.00	0.00	0.00	0.00
30	5	0.00	1.00	14.00	0.31	113.47
31	5	0.00	1.00	13.50	0.35	109.87
32	5	0.00	1.00	13.00	0.40	106.28
33	5	0.00	1.00	12.50	0.46	102.68
34	5	0.00	1.00	12.00	0.53	99.09
35	5	0.00	1.00	11.50	0.63	95.49
36	5	0.00	1.00	11.00	0.75	91.90
37	5	0.00	1.00	10.50	0.90	88.30
38	5	0.00	1.00	10.00	1.11	84.71
39	4	0.00	1.00	9.50	2.46	81.11
40	4	0.00	1.00	9.00	3.17	77.52
41	4	0.00	1.00	8.50	4.13	73.92
42	4	0.00	1.00	8.00	4.36	70.33
43	4	0.00	1.00	7.50	4.46	66.73
44	4	0.00	1.00	7.00	4.46	63.14
45	4	0.00	1.00	6.50	4.44	59.54
46	4	0.00	1.00	6.00	4.33	55.95
47	3	0.00	1.00	5.50	5.91	52.35
48	3	0.00	1.00	5.00	4.55	48.76
49	3	0.00	1.00	4.50	3.51	45.16
50	3	0.00	1.00	4.00	2.84	41.57
51	3	0.00	1.00	3.50	2.34	37.97
52	3	0.00	1.00	3.00	1.96	34.38
53	2	0.00	1.00	2.50	1.67	30.29
54	2	0.00	1.00	2.00	1.44	26.19
55	2	0.00	1.00	1.50	1.08	22.09
56	2	0.00	1.00	1.00	4.18	18.00
57	1	0.00	1.00	0.50	0.00	9.00
58	1	0.00	1.00	0.00	0.00	0.00
59	5	9.00	2.00	14.00	0.13	113.47
60	5	9.00	2.00	13.50	0.14	109.87
61	5	9.00	2.00	13.00	0.14	106.28
62	5	9.00	2.00	12.50	0.15	102.68
63	5	9.00	2.00	12.00	0.16	99.09
64	5	9.00	2.00	11.50	0.17	95.49
65	5	9.00	2.00	11.00	0.17	91.90

66	5	9.00	2.00	10.50	0.20	88.30
67	5	9.00	2.00	10.00	0.21	84.71
68	4	9.00	2.00	9.50	0.36	81.11
69	4	9.00	2.00	9.00	0.37	77.52
70	4	9.00	2.00	8.50	0.37	73.92
71	4	9.00	2.00	8.00	0.38	70.33
72	4	9.00	2.00	7.50	0.38	66.73
73	4	9.00	2.00	7.00	0.38	63.14
74	4	9.00	2.00	6.50	0.38	59.54
75	4	9.00	2.00	6.00	0.38	55.95
76	3	9.00	2.00	5.50	0.51	52.35
77	3	9.00	2.00	5.00	0.51	48.76
78	3	9.00	2.00	4.50	0.53	45.16
79	3	9.00	2.00	4.00	0.52	41.57
80	3	9.00	2.00	3.50	0.51	37.97
81	3	9.00	2.00	3.00	0.49	34.38
82	2	9.00	2.00	2.50	0.47	30.29
83	2	9.00	2.00	2.00	0.46	26.19
84	2	9.00	2.00	1.50	0.43	22.09
85	2	9.00	2.00	1.00	0.41	18.00
86	1	9.00	2.00	0.50	0.00	9.00
87	1	9.00	2.00	0.00	0.00	0.00
88	5	0.00	3.00	14.00	0.28	113.47
89	5	0.00	3.00	13.50	0.32	109.87
90	5	0.00	3.00	13.00	0.35	106.28
91	5	0.00	3.00	12.50	0.40	102.68
92	5	0.00	3.00	12.00	0.44	99.09
93	5	0.00	3.00	11.50	0.50	95.49
94	5	0.00	3.00	11.00	0.57	91.90
95	5	0.00	3.00	10.50	0.65	88.30
96	5	0.00	3.00	10.00	0.73	84.71
97	4	0.00	3.00	9.50	1.45	81.11
98	4	0.00	3.00	9.00	1.62	77.52
99	4	0.00	3.00	8.50	1.81	73.92
100	4	0.00	3.00	8.00	1.97	70.33
101	4	0.00	3.00	7.50	2.08	66.73
102	4	0.00	3.00	7.00	2.12	63.14
103	4	0.00	3.00	6.50	2.08	59.54
104	4	0.00	3.00	6.00	2.03	55.95
105	3	0.00	3.00	5.50	2.59	52.35
106	3	0.00	3.00	5.00	2.32	48.76
107	3	0.00	3.00	4.50	2.08	45.16
108	3	0.00	3.00	4.00	1.86	41.57
109	3	0.00	3.00	3.50	1.67	37.97
110	3	0.00	3.00	3.00	1.47	34.38
111	2	0.00	3.00	2.50	1.31	30.29
112	2	0.00	3.00	2.00	1.17	26.19
113	2	0.00	3.00	1.50	1.04	22.09
114	2	0.00	3.00	1.00	0.59	18.00
115	1	0.00	3.00	0.50	0.00	9.00
116	1	0.00	3.00	0.00	0.00	0.00
117	5	0.00	5.00	14.00	0.23	113.47
118	5	0.00	5.00	13.50	0.25	109.87
119	5	0.00	5.00	13.00	0.27	106.28
120	5	0.00	5.00	12.50	0.29	102.68
121	5	0.00	5.00	12.00	0.32	99.09
122	5	0.00	5.00	11.50	0.35	95.49
123	5	0.00	5.00	11.00	0.38	91.90
124	5	0.00	5.00	10.50	0.41	88.30

125	5	0.00	5.00	10.00	0.44	84.71
126	4	0.00	5.00	9.50	0.81	81.11
127	4	0.00	5.00	9.00	0.91	77.52
128	4	0.00	5.00	8.50	0.96	73.92
129	4	0.00	5.00	8.00	0.99	70.33
130	4	0.00	5.00	7.50	1.02	66.73
131	4	0.00	5.00	7.00	1.02	63.14
132	4	0.00	5.00	6.50	1.02	59.54
133	4	0.00	5.00	6.00	0.99	55.95
134	3	0.00	5.00	5.50	1.39	52.35
135	3	0.00	5.00	5.00	1.32	48.76
136	3	0.00	5.00	4.50	1.24	45.16
137	3	0.00	5.00	4.00	1.17	41.57
138	3	0.00	5.00	3.50	1.09	37.97
139	3	0.00	5.00	3.00	1.00	34.38
140	2	0.00	5.00	2.50	0.94	30.29
141	2	0.00	5.00	2.00	0.86	26.19
142	2	0.00	5.00	1.50	2.78	22.09
143	2	0.00	5.00	1.00	1.13	18.00
144	1	0.00	5.00	0.50	0.00	9.00
145	1	0.00	5.00	0.00	0.00	0.00
146	5	0.00	7.00	14.00	0.17	113.47
147	5	0.00	7.00	13.50	0.19	109.87
148	5	0.00	7.00	13.00	0.20	106.28
149	5	0.00	7.00	12.50	0.21	102.68
150	5	0.00	7.00	12.00	0.23	99.09
151	5	0.00	7.00	11.50	0.24	95.49
152	5	0.00	7.00	11.00	0.26	91.90
153	5	0.00	7.00	10.50	0.27	88.30
154	5	0.00	7.00	10.00	0.28	84.71
155	4	0.00	7.00	9.50	0.55	81.11
156	4	0.00	7.00	9.00	0.57	77.52
157	4	0.00	7.00	8.50	0.59	73.92
158	4	0.00	7.00	8.00	0.59	70.33
159	4	0.00	7.00	7.50	0.60	66.73
160	4	0.00	7.00	7.00	0.60	63.14
161	4	0.00	7.00	6.50	0.60	59.54
162	4	0.00	7.00	6.00	0.59	55.95
163	3	0.00	7.00	5.50	0.81	52.35
164	3	0.00	7.00	5.00	0.83	48.76
165	3	0.00	7.00	4.50	0.81	45.16
166	3	0.00	7.00	4.00	0.79	41.57
167	3	0.00	7.00	3.50	0.75	37.97
168	3	0.00	7.00	3.00	0.70	34.38
169	2	0.00	7.00	2.50	0.66	30.29
170	2	0.00	7.00	2.00	0.64	26.19
171	2	0.00	7.00	1.50	0.60	22.09
172	2	0.00	7.00	1.00	0.56	18.00
173	1	0.00	7.00	0.50	0.00	9.00
174	1	0.00	7.00	0.00	0.00	0.00
175	5	0.00	10.00	14.00	0.12	113.47
176	5	0.00	10.00	13.50	0.12	109.87
177	5	0.00	10.00	13.00	0.13	106.28
178	5	0.00	10.00	12.50	0.13	102.68
179	5	0.00	10.00	12.00	0.14	99.09
180	5	0.00	10.00	11.50	0.14	95.49
181	5	0.00	10.00	11.00	0.17	91.90
182	5	0.00	10.00	10.50	0.17	88.30
183	5	0.00	10.00	10.00	0.18	84.71

184	4	0.00	10.00	9.50	0.31	81.11
185	4	0.00	10.00	9.00	0.32	77.52
186	4	0.00	10.00	8.50	0.32	73.92
187	4	0.00	10.00	8.00	0.33	70.33
188	4	0.00	10.00	7.50	0.33	66.73
189	4	0.00	10.00	7.00	0.33	63.14
190	4	0.00	10.00	6.50	0.33	59.54
191	4	0.00	10.00	6.00	0.33	55.95
192	3	0.00	10.00	5.50	0.45	52.35
193	3	0.00	10.00	5.00	0.44	48.76
194	3	0.00	10.00	4.50	0.43	45.16
195	3	0.00	10.00	4.00	0.46	41.57
196	3	0.00	10.00	3.50	0.44	37.97
197	3	0.00	10.00	3.00	0.43	34.38
198	2	0.00	10.00	2.50	0.41	30.29
199	2	0.00	10.00	2.00	0.39	26.19
200	2	0.00	10.00	1.50	0.35	22.09
201	2	0.00	10.00	1.00	0.28	18.00
202	1	0.00	10.00	0.50	0.00	9.00
203	1	0.00	10.00	0.00	0.00	0.00

Dealing Charge No. 1 DIRECTION NO. 1

Dealing Charge No. 1 DIRECTION NO. 2

Dealing Charge No. 1 DIRECTION NO. 3

Dealing Charge No. 1 DIRECTION NO. 4

Dealing Charge No. 1 DIRECTION NO. 5

Dealing Charge No. 1 DIRECTION NO. 6

****** PEAK DYNAMIC RESPONSE DURING BLASTING **

NODE	X	Y	Z	ACC(g)	VELO	PRESSURE	SH.STRAIN(%)	VOL.STRAIN(%)
1	0.00	0.00	14.00	142.379	0.815	2012.62	0.06	0.05
2	0.00	0.00	13.50	161.706	0.919	2261.33	0.07	0.05
3	0.00	0.00	13.00	183.839	1.040	2544.96	0.08	0.06
4	0.00	0.00	12.50	214.652	1.174	2856.79	0.10	0.07
5	0.00	0.00	12.00	261.128	1.367	3307.73	0.11	0.08
6	0.00	0.00	11.50	316.818	1.587	3818.69	0.13	0.09
7	0.00	0.00	11.00	401.494	1.903	4531.30	0.16	0.11
8	0.00	0.00	10.50	527.969	2.350	5537.92	0.21	0.13
9	0.00	0.00	10.00	722.765	2.982	6945.31	0.27	0.16
10	0.00	0.00	9.501008.547		3.871	8814.95	0.38	0.21
11	0.00	0.00	9.001483.502		5.276	11682.38	0.56	0.28
12	0.00	0.00	8.501771.330		6.059	13244.65	0.64	0.32
13	0.00	0.00	8.001771.330		6.059	13244.65	0.64	0.32
14	0.00	0.00	7.501771.330		6.059	13244.65	0.64	0.32
15	0.00	0.00	7.001771.330		6.059	13244.65	0.64	0.32
16	0.00	0.00	6.501832.316		6.169	13404.30	0.66	0.33
17	0.00	0.00	6.001832.316		6.169	13404.30	0.66	0.33
18	0.00	0.00	5.501832.316		6.169	13404.30	0.66	0.33
19	0.00	0.00	5.001540.242		5.380	11835.13	0.58	0.29
20	0.00	0.00	4.501043.830		3.969	8941.92	0.38	0.22
21	0.00	0.00	4.00	759.761	3.089	7078.33	0.29	0.17

22	0.00	0.00	3.50	570.466	2.459	5742.72	0.22	0.14
23	0.00	0.00	3.00	436.746	1.985	4893.88	0.17	0.12
24	0.00	0.00	2.50	352.787	1.676	4173.56	0.14	0.10
25	0.00	0.00	2.00	294.608	1.454	3644.01	0.12	0.09
26	0.00	0.00	1.50	258.867	1.401	2959.07	0.10	0.07
27	0.00	0.00	1.00	291.450	1.476	1427.83	0.29	0.26
28	0.00	0.00	0.50	142.046	0.980	1080.34	0.19	0.20
29	0.00	0.00	0.00	0.000	0.000	0.00	0.00	0.00
30	0.00	1.00	14.00	137.685	0.790	1953.40	0.06	0.05
31	0.00	1.00	13.50	156.453	0.892	2196.47	0.07	0.05
32	0.00	1.00	13.00	178.090	1.008	2470.40	0.08	0.06
33	0.00	1.00	12.50	206.155	1.140	2778.40	0.09	0.07
34	0.00	1.00	12.00	251.160	1.325	3213.14	0.11	0.08
35	0.00	1.00	11.50	305.715	1.543	3713.32	0.13	0.09
36	0.00	1.00	11.00	386.708	1.847	4410.77	0.16	0.10
37	0.00	1.00	10.50	488.907	2.211	5222.05	0.20	0.12
38	0.00	1.00	10.00	641.448	2.726	6381.78	0.25	0.15
39	0.00	1.00	9.50	866.848	3.444	7985.44	0.33	0.19
40	0.00	1.00	9.00	1250.152	4.593	10279.74	0.46	0.25
41	0.00	1.00	8.50	1771.330	6.059	13244.65	0.64	0.32
42	0.00	1.00	8.00	1771.330	6.059	13244.65	0.64	0.32
43	0.00	1.00	7.50	1771.330	6.059	13244.65	0.64	0.32
44	0.00	1.00	7.00	1771.330	6.059	13244.65	0.64	0.32
45	0.00	1.00	6.50	1779.801	6.094	13152.38	0.63	0.32
46	0.00	1.00	6.00	1779.801	6.094	13152.38	0.63	0.32
47	0.00	1.00	5.50	1823.443	6.155	13366.68	0.66	0.33
48	0.00	1.00	5.00	1289.967	4.674	10378.40	0.48	0.26
49	0.00	1.00	4.50	907.082	3.540	8024.80	0.34	0.20
50	0.00	1.00	4.00	682.252	2.835	6531.89	0.26	0.16
51	0.00	1.00	3.50	531.703	2.329	5433.99	0.21	0.13
52	0.00	1.00	3.00	421.341	1.927	4765.59	0.17	0.11
53	0.00	1.00	2.50	339.231	1.631	4061.87	0.14	0.10
54	0.00	1.00	2.00	284.113	1.418	3546.79	0.12	0.08
55	0.00	1.00	1.50	268.564	1.479	2660.93	0.09	0.06
56	0.00	1.00	1.00	239.283	1.312	1267.35	0.26	0.23
57	0.00	1.00	0.50	127.467	0.974	1028.35	0.17	0.19
58	0.00	1.00	0.00	0.000	0.000	0.00	0.00	0.00
59	9.00	2.00	14.00	62.577	0.375	949.90	0.03	0.02
60	9.00	2.00	13.50	66.399	0.397	1002.26	0.03	0.02
61	9.00	2.00	13.00	68.531	0.408	1030.10	0.03	0.02
62	9.00	2.00	12.50	70.761	0.420	1060.19	0.03	0.02
63	9.00	2.00	12.00	75.360	0.446	1124.12	0.03	0.03
64	9.00	2.00	11.50	77.977	0.460	1158.10	0.03	0.03
65	9.00	2.00	11.00	80.681	0.474	1193.51	0.04	0.03
66	9.00	2.00	10.50	93.823	0.526	1315.61	0.04	0.03
67	9.00	2.00	10.00	96.928	0.542	1354.34	0.04	0.03
68	9.00	2.00	9.50	96.928	0.542	1354.34	0.04	0.03
69	9.00	2.00	9.00	100.074	0.559	1394.20	0.04	0.03
70	9.00	2.00	8.50	100.074	0.559	1394.20	0.04	0.03
71	9.00	2.00	8.00	103.296	0.576	1435.31	0.04	0.03
72	9.00	2.00	7.50	103.296	0.576	1435.31	0.04	0.03
73	9.00	2.00	7.00	103.296	0.576	1435.31	0.04	0.03
74	9.00	2.00	6.50	103.296	0.576	1435.31	0.04	0.03
75	9.00	2.00	6.00	103.296	0.576	1435.31	0.04	0.03
76	9.00	2.00	5.50	100.074	0.559	1394.20	0.04	0.03
77	9.00	2.00	5.00	100.074	0.559	1394.20	0.04	0.03
78	9.00	2.00	4.50	100.988	0.553	1436.03	0.04	0.03
79	9.00	2.00	4.00	100.988	0.553	1436.03	0.04	0.03
80	9.00	2.00	3.50	97.948	0.537	1395.91	0.04	0.03

81	9.00	2.00	3.00	94.829	0.521	1356.21	0.04	0.03
82	9.00	2.00	2.50	91.958	0.506	1316.88	0.04	0.03
83	9.00	2.00	2.00	88.890	0.492	1281.92	0.04	0.03
84	9.00	2.00	1.50	77.891	0.466	1212.32	0.04	0.03
85	9.00	2.00	1.00	67.187	0.458	1174.21	0.03	0.03
86	9.00	2.00	0.50	65.921	0.460	1122.07	0.03	0.03
87	9.00	2.00	0.00	0.000	0.000	0.00	0.00	0.00
88	0.00	3.00	14.00	128.956	0.733	1820.57	0.06	0.04
89	0.00	3.00	13.50	142.200	0.804	1991.55	0.06	0.05
90	0.00	3.00	13.00	156.980	0.883	2181.07	0.07	0.05
91	0.00	3.00	12.50	178.774	0.999	2456.31	0.08	0.06
92	0.00	3.00	12.00	198.273	1.096	2684.38	0.09	0.06
93	0.00	3.00	11.50	232.285	1.239	3021.48	0.10	0.07
94	0.00	3.00	11.00	273.192	1.400	3392.20	0.12	0.08
95	0.00	3.00	10.50	319.966	1.582	3814.93	0.13	0.09
96	0.00	3.00	10.00	376.236	1.786	4293.94	0.15	0.10
97	0.00	3.00	9.50	437.515	2.009	4806.50	0.18	0.12
98	0.00	3.00	9.00	508.611	2.263	5322.00	0.20	0.13
99	0.00	3.00	8.50	587.857	2.541	5932.72	0.23	0.14
100	0.00	3.00	8.00	654.910	2.764	6423.43	0.25	0.15
101	0.00	3.00	7.50	704.478	2.925	6772.42	0.27	0.16
102	0.00	3.00	7.00	730.727	3.009	6954.32	0.28	0.17
103	0.00	3.00	6.50	704.478	2.925	6772.42	0.27	0.16
104	0.00	3.00	6.00	673.080	2.812	6474.72	0.26	0.16
105	0.00	3.00	5.50	604.922	2.586	5980.87	0.23	0.15
106	0.00	3.00	5.00	522.681	2.310	5385.79	0.20	0.13
107	0.00	3.00	4.50	453.857	2.063	4842.78	0.18	0.12
108	0.00	3.00	4.00	392.580	1.845	4352.43	0.16	0.11
109	0.00	3.00	3.50	337.503	1.626	4049.76	0.14	0.10
110	0.00	3.00	3.00	292.291	1.450	3630.13	0.12	0.09
111	0.00	3.00	2.50	253.851	1.295	3261.08	0.11	0.08
112	0.00	3.00	2.00	219.277	1.156	2923.15	0.10	0.07
113	0.00	3.00	1.50	199.129	1.095	2638.05	0.08	0.06
114	0.00	3.00	1.00	260.389	1.295	1526.52	0.06	0.04
115	0.00	3.00	0.50	161.001	0.953	926.10	0.19	0.17
116	0.00	3.00	0.00	0.000	0.000	0.00	0.00	0.00
117	0.00	5.00	14.00	105.629	0.609	1520.39	0.05	0.04
118	0.00	5.00	13.50	112.867	0.647	1615.24	0.05	0.04
119	0.00	5.00	13.00	120.697	0.689	1715.68	0.05	0.04
120	0.00	5.00	12.50	133.095	0.757	1878.24	0.06	0.04
121	0.00	5.00	12.00	142.200	0.804	1991.55	0.06	0.05
122	0.00	5.00	11.50	156.980	0.883	2181.07	0.07	0.05
123	0.00	5.00	11.00	167.327	0.939	2314.56	0.08	0.05
124	0.00	5.00	10.50	184.699	1.031	2530.48	0.08	0.06
125	0.00	5.00	10.00	198.273	1.096	2684.38	0.09	0.06
126	0.00	5.00	9.50	215.132	1.164	2844.25	0.10	0.07
127	0.00	5.00	9.00	244.360	1.276	3086.13	0.10	0.07
128	0.00	5.00	8.50	262.593	1.352	3263.28	0.11	0.08
129	0.00	5.00	8.00	273.009	1.392	3354.01	0.12	0.08
130	0.00	5.00	7.50	282.286	1.430	3444.15	0.12	0.08
131	0.00	5.00	7.00	282.286	1.430	3444.15	0.12	0.08
132	0.00	5.00	6.50	282.286	1.430	3444.15	0.12	0.08
133	0.00	5.00	6.00	273.009	1.392	3354.01	0.12	0.08
134	0.00	5.00	5.50	273.770	1.386	3315.07	0.12	0.08
135	0.00	5.00	5.00	255.312	1.311	3145.09	0.11	0.08
136	0.00	5.00	4.50	237.172	1.236	2972.17	0.10	0.07
137	0.00	5.00	4.00	220.793	1.168	2816.13	0.10	0.07
138	0.00	5.00	3.50	207.065	1.103	2665.97	0.09	0.07
139	0.00	5.00	3.00	189.592	1.011	2452.43	0.08	0.06

140	0.00	5.00	2.50	178.637	0.953	2316.63	0.08	0.06
141	0.00	5.00	2.00	164.789	0.874	2133.43	0.07	0.05
142	0.00	5.00	1.50	107.119	0.785	858.84	0.16	0.16
143	0.00	5.00	1.00	161.810	1.120	358.85	0.06	0.06
144	0.00	5.00	0.50	161.810	1.120	358.85	0.06	0.06
145	0.00	5.00	0.00	0.000	0.000	0.00	0.00	0.00
146	0.00	7.00	14.00	80.681	0.474	1193.51	0.04	0.03
147	0.00	7.00	13.50	86.246	0.505	1267.88	0.04	0.03
148	0.00	7.00	13.00	92.238	0.537	1347.70	0.04	0.03
149	0.00	7.00	12.50	98.634	0.572	1432.45	0.04	0.03
150	0.00	7.00	12.00	105.629	0.609	1520.39	0.05	0.04
151	0.00	7.00	11.50	109.222	0.628	1568.35	0.05	0.04
152	0.00	7.00	11.00	116.654	0.668	1665.42	0.05	0.04
153	0.00	7.00	10.50	120.697	0.689	1715.68	0.05	0.04
154	0.00	7.00	10.00	128.956	0.733	1820.57	0.06	0.04
155	0.00	7.00	9.50	145.521	0.799	1968.55	0.06	0.05
156	0.00	7.00	9.00	150.094	0.821	2023.05	0.06	0.05
157	0.00	7.00	8.50	154.879	0.847	2083.94	0.07	0.05
158	0.00	7.00	8.00	154.879	0.847	2083.94	0.07	0.05
159	0.00	7.00	7.50	159.346	0.873	2144.14	0.07	0.05
160	0.00	7.00	7.00	159.346	0.873	2144.14	0.07	0.05
161	0.00	7.00	6.50	159.346	0.873	2144.14	0.07	0.05
162	0.00	7.00	6.00	154.879	0.847	2083.94	0.07	0.05
163	0.00	7.00	5.50	154.879	0.847	2083.94	0.07	0.05
164	0.00	7.00	5.00	160.864	0.848	2074.15	0.07	0.05
165	0.00	7.00	4.50	156.057	0.823	2022.64	0.07	0.05
166	0.00	7.00	4.00	150.445	0.795	1971.68	0.06	0.05
167	0.00	7.00	3.50	137.338	0.741	1890.01	0.06	0.05
168	0.00	7.00	3.00	133.079	0.719	1851.91	0.06	0.04
169	0.00	7.00	2.50	124.958	0.678	1749.74	0.05	0.04
170	0.00	7.00	2.00	121.394	0.659	1702.17	0.05	0.04
171	0.00	7.00	1.50	114.259	0.622	1608.28	0.05	0.04
172	0.00	7.00	1.00	107.371	0.587	1519.32	0.05	0.04
173	0.00	7.00	0.50	100.988	0.553	1436.03	0.04	0.03
174	0.00	7.00	0.00	0.000	0.000	0.00	0.00	0.00
175	0.00	10.00	14.00	57.328	0.346	878.10	0.03	0.02
176	0.00	10.00	13.50	58.942	0.356	901.19	0.03	0.02
177	0.00	10.00	13.00	62.577	0.375	949.90	0.03	0.02
178	0.00	10.00	12.50	64.469	0.386	975.61	0.03	0.02
179	0.00	10.00	12.00	66.399	0.397	1002.26	0.03	0.02
180	0.00	10.00	11.50	68.531	0.408	1030.10	0.03	0.02
181	0.00	10.00	11.00	80.315	0.455	1140.94	0.03	0.03
182	0.00	10.00	10.50	82.668	0.468	1172.33	0.04	0.03
183	0.00	10.00	10.00	85.389	0.481	1204.81	0.04	0.03
184	0.00	10.00	9.50	85.389	0.481	1204.81	0.04	0.03
185	0.00	10.00	9.00	88.101	0.495	1240.68	0.04	0.03
186	0.00	10.00	8.50	88.101	0.495	1240.68	0.04	0.03
187	0.00	10.00	8.00	90.832	0.511	1277.78	0.04	0.03
188	0.00	10.00	7.50	90.832	0.511	1277.78	0.04	0.03
189	0.00	10.00	7.00	90.832	0.511	1277.78	0.04	0.03
190	0.00	10.00	6.50	90.832	0.511	1277.78	0.04	0.03
191	0.00	10.00	6.00	90.832	0.511	1277.78	0.04	0.03
192	0.00	10.00	5.50	88.101	0.495	1240.68	0.04	0.03
193	0.00	10.00	5.00	88.101	0.495	1240.68	0.04	0.03
194	0.00	10.00	4.50	85.389	0.481	1204.81	0.04	0.03
195	0.00	10.00	4.00	88.890	0.492	1281.92	0.04	0.03
196	0.00	10.00	3.50	84.761	0.479	1247.26	0.04	0.03
197	0.00	10.00	3.00	77.891	0.466	1212.32	0.04	0.03
198	0.00	10.00	2.50	67.187	0.458	1174.21	0.03	0.03

199	0.00	10.00	2.00	65.921	0.460	1122.07	0.03	0.03
200	0.00	10.00	1.50	67.302	0.486	1033.16	0.03	0.02
201	0.00	10.00	1.00	91.426	0.534	885.41	0.03	0.02
202	0.00	10.00	0.50	95.848	0.530	524.54	0.10	0.09
203	0.00	10.00	0.00	0.000	0.000	0.00	0.00	0.00

****** RESIDUAL RESPONSE AT THE END OF BLASTING **

(SETT = total settlement including contribution by EPV0
VOL = total volumetric strain including EPV0
D-VOL = VOL - EPV0
PPR = pore water pressure ratio at the end of this analysis when PWP0 due to EPV0 is held undrained
D-PPR = pore water pressure ratio when PWP0 has fully dissipated or EPV0 has consolidated)

NODE	X	Y	Z	SETT.	SIG-V0	PPR	VOL(%)	D-PPR	D-VOL(%)
1	0.00	0.00	14.00	0.000	113.47	0.80	0.36	0.18	0.04
2	0.00	0.00	13.50	0.002	109.87	0.84	0.41	0.20	0.05
3	0.00	0.00	13.00	0.004	106.28	0.88	0.47	0.23	0.05
4	0.00	0.00	12.50	0.007	102.68	0.91	0.53	0.25	0.06
5	0.00	0.00	12.00	0.010	99.09	0.94	0.62	0.29	0.07
6	0.00	0.00	11.50	0.013	95.49	0.96	0.73	0.33	0.08
7	0.00	0.00	11.00	0.017	91.90	0.98	0.88	0.39	0.10
8	0.00	0.00	10.50	0.022	88.30	0.99	1.08	0.46	0.12
9	0.00	0.00	10.00	0.028	84.71	1.00	1.36	0.55	0.16
10	0.00	0.00	9.50	0.039	81.11	1.00	3.07	0.81	0.35
11	0.00	0.00	9.00	0.057	77.52	1.00	4.10	0.91	0.47
12	0.00	0.00	8.50	0.079	73.92	1.00	4.82	0.94	0.52
13	0.00	0.00	8.00	0.104	70.33	1.00	4.97	0.94	0.50
14	0.00	0.00	7.50	0.129	66.73	1.00	4.97	0.94	0.50
15	0.00	0.00	7.00	0.153	63.14	1.00	4.97	0.94	0.50
16	0.00	0.00	6.50	0.179	59.54	1.00	5.15	0.95	0.52
17	0.00	0.00	6.00	0.204	55.95	1.00	5.15	0.95	0.52
18	0.00	0.00	5.50	0.235	52.35	1.00	6.93	0.98	0.75
19	0.00	0.00	5.00	0.267	48.76	1.00	5.90	0.97	0.68
20	0.00	0.00	4.50	0.293	45.16	1.00	4.42	0.90	0.51
21	0.00	0.00	4.00	0.312	41.57	1.00	3.47	0.81	0.40
22	0.00	0.00	3.50	0.328	37.97	1.00	2.80	0.71	0.33
23	0.00	0.00	3.00	0.341	34.38	1.00	2.29	0.61	0.27
24	0.00	0.00	2.50	0.351	30.29	0.99	1.94	0.54	0.22
25	0.00	0.00	2.00	0.360	26.19	0.99	1.67	0.48	0.20
26	0.00	0.00	1.50	0.368	22.09	0.97	1.35	0.39	0.15
27	0.00	0.00	1.00	0.384	18.00	1.00	5.23	0.94	0.60
28	0.00	0.00	0.50	0.397	9.00	0.00	0.00	0.00	0.00
29	0.00	0.00	0.00	0.397	0.00	0.00	0.00	0.00	0.00
30	0.00	1.00	14.00	0.000	113.47	0.79	0.35	0.17	0.04
31	0.00	1.00	13.50	0.002	109.87	0.83	0.40	0.19	0.05
32	0.00	1.00	13.00	0.004	106.28	0.87	0.46	0.22	0.05
33	0.00	1.00	12.50	0.006	102.68	0.90	0.52	0.25	0.06
34	0.00	1.00	12.00	0.009	99.09	0.93	0.60	0.28	0.07
35	0.00	1.00	11.50	0.013	95.49	0.96	0.71	0.32	0.08
36	0.00	1.00	11.00	0.016	91.90	0.98	0.85	0.38	0.10
37	0.00	1.00	10.50	0.021	88.30	0.99	1.01	0.44	0.12
38	0.00	1.00	10.00	0.027	84.71	1.00	1.25	0.51	0.14
39	0.00	1.00	9.50	0.037	81.11	1.00	2.78	0.77	0.32
40	0.00	1.00	9.00	0.053	77.52	1.00	3.59	0.87	0.42

41	0.00	1.00	8.50	0.073	73.92	1.00	4.66	0.94	0.54
42	0.00	1.00	8.00	0.097	70.33	1.00	4.87	0.94	0.51
43	0.00	1.00	7.50	0.122	66.73	1.00	4.97	0.94	0.50
44	0.00	1.00	7.00	0.147	63.14	1.00	4.97	0.94	0.50
45	0.00	1.00	6.50	0.171	59.54	1.00	4.94	0.94	0.50
46	0.00	1.00	6.00	0.196	55.95	1.00	4.84	0.94	0.51
47	0.00	1.00	5.50	0.225	52.35	1.00	6.68	0.98	0.77
48	0.00	1.00	5.00	0.254	48.76	1.00	5.15	0.94	0.60
49	0.00	1.00	4.50	0.277	45.16	1.00	3.97	0.86	0.46
50	0.00	1.00	4.00	0.295	41.57	1.00	3.21	0.77	0.37
51	0.00	1.00	3.50	0.310	37.97	1.00	2.65	0.68	0.31
52	0.00	1.00	3.00	0.322	34.38	1.00	2.22	0.60	0.26
53	0.00	1.00	2.50	0.332	30.29	0.99	1.88	0.52	0.22
54	0.00	1.00	2.00	0.341	26.19	0.99	1.63	0.46	0.19
55	0.00	1.00	1.50	0.348	22.09	0.96	1.21	0.35	0.14
56	0.00	1.00	1.00	0.363	18.00	1.00	4.71	0.91	0.53
57	0.00	1.00	0.50	0.375	9.00	0.00	0.00	0.00	0.00
58	0.00	1.00	0.00	0.375	0.00	0.00	0.00	0.00	0.00
59	9.00	2.00	14.00	0.000	113.47	0.48	0.15	0.08	0.02
60	9.00	2.00	13.50	0.001	109.87	0.50	0.16	0.08	0.02
61	9.00	2.00	13.00	0.002	106.28	0.52	0.16	0.08	0.02
62	9.00	2.00	12.50	0.002	102.68	0.53	0.17	0.09	0.02
63	9.00	2.00	12.00	0.003	99.09	0.56	0.18	0.09	0.02
64	9.00	2.00	11.50	0.004	95.49	0.57	0.19	0.10	0.02
65	9.00	2.00	11.00	0.005	91.90	0.58	0.20	0.10	0.02
66	9.00	2.00	10.50	0.006	88.30	0.64	0.23	0.12	0.03
67	9.00	2.00	10.00	0.007	84.71	0.65	0.23	0.12	0.03
68	9.00	2.00	9.50	0.009	81.11	0.75	0.41	0.16	0.05
69	9.00	2.00	9.00	0.011	77.52	0.76	0.42	0.16	0.05
70	9.00	2.00	8.50	0.013	73.92	0.76	0.42	0.16	0.05
71	9.00	2.00	8.00	0.015	70.33	0.77	0.43	0.17	0.05
72	9.00	2.00	7.50	0.017	66.73	0.77	0.43	0.17	0.05
73	9.00	2.00	7.00	0.020	63.14	0.77	0.43	0.17	0.05
74	9.00	2.00	6.50	0.022	59.54	0.77	0.43	0.17	0.05
75	9.00	2.00	6.00	0.024	55.95	0.77	0.43	0.17	0.05
76	9.00	2.00	5.50	0.026	52.35	0.78	0.58	0.18	0.07
77	9.00	2.00	5.00	0.029	48.76	0.78	0.58	0.18	0.07
78	9.00	2.00	4.50	0.032	45.16	0.79	0.59	0.18	0.07
79	9.00	2.00	4.00	0.035	41.57	0.79	0.59	0.18	0.07
80	9.00	2.00	3.50	0.038	37.97	0.77	0.57	0.18	0.07
81	9.00	2.00	3.00	0.041	34.38	0.76	0.55	0.17	0.07
82	9.00	2.00	2.50	0.044	30.29	0.75	0.53	0.16	0.06
83	9.00	2.00	2.00	0.046	26.19	0.74	0.52	0.16	0.06
84	9.00	2.00	1.50	0.049	22.09	0.72	0.49	0.15	0.06
85	9.00	2.00	1.00	0.051	18.00	0.70	0.46	0.14	0.06
86	9.00	2.00	0.50	0.052	9.00	0.00	0.00	0.00	0.00
87	9.00	2.00	0.00	0.052	0.00	0.00	0.00	0.00	0.00
88	0.00	3.00	14.00	0.000	113.47	0.76	0.32	0.16	0.04
89	0.00	3.00	13.50	0.002	109.87	0.80	0.36	0.18	0.04
90	0.00	3.00	13.00	0.004	106.28	0.83	0.40	0.19	0.05
91	0.00	3.00	12.50	0.006	102.68	0.87	0.45	0.22	0.05
92	0.00	3.00	12.00	0.008	99.09	0.89	0.50	0.24	0.06
93	0.00	3.00	11.50	0.011	95.49	0.92	0.57	0.27	0.07
94	0.00	3.00	11.00	0.014	91.90	0.94	0.64	0.30	0.07
95	0.00	3.00	10.50	0.017	88.30	0.96	0.73	0.33	0.08
96	0.00	3.00	10.00	0.021	84.71	0.98	0.83	0.37	0.10
97	0.00	3.00	9.50	0.027	81.11	1.00	1.64	0.54	0.19
98	0.00	3.00	9.00	0.036	77.52	1.00	1.83	0.58	0.21
99	0.00	3.00	8.50	0.046	73.92	1.00	2.04	0.63	0.24

159	0.00	7.00	7.50	0.026	66.73	0.90	0.69	0.26	0.08
160	0.00	7.00	7.00	0.029	63.14	0.90	0.69	0.26	0.08
161	0.00	7.00	6.50	0.033	59.54	0.90	0.69	0.26	0.08
162	0.00	7.00	6.00	0.036	55.95	0.90	0.67	0.25	0.08
163	0.00	7.00	5.50	0.040	52.35	0.91	0.92	0.28	0.11
164	0.00	7.00	5.00	0.045	48.76	0.91	0.94	0.28	0.11
165	0.00	7.00	4.50	0.049	45.16	0.91	0.91	0.27	0.11
166	0.00	7.00	4.00	0.054	41.57	0.90	0.89	0.27	0.10
167	0.00	7.00	3.50	0.058	37.97	0.89	0.85	0.25	0.10
168	0.00	7.00	3.00	0.062	34.38	0.87	0.80	0.24	0.09
169	0.00	7.00	2.50	0.066	30.29	0.86	0.75	0.23	0.09
170	0.00	7.00	2.00	0.070	26.19	0.85	0.72	0.22	0.09
171	0.00	7.00	1.50	0.073	22.09	0.83	0.68	0.21	0.08
172	0.00	7.00	1.00	0.077	18.00	0.81	0.64	0.19	0.07
173	0.00	7.00	0.50	0.078	9.00	0.00	0.00	0.00	0.00
174	0.00	7.00	0.00	0.078	0.00	0.00	0.00	0.00	0.00
175	0.00	10.00	14.00	0.000	113.47	0.45	0.13	0.07	0.02
176	0.00	10.00	13.50	0.001	109.87	0.46	0.14	0.07	0.02
177	0.00	10.00	13.00	0.001	106.28	0.48	0.15	0.08	0.02
178	0.00	10.00	12.50	0.002	102.68	0.49	0.15	0.08	0.02
179	0.00	10.00	12.00	0.003	99.09	0.51	0.16	0.08	0.02
180	0.00	10.00	11.50	0.004	95.49	0.52	0.16	0.08	0.02
181	0.00	10.00	11.00	0.005	91.90	0.58	0.19	0.10	0.02
182	0.00	10.00	10.50	0.006	88.30	0.59	0.20	0.10	0.02
183	0.00	10.00	10.00	0.007	84.71	0.60	0.20	0.10	0.02
184	0.00	10.00	9.50	0.008	81.11	0.70	0.35	0.14	0.04
185	0.00	10.00	9.00	0.010	77.52	0.71	0.36	0.14	0.04
186	0.00	10.00	8.50	0.012	73.92	0.71	0.36	0.14	0.04
187	0.00	10.00	8.00	0.013	70.33	0.72	0.38	0.15	0.04
188	0.00	10.00	7.50	0.015	66.73	0.72	0.38	0.15	0.04
189	0.00	10.00	7.00	0.017	63.14	0.72	0.38	0.15	0.04
190	0.00	10.00	6.50	0.019	59.54	0.72	0.38	0.15	0.04
191	0.00	10.00	6.00	0.021	55.95	0.72	0.38	0.15	0.04
192	0.00	10.00	5.50	0.023	52.35	0.73	0.51	0.15	0.06
193	0.00	10.00	5.00	0.026	48.76	0.73	0.50	0.15	0.06
194	0.00	10.00	4.50	0.028	45.16	0.72	0.49	0.15	0.06
195	0.00	10.00	4.00	0.031	41.57	0.74	0.52	0.16	0.06
196	0.00	10.00	3.50	0.033	37.97	0.73	0.50	0.15	0.06
197	0.00	10.00	3.00	0.036	34.38	0.72	0.49	0.15	0.06
198	0.00	10.00	2.50	0.038	30.29	0.70	0.47	0.14	0.05
199	0.00	10.00	2.00	0.040	26.19	0.68	0.44	0.13	0.05
200	0.00	10.00	1.50	0.042	22.09	0.64	0.40	0.12	0.05
201	0.00	10.00	1.00	0.044	18.00	0.57	0.32	0.10	0.04
202	0.00	10.00	0.50	0.045	9.00	0.00	0.00	0.00	0.00
203	0.00	10.00	0.00	0.045	0.00	0.00	0.00	0.00	0.00